Development and characterization of aptamer-amphiphiles against fractalkine for targeted drug delivery

A Dissertation
SUBMITTED TO THE FACULTY OF
UNIVERSITY OF MINNESOTA
BY

Brett M. Waybrant

IN PARTIAL FULFILLMENT OF THE REQUIREMENTS
FOR THE DEGREE OF
DOCTOR OF PHILOSOPHY

Adviser: Efrosini Kokkoli

December 2013

Acknowledgements

I came to the University of Minnesota for two reasons, the quality of the department and the people. Looking back on my graduate experience, both exceeded expectations. The faculty, coursework, and facilities was certainly top notch. The friendships developed though the first semester late night homework sessions, roundtable shenanigans, and graduate school highs and lows are priceless. I want to thank all my fellow classmates for the memories. The nights in downtown Minneapolis, Saturday golf outings, weekend cabin trips, and winter ice hockey have enriched my life with experiences I probably would not have gotten elsewhere. I also want to thank my family and especially my long suffering wife, Julia, for dealing with the late nights, unpredictable schedules, lonely weekends, and for providing the emotional support though the struggles of grad school.

I would also like to also thank my advisor, Prof. Efie Kokkoli, for the technical, creative brainstorming, and funding support. The meetings and discussions lead to many creative solutions to difficult the problems encountered during research. Among those key to this work are the Kokkoli group members Tim Pearce, Kamlesh Schroff, Maroof Adil, Matt Petersen, Brett Waybrant, Rachael Levine, Nicole Atchison, Emilie Rexeisen, Todd Pangburn, Ashish Garg, Carolyn Scott, and Frankie Pelaez. The lab discussions were not only very helpful but also wonderfully entertaining. In particular I would like to thank Tim Pearce who was tremendously patent and accommodating. Thanks to you all.

Abstract

A foundation of modern diagnostics and therapeutics is the ability to non-covalently bind to a molecule of interest. These affinity molecules are behind a broad array of products ranging from therapeutics to HIV tests. Currently, antibodies are used as the affinity molecule. Despite the success of antibodies, alternatives are needed due to high development and production costs, and issues with stability. Aptamers are an exciting alternative to antibodies. Aptamers are short sequences of single stranded DNA or RNA that bind molecular targets with high affinity and specificity. Aptamers are inexpensive to produce, are very stable, have long shelf lives, and could potentially replace antibodies in a number of applications. One potential application of aptamers is targeted drug delivery. The goal of targeted drug delivery is to selectively deliver a therapeutic payload to the site of action thereby increasing efficacy and decreasing side effects. Fractalkine is a cell surface protein expressed at sites of inflammation. It is expressed on several types of cancerous tissues and it is involved in the patheogenisis of arthritis, asthma, and atherosclerosis. This work describes the development and characterization of an aptamer that binds fractalkine with high affinity. The aptamer was modified with a hydrophobic tail, creating an aptamer-amphiphile, for use in a model drug delivery vesicle called a liposome. The aptamer-amphiphile was optimized for a high affinity interaction with fractalkine by adding a spacer molecule between the aptamer headgroup and the hydrophobic tail. The optimized amphiphile had high affinity for fractalkine and self-assembled into micelles and an interesting nanotape morphology. Finally, as a proof of concept, the optimized aptamer-amphiphile was incorporated into a liposome and targeted to fractalkine expressing cells. This work highlights the development of aptamers as affinity ligands, and demonstrates their use as potential drug delivery agents.

Contents

List of Tables

List of Figures

1 Introduction

The ability to bind molecules is an essential tool in modern science, especially in biological and medical disciplines.[1, 2] These molecular recognition tools specifically bind to target molecules through non-covalent interactions. Antibodies are the most widely used molecular detection ligand and have been used for decades in therapeutics, sensors, diagnostic tests, and imaging agents with great success.[3] However, there is a drive to develop antibody alternatives that maintain the high affinity binding to the target molecules but have properties better suited for the particular application.[1, 4]

Aptamers are an alternative molecular detection ligand made of single stranded DNA or RNA.[5-9] Aptamers have potential uses in sensors and diagnostic assays,[9, 10] affinity separations,[11] imaging, and drug delivery applications.[6, 12-16] Even though they were discovered in the 1990's, a significant amount of research is needed before aptamers are ready for commercial applications primarily because antibodies are well studied and developed.[1] This work investigates the development, modification, and characterization of an aptamer that binds a cell surface protein called fractalkine, and uses the aptamer as a ligand for targeted drug delivery.

1.1 Aptamers

1.1.1 What are aptamers

Aptamers are sequences of single stranded DNA (ssDNA) or RNA that bind to a specific molecule. Although typically short, 15-60 nucleotides in length, aptamers fold into complex three-dimensional structures either in free solution or upon binding to the target

molecule.[17] The complex shape allows the aptamer to strongly interact with the target molecule through hydrogen bonding, base stacking, van der Waals forces, and electrostatic interactions to produce a high affinity interaction.

At first thought, it seems strange that ssDNA can bind molecular targets. We typically think of DNA as a passive carrier of genetic information. However, this is a naive viewpoint. Not only do nucleic acids interact with and bind proteins with in the cell, they are active members of the cellular arsenal being involved in protein synthesis (ribosomes), mRNA splicing (splicesomes), and protein regulation (riboswitch).[18] It was the discovery of this active role of RNA that led to the discovery of aptamers in the early 1990s by three independent groups with the Szostak and Gold labs developing in vitro selection techniques.[19-21]

Aptamers can be either RNA based or DNA based. Some have suggested RNA aptamers may be better binders than DNA aptamer because the increased flexibility of RNA allows for more complex folding.[1, 13, 22] However, most often there is little to no difference between DNA aptamers and RNA aptamers except that DNA is inherently more stable.[8, 22] Several DNA and RNA aptamers have been selected against the same target molecule like thrombin,[23-25], interferon ɣ,[26, 27] and immunoglobulin E.[28, 29] DNA and RNA aptamers are typically not interchangeable; an RNA aptamer that is converted to DNA usually does not bind. However, there are cases where DNA and RNA aptamers with the same sequence do bind the same target.[30-32] Certain structural motifs may translate well between the nucleic acids while others do not.[32]

Aptamers are widely touted as antibody alternatives and are used in applications such as sensors and diagnostic assays,[9, 10] affinity chromatography,[11, 16] and therapeutic and imaging agents.[6, 12-15] Antibodies are currently the dominant molecular detection ligand used for therapeutics and diagnostics. However, aptamers are well suited in many applications where antibodies are currently used, and present several advantages to antibodies.

1.1.2 Advantages and drawbacks of aptamers

Affinity and specificity are important properties of any binding ligand like antibodies or aptamers. Affinity is a measure of how strongly the ligand binds its target molecule. It is quantified by the equilibrium dissociation constant (K_D). Aptamers have affinities that are similar to those of antibodies, varying from the low micromolar to picomolar, with the low nanomolar affinities being typical.[10, 33] Specificity is the preferential binding to the target molecule over similar molecules.[34] Aptamers are highly specific molecules. They can distinguish between isozymes,[35, 36] molecules differing by a single functional group,[37, 38] and even enantiomers.[39, 40] Perhaps the best known example of specificity is an aptamer that was designed to bind theophylline but not caffeine. Theophylline and caffeine differ in structure by a single methyl yet the aptamer has a 10,000 fold difference in affinity between the two molecules.[41]

A major advantage of aptamers is the in vitro identification process.[7] Antibodies are often made though the immunization of animals. The target molecule, the antigen, is injected into an animal resulting in an immune response. The immune system develops antibodies against the antigen and those antibodies are collected (to make poly-clonal antibodies) or

the spleen is harvested and the antibody producing cells are hybridized to produce a monoclonal antibody cell line. The process is typically done in vivo. Aptamer selection, on the other hand, is done in vitro. Because of this, aptamers can be selected against molecules that are poorly immunogenic.[13] Target molecule include small ions like Zn^{+},[42] small molecules,[43, 44] proteins,[23, 45] carbohydrates,[46, 47] toxins,[48, 49] and even whole organisms like bacteria and viruses.[50-52] However aptamers selected against small molecules tend to have lower affinity because of fewer target-aptamer interactions.[3] In vitro selections also allow the aptamer binding conditions to be optimized to the intended application. Buffers, salt concentrations, temperature, pH, and organic solvent content affect the binding affinity of ligands. With aptamers, the in vitro selection procedure can mimic the conditions in the intended application.[53] Aptamers have been selected to tolerate high concentrations of organic solvents (20% methanol) where antibodies failed to bind.[54] Similarly, an aptamer was developed for affinity chromatography that retained activity in a mobile buffer phase containing 30% acetonitrile.[55]

In addition to the in vitro selection process, aptamers are synthesized chemically unlike antibodies which are produced in vivo or in bioreactors. Because of the cellular origins, the production of antibodies is highly variable. Changes in the secondary and tertiary structure, glycosylation patterns, and drug-antibody conjugation efficiency, biological function can vary considerably from batch to batch. This makes regulating the production of antibodies for therapeutic use difficult requiring multiple assays to ensure proper biological activity. The glycosylation patterns require the use of mammalian cell lines for production greatly increasing the costs.[1] Aptamers, on the other hand, are synthesized chemically. This significantly reduces the cost of production because mammalian cell

culture is avoided. It also increases the consistency. There is little batch to batch variation. And the chemical synthesis allows for easy and site specific modifications at the 5' or 3' ends of the aptamer, but also within the aptamer strand itself.[7, 56, 57]

The relative simplicity of aptamers serves both as an advantage and disadvantage. Aptamers are composed of just 4 building blocks, adenine, guanine, cytosine and thymine/uracil while antibodies are built from 20 amino acids. Antibodies are large proteins, around 150 kDa, with a complex tertiary structure and glycosylation patterns. Aptamers, while they do form complex shapes, are much less complex than the intricate folding required of antibodies. Aptamers can be denatured like antibodies by heat, pH, and chemical solvents. However, unlike antibodies, aptamers undergo reversible denaturation. Aptamers are refolded by heating the aptamer above its melting temperature in the appropriate buffer and cooling to room temperature. This reversible denaturation, along with the chemical stability of nucleic acids, especially DNA, greatly extends the shelf life of the aptamer. Aptamers stored as lyophilized or dried powder have a shelf life of decades.

This simplicity also limits aptamers. Some molecular targets, especially negatively charged proteins, evade aptamer selection.[58] This is likely because there are only 4 base options compared to the 20 for antibodies limiting the chemical diversity to interact with the target molecule.[59] To overcome this, several alternative or modified bases have been developed.[56, 60] These modified bases have enabled aptamers to bind targets that previously avoided selection.[61]

1.1.3 Aptamers and the structure of DNA

Aptamers form complex three dimensional shapes and this shape is essential to the target affinity and specificity.[17] Aptamers also form several secondary structures that influence binding like step-loops, pseudoknots, and G-quadruplex structures.[4] Furthermore, the aptamer interacts with the target molecule through a variety of forces including van der Waals forces, hydrogen bonding, aromatic stacking interactions, and electrostatic forces. The structure of DNA is essential in understanding these interactions.

DNA and RNA are a linear biopolymers of repeating adenine (A), thymine (T), cytosine (C), guanine (G) and uracil (U) nucleobases connected though a sugar-phosphate backbone. Figure 1.1 shows the structures of the nucleobases. The bases are derivatives of pyrimidines (C, T, U) and purine (A, G). The bases are attached to a sugar molecule, deoxyribose for DNA and ribose for RNA, though a β-glycosidic linkage. The structure of deoxyribose is shown in Figure 1.2. In RNA, the 2' hydrogen is replaced with an –OH group. The nucleobases are attached at the 1' position to form a nucleoside. The nucleosides are joined by a phosphodiester linkage through the 5' and 3' positions of the sugar. The structure of DNA is shown in Figure 1.3. The two major forces between DNA strands are hydrogen bonding and aromatic base stacking.[62] Hydrogen bonding occurs between the bases to form the traditional Watson-Crick base paring, A to T and C to G. However, alternative base paring is also possible.[63, 64]

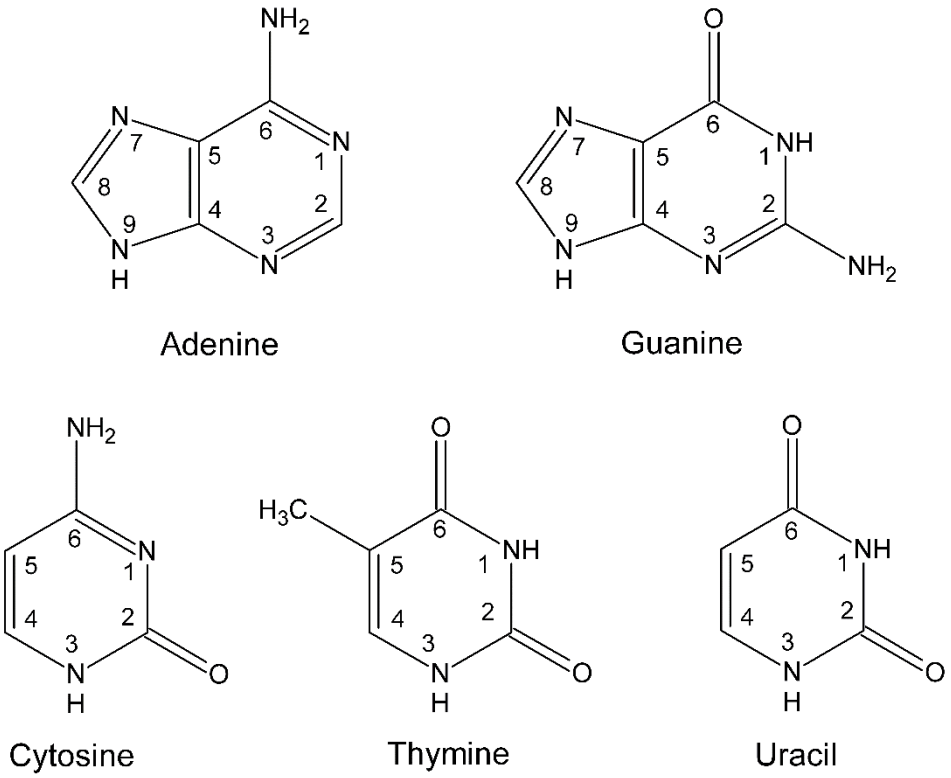

Figure 1.1: Structures of the nucleobases with the carbon atoms numbered. The base attaches to the ribose sugar through C_9 for Adenine and Guanine and C_3 for cytosine, thymine, and uracil.

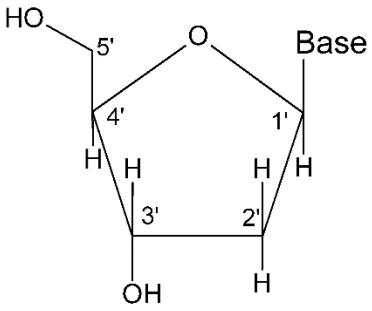

Figure 1.2: Structure of the deoxyribose sugar that makes up DNA. RNA is made from a similar sugar except the 2' hydrogen is replaced with an -OH group. The carbons are labeled with primes to distinguish from the nucleobase carbons.

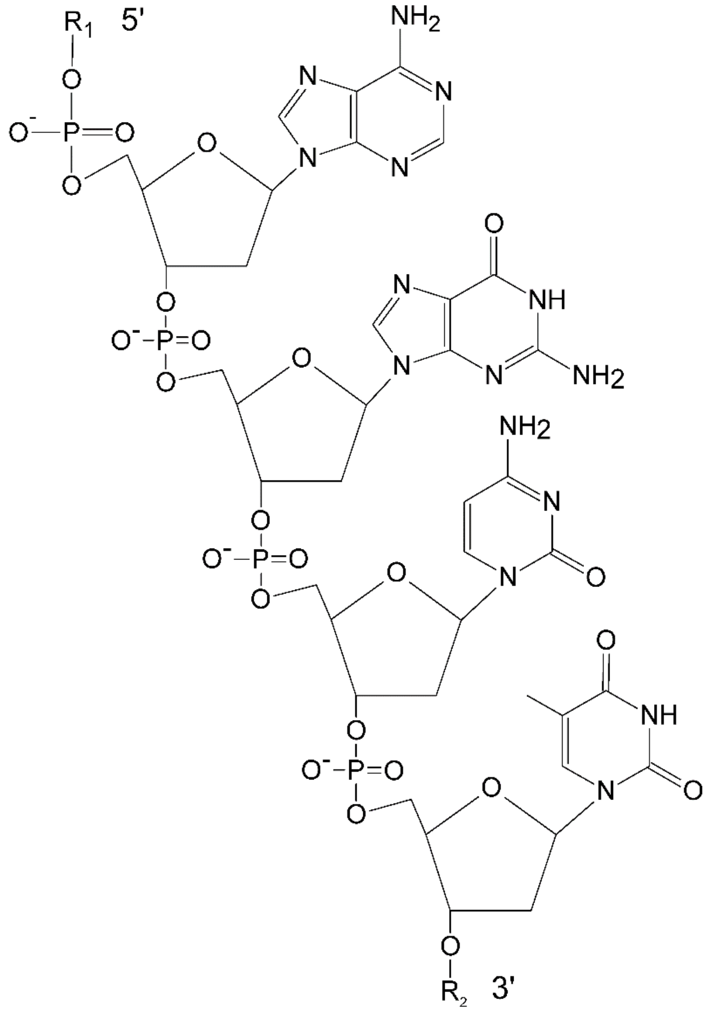

Figure 1.3: Structure of DNA with each nucleoside. The DNA strands have a directionality based on the 5’ and 3’ phosphodiester bonds.

1.1.4 Secondary structure of DNA

Nucleic acids can adopt a variety of secondary and tertiary structures. Perhaps the most well known, however, is the double helix. The DNA double helix forms when two complimentary strands of DNA pair together with one strand running in the 5' to 3' direction and the other strand running in the 3' to 5' direction.[64] The bases interact through Watson-Crick base pairing and base stacking. Each base pair is offset from the pair above giving rise to the helical structure of the double stranded DNA. Double stranded DNA can occur in several different conformations. Only three conformations, A-form, B-form, and Z-form, have been observed in nature with the majority of double stranded DNA taking the B-form.[65, 66] B-form DNA, first characterized by Watson and Crick, forms a right handed double helix with a strand diameter of 2 nm and a complete rotation of the helix approximately every 10 base pairs or 3.4 nm of strand length.[64]

1.1.5 Stem-loop structure

The stem-loop structure, also known as a hairpin structure, is one of the most common secondary structures found in DNA and RNA. Stem-loop structures occur when complementary sequences within a single DNA or RNA strand hybridize forming a double stranded stem region, and a single stranded loop region where the nucleic acid folds on itself and reverses direction.[67] Figure 1.4 is a diagram of a stem-loop structure. The base paring in the stem portion is in the double helix B-form conformation.[68]

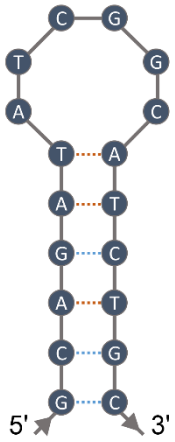

Figure 1.4: Diagram of a stem-loop structure.

1.1.6 G-quadruplex structure

A guanine rich DNA or RNA sequence often forms a G-quadruplex structure. Guanine is different from the other nucleobases in that it self-assembles into a tetrameric structure called a G-tetrad. A G-tetrad is a square planar arrangement of 4 guanine nuclobases with each corner of the square occupied by guanine. Each guanine forms two hydrogen bonds (through Hoogsteen base paring) with each adjacent guanine completing the sides of the square. The structure of a G-tetrad is show in Figure 1.5.

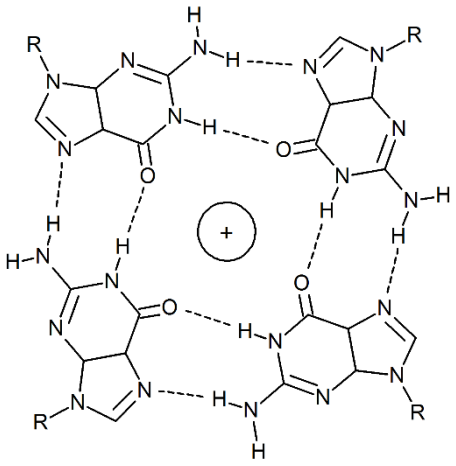

Figure 1.5: Structure of a G-tetrad.

Two or more of the G-tetrads stack on top of each other due to π bond stacking forming a G-quadruplex.[69] The structures of several G-quadruplex formations are shown in Figure 1.6. G-quadruplexes are broadly categorized into two groups based on the orientation and number of strands that make up the quadruplex. DNA and RNA have a 5' end and a 3' end based in the phosphodiester bond between the nucleotides. See Figure 1.2 and Figure 1.3. A G-quadruplex with all four strands oriented in the same direction are called parallel while a G-quadruplex with at least one strand oriented in the opposite direction to the others is called anti-parallel.[69] Figure 1.6 A and B show a parallel and an anti-parallel G-quadruplex respectively. In Figure 1.6A, the parallel G-quadruplex has all four strands are oriented in the same 5' to 3' orientation as denoted by the arrows; in Figure 1.6B, the anti-parallel G-quadruplex has two strands orientated in the 5' to 3' and two strands in the 3' to 5' direction. However, only one strand needs to be oriented in the opposite direction to qualify as an anti-parallel G-quadruplex.

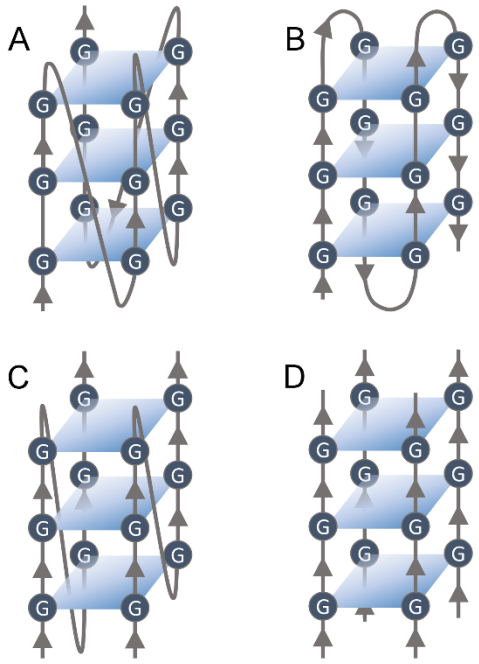

Figure 1.6: Structures of a (A) parallel unimolecular G-quadruplex, (B) anti-parallel unimolecular G-quadruplex. Parallel G-quadruplexes can also be (C) bimolecular and (D) tetramolecular. There are several additional G-quadruplex structures not shown.

The G-quadruplexes in Figure 1.6 A and B are composed of one strand. However, they can also form from two (Figure 1.6 A) or four strands (Figure 1.6 B) coming together. There are two naming conventions to describe the molecularity of G-quadruplexes. The first classifies G-quadruplexes as either intramolecular, composed of a single strand, or intermolecular, composed of several strands. They are also classified by the number of strands, unimolecular, bimolecular and tetramolecular G-quadruplexes are composed of 1, 2, and 4 strands respectively.[70]

The quadruplex is strengthened by the addition of cations, notably K+, that coordinate between the tetrads. The positive cation interacts with the O6 oxygen atom of guanine (see Figure 1.1) stabilizing the complex.[71] Both monovalent and divalent cations stabilize

the G-quadruplex but monovalents are usually better at stabilizing the quadruplex.[72] The ability of monovalent cations to strengthen the G-quadruplex is K^{1+}> Rb^{1+}> Na^{1+}> Cs^{1+}>Li^{1+} and for Sr^{2+}> Ba^{2+}> Ca^{2+}> Mg^{2+} for divalent cations.[71, 72] However, the monovalent cations typically stabilize the G-quadruplex better than divalent cations.[72] The stabilizing ability of the different cations is largely dependent on the ionic radius of the cation. Ions with an ionic radii between 1.3 and 1.5 best stabilize the G-quadruplex.[71]

1.1.7 Circular dichroism (CD) spectroscopy

Circular dichroism (CD) spectroscopy is a technique to probe the secondary structure of DNA and RNA.[73] CD spectroscopy measure the differential absorption of left and right handed circularly polarized light by chiral molecules. The difference in absorption, called the ellipticity, is characteristic of different secondary structures. B-form or stem-loops, parallel G-quadrupexes, and anti-parallel G-quadruplexes can be identified from the CD spectrum.[73-75] The CD spectra of the different secondary structures will be discussed in section 3.2.3. The CD signal in double stranded DNA arises from several factors including the electronic dipoles of the nucleobases, interactions between the bases, bond angles between the base and sugar, and bond angles between the sugar and the phosphate backbone.[76, 77] CD spectroscopy can distringuish between A-, B-, Z-forms of DNA.[78] For G-quadruplexes, the CD spectrum arrises from the interations between the G-tetrads. The directionality of the strands affects the conformation of the sugar-base N-glycosidic bond. All the bonds are in the anti conformation for parallel G-quadruplexes, but the bonds are in both the anti and syn conformations in anti-parallel G-quadruplexes. This causes different polarities of the hydrogen bonds making up the G-tetrad.[79] The CD signal arises from the stacking between G-tetrads of the same or different polarities leading to the

characteristic CD spectra.[80, 81]

1.1.8 Selection of aptamers - SELEX

There are several methods to identify and isolate aptamer, but the systematic evolution of ligands by exponential enrichment (SELEX) process is most commonly used. SELEX is an iterative, combinatorial approach of exposure, isolation, and amplification. The process starts with a large random pool of oligonucleotides, usually 10^{14} to 10^{15} unique sequences. (Here we distinguish between oligonucleotides and aptamers. Oligonucleotides are short single stranded nucleic acid sequences that do not bind a specific target molecule; aptamers are single stranded nucleic acid sequences that bind a specific target molecule.) The oligonucleotides have a random region, usually 25 to 60 bases long flanked with primer regions which are 15-26 nucleotides long.[82] The primer regions are used during amplification of the oligonucleotide pool. A schematic of the oligonucleotide is shown in Figure 1.7A. The random oligonucleotide pool, called a library, is synthesized chemically. The random pool is generated by adding all four nucleotides at once during the stepwise synthesis of the pool. Each nucleotide has an equal probability of reacting resulting in a random sequence. Some care must be taken when synthesizing the library because the nucleotide precursors have slightly different reaction yields.[83] Random pools are easily synthesized by DNA synthesis companies.

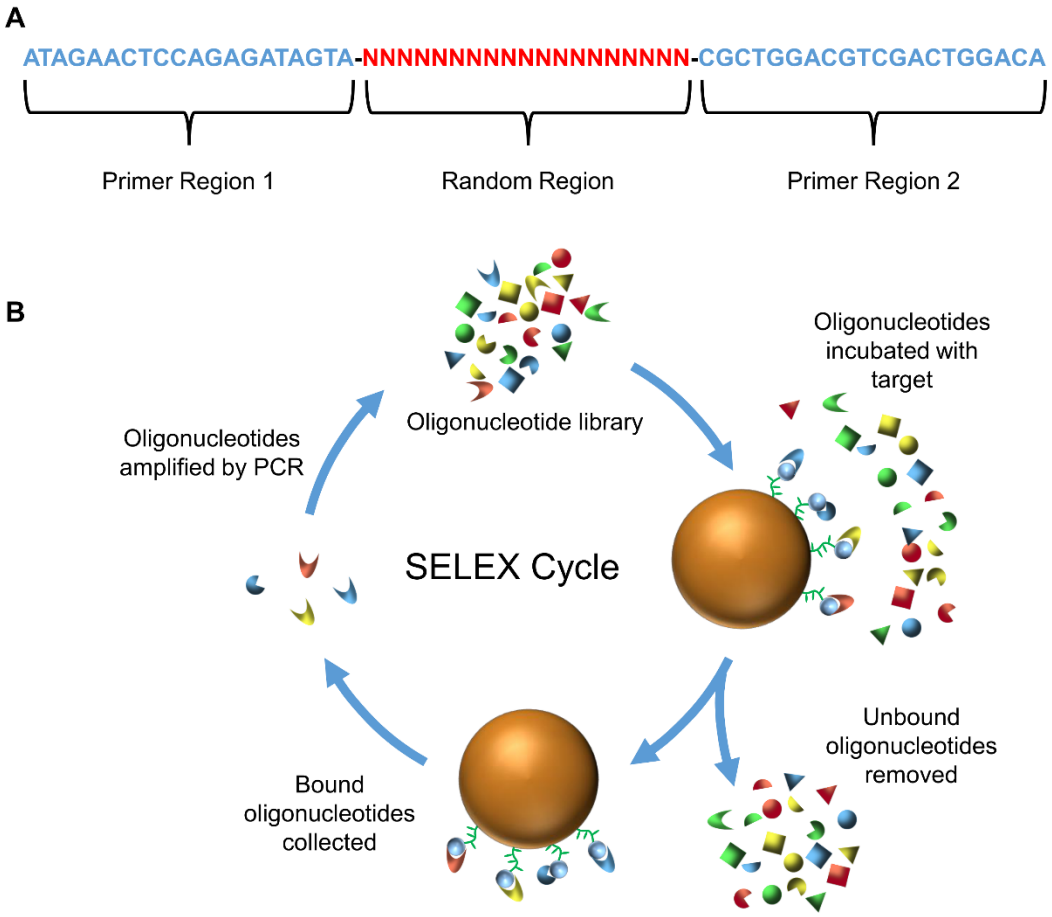

Figure 1.7: (A) Schematic of the oligonucleotide and (B) a diagram of the SELEX cycle.

SELEX is deceptively simple. A diagram of the process is shown in Figure 1.7. The oligonucleotide library is then exposed to the target molecule. Because of the large number of oligonucleotides, some have the right shape and properties to bind the target. Roughly one in 10^9 to 10^{13} oligonucleotides have sufficient affinity with higher affinity sequences being more rare.[84] Those oligonucleotides with affinity bind the target molecule while the oligonucleotides with no affinity remain in solution. The bound oligonucleotides are then isolated from non-binders and amplified by polymerase chain reaction (PCR).

The amplified oligonucleotide library is again exposed to the target molecule and the cycle is repeated. With each cycle, the oligonucleotide library is enriched with binding sequences and depleted of non-binding sequences. Several cycles are needed because of the rarity of the high affinity oligonucleotides in the initial aptamer pool and because the isolation methods are not 100% efficient. Six to fifteen cycles are typically needed to isolate the highest affinity aptamers after which the aptamer pool is cloned and sequenced.

1.1.9 Immobilization

The immobilization of the target molecule is an essential step in the SELEX process.[85] Immobilization facilitates efficient separation of the bound from the unbound oligonucleotides and collection of the aptamer-target complex.[85] Therefore it is important to select an immobilization system that has a high partition efficiency, defined as the percentage of the aptamer-target complex that is retained after isolation, and that efficiently removed the non-specific oligonucleotides. The partition efficiency and background removal are crucially important in reducing the number of cycles and therefore the time and cost of SELEX.[82, 86, 87] The partition efficiency is largely determined by the immobilization method and background removal is achieved by thorough washing steps. Another concern of the immobilization method, especially with proteins, is retaining the tertiary structure of the target molecules. Aptamers are sensitive to changes in the conformation of the target molecule and immobilization methods that alter the 3D shape can cause failure to identify aptamers with high affinity.[58]

There are a large number of immobilization methods and two will be highlighted here.[85]

The initial SELEX methods used affinity chromatography columns. In this system, the target molecule is covalently conjugated to a chromatographic medium, often a cross linked agarose bead. The column is equilibrated with the binding buffer and the oligonucleotide library exposed to the medium. The column is then washed with several column volumes of buffer to remove the oligonucleotides that do not bind. The aptamer is recovered by adding an appropriate elution buffer to the column, often deionized water, a high salt buffer, or a chelating agent like EDTA, which causes the aptamer to dissociate. The elution is then amplified by PCR and the process repeated. The second method uses the polyhistidine-nickel interaction to immobilize the target to the surface of magnetic agarose beads.[88, 89] Recombinant proteins are often expressed with a polyhistidine tag to facilitate purification from the cell culture. The polyhistidine tag non-covalently binds to nickel allowing for reversible immobilization. The protein is first incubated with commercially available magnetic agarose beads that have a Ni^{2+} ion chelated onto the surface. Next, the oligonucleotide library is exposed to the beads and non-binding oligonucleotides removed by washing with buffer. The aptamer-target complex is then eluted using an acidic buffer or adding an excess of imidazole. The aptamer is then recovered from the supernatant and used in subsequent cycles. With this system, the aptamer-target complex is easily isolated because of the selective elution of the polyhistidine-Ni^{2+} interaction and the easy partitioning of the magnetic beads.

1.1.10 Stringency of selection

SELEX can be simplified into two phases. In the initial phase, the high affinity aptamers are an extremely small percentage of the library. It is critical that these aptamers are collected and passed on to subsequent rounds. Therefore incubation times are long and

washing steps are gentle. The selection in less stringent. In the second phase, after the majority of the non-binding oligonucleotides are removed, the selection conditions must become more stringent to isolate those aptamers with the highest affinity from those with mediocre affinity. If the selection stringency is not increased, only the aptamers with mediocre affinity will be isolated.[86] This is because the library contains a large number of mediocre affinity aptamers and a relatively few number of high affinity aptamers. If too many of the mediocre affinity aptamers are retained they overwhelm the high affinity aptamers. The selection conditions must be such that the high affinity aptamers compete with and displace the more numerous mediocre affinity aptamers. The selection stringency is controlled by several methods like increasing salt concentration and reducing incubation time. But the preferred method is reduction of the target molecule concentration. By reducing the target concentration the aptamers with highest affinity occupy the majority of the binding sites while the lower affinity aptamers remain unbound and are removed during the isolation steps.

1.1.11 Negative and counter selection

It is important to amplify only those aptamer that bind the target molecule. SELEX is a non-discriminatory process; aptamers will be selected against any molecule in the system.[90] In most systems there are multiple potential non-specific molecules like the immobilization system, carrier proteins like bovine serum albumin, and even different epitopes on the target molecule. These off-target aptamers complicate the identification of the target aptamer and can reduce the affinity of the aptamers.[91] A negative selection round is usually performed to remove the aptamers that bind the off-target molecules. Negative selection is done by performing one or more SELEX cycles with the target

molecule absent and collecting what does not bind. Aptamers that bind off-target molecules are removed but the target molecule aptamers remain. A similar method called counter SELEX is done to isolate aptamers that bind a specific epitope, or to increase aptamer selectivity. Here, the oligonucleotide library is exposed to a molecule that is similar to the target molecule. Those aptamers that have affinity for the off-target molecule bind and are removed. But the aptamers that bind the target molecule, but not the off-target molecule remain. Using this method, aptamers can be isolated that discriminate between molecules that differ by a methyl or hydroxyl group.[2]

Aptamers have several characteristics that make them excellent affinity ligands like high affinity and selectivity for the target molecule, low cost of production, high stability, and in vitro selection methods. Aptamers are just now entering into commercial use in diagnostic assays and as therapies.[92, 93] However, a significant amount of research is needed before aptamers are ready for use in mainstream applications.

1.2 Fractalkine

Fractalkine is a cell surface protein that is an exciting and unexplored target molecule for aptamers. Fractalkine is part of the chemokine family consisting of small proteins involved in the immune response and inflammation pathways.[94] Fractalkine's structure and physiological function make it a great target for novel therapeutics in pain management, inflammatory diseases such as asthma, and cancer treatments. Despite fractalkine's potential, there are no such therapeutics in clinical use.[95]

1.2.1 Chemokines

Chemokines are a family of approximately 50 structurally related proteins involved in, among other things, inflammation, immune response, and tumor development through the recruitment and regulation of leukocytes (white blood cells).[94, 96-98] Chemokines are part of a larger family of signaling proteins called cytokines. What sets chemokines apart is the ability to induce chemotaxis, which is cell migration in response to a chemical gradient. There are four sub-classifications of chemokines, CC, CXC, XC, and CX3C, distinguished by four cysteine residues that form two disulfide bonds essential for structure and function, although this system is slowly being replaced by one based on function rather than structure.[96, 99] Chemokines are named by their sub-family classification, for example CC, followed by whether it is a receptor (R) or ligand (L) status and a number designator. So CCL11 is ligand 11 of the CC chemokine family.

1.2.2 Function of fractalkine

Fractalkine (or CX_3CL1), discovered in 1997 and known as neurotactin in mice, is the only member of the CX_3C family.[100, 101] Fractalkine, and its analog CXCL16, are the only chemokines that exist in both membrane bound and soluble forms with each form providing a different physiological function.[102] In the membrane bound form, fractalkine serves primarily as an integrin independent adhesion molecule for circulating leukocytes.[103] The unique structure of membrane bound fractalkine, shown in Figure 1.8, makes fractalkine an excellent adhesion molecule. Fractalkine binds to its receptor CX3CR1 exclusively though the chemokine domain which sits atop an extended mucin-like stalk. The chemokine domain and mucin-like stalk are anchored to the cell membrane through a single pass transmembrane domain with a short cytoplasmic tail. The heavily

glycosylated mucin-like stalk functions exclusively as a tether for the chemokine domain extending it though the extracellular matrix to increase accessibility to leukocytes.[104] Replacement of the mucin-like stalk with a short repeat consensus sequence of E-selectin of the same length as the mucin stalk showed similar binding wild type fractalkine while mucin alone exhibited no binding and the chemokine domain without a tether showed significantly reduced binding.[104] Furthermore, capture of leukocytes to fractalkine occurs in an integrin independent manner[105, 106] and under physiological shear stresses.[103, 107, 108] Membrane bound fractalkine has been found on dendritic cells,[109, 110] neurons,[111, 112] and astrocytes,[113] and is believed to play an important role in cellular communication within the nervous system.[114]

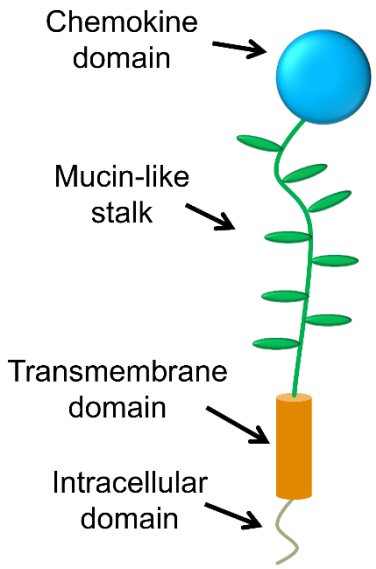

Figure 1.8: Cartoon showing the structure of membrane bound fractalkine.

The soluble form is a chemoattractant for natural killer cells, monocytes and subsets of T-cells.[100, 101, 115] The soluble form of fractalkine is created by cleavage of membrane bound fractalkine though both constitutive and induced cleavage of the mucin like stalk near the cell membrane creating a 95 kDa soluble protein. Constitutive shedding occurs through the ADAM10 metalloproteinase[116, 117] while induced cleavage is done by tumor necrosis factor-α-converting enzyme (TACE or ADAM17).[118, 119] The soluble fractalkine concentration in the blood is very low. The majority (85%) of healthy volunteers and colorectal cancer patients had undetectable soluble fractalkine levels ranging from 1.8 to 44.8 ng/mL.[120]

1.2.3 Fractalkine's role in disease

The role of fractalkine in disease is just beginning to be understood. It is involved in atherosclerosis, cardiac allograft rejection, asthma, age related macular degeneration, and neuropathic pain.[95, 121] Much of fractalkine's role in diseases is due to the bodies inflammatory response. After an injury or at the site of infection, chemokines and adhesion molecule recruit and direct leukocytes as part of the inflammatory response.[122] Fractalkine takes part in this process by recruiting leukocytes through chemotaxis and by serving as an adhesion molecule. In the vasculature system, fractalkine is only expressed at sites of inflammation or injury upon stimulation by pro-inflammatory cytokines TNF-α, IFN-γ and IL-1β.[100, 123-125] But fractalkine is involved in several other diseases. Several diseases are discussed in more detail below.

Cancer

Fractalkine is involved in a variety of different cancers including human gioblastoma,[126] hepatocellular carcinoma,[127, 128] B16-F0 melanoma,[129] neuroblastoma,[130] lung cancer epithelium,[131] epithelial ovarian cancer,[132] and is implicated in the metastasis of prostate,[133, 134] breast, pancreatic and melanoma brain cancers. The expression of fractalkine leads to better prognosis due to the increased recruitment of leukocytes to the cancer sites. Studies by Hyakudomi et al and Ohta et al on gastric adenocarcinoma and colorectal cancer respectively both showed better prognosis and disease free survival that correlated with increased fractalkine expression.[135, 136] Fractalkine has also shown to attract natural killer cells to tumor sites resulting in a strong antitumor effect.[137-139]

Rheumatoid arthritis

Rheumatoid arthritis is characterized by chronic inflammation of joint tissues leading to leukocyte infiltration and eventually joint destruction.[140] The synovium of rheumatoid arthritis patients show infiltration of monocytes, macrophages and CD4+ T lymphocytes which promote secretion of inflammatory cytokines.[141] It is therefore not surprising that fractalkine is significantly expressed in endothelial cells, monocytes and macrophages, and dendritic cells while macrophages, fibroblasts and dendritic cells expressed CX3CR1.[142, 143] Soluble fractalkine is also significantly increased in the synovial fluid of patients with rheumatoid arthritis compared to healthy individuals.[144-146] The increased fractalkine concentration likely leads to chemotaxis of leukocytes.[141] Fractalkine levels were correlated with increased joint stiffness suggesting fractalkine induced chemotaxis of monocytes is a factor in rheumatoid arthritis suggesting fractalkine is an important contributor to the disease.[142] Additionally, a study in mice by Nanki et al showed that

inhibition of fractalkine by an anti-fractalkine antibody inhibited the infiltration of macrophages into the synovium by 40% and reduced the symptoms of arthritis in a murine model.[147] A fractalkine antagonist has real potential as a therapy for rheumatoid arthritis.

Asthma

Both fractalkine and its receptor, CX3CR1 play crucial roles in asthma. Asthma is characterized by chronic inflammation of the airway and the primary driver is the T_H2 inflammatory response.[148-152] In asthmatic individuals, airway smooth muscle cells (ASMCs) constitutively express fractalkine.[153] Immunostaining of bronchial biopsies showed fractalkine expression 6.5 times higher in asthmatic patients compared to controls with significant expression in the epithelium, submucosa, and smooth muscle cells. Fractalkine is upregulated in patients with asthma and rhinitis compared to healthy patients. Rimaniol et al. studied the fractalkine expression in 19 control and 55 patients with symptomatic allergic rhinitis and asthma.[154] Immunohistochemistry staining of bronchial mucosal biopsy shows high levels of membrane bound fractalkine in endothelial and epithelial cells pre and post challenge. A second study also showed constitutive fractalkine expression in bronchoscopy and bronchial mucosal biopsies.[155] The expression of membrane bound fractalkine in the airways of asthmatic individuals makes fractalkine an excellent molecule for targeted delivery of therapeutics.

Atherosclerosis

Atherosclerosis is a chronic inflammatory disease of the arterial wall. Monocytes and lymphocytes accumulate in the arterial lesion in response to chemokines leading to the migration of smooth muscle cells and the buildup of plaque.[156] Several studies have shown

fractalkine to be a key contributor to atherosclerosis. Two studies showed polymorphic mutations in CX3CR1 correlated with a decreased risk of coronary artery disease.[157, 158] Studies of CX3CL1 and CX3CL1 knockout mice show dramatic reduction in lesion size.[159-162] A study in fractalkine knockout mice by Teupser et al showed up to 85% reduction in lesion area compared to controls.[161]

Pain Management

Fractalkine expressed within the nervous system, primarily on neurons, and is thought to function as a signaling molecule between neurons and microglia.[111, 163] Intrathecal fractalkine induces a pain response in rats which is modulated by anti-CX3CR1 antibody.[164] Several studies implicate fractalkine as a neuron to gila signaling molecule inducing a pain response.[165, 166] Furthermore, in CX3CR1 knockout mice showed significantly reduced pain response.[167] Additionally, injury releases fractalkine from neurons. The fractalkine stimulates microglia cells leading to activation of the pain pathways. Addition of an anti-fractalkine antibody prevented activation of the pain pathway in a rat model indicating fractalkine is an important pain mediator.[168]

Fractalkine is a good target for therapeutic applications because of its unique structure and function. It is involved in several diseases by recruiting and capturing leukocytes at sites of infection and inflammation. Currently there are no therapeutics targeting fractalkine.[95]

1.3 Targeted delivery

Most injected therapeutic drugs rapidly distribute throughout the body. Large doses are therefore required to achieve therapeutically effective concentrations at the tumor site. As a result, there is significant toxicity to the healthy tissues of the body leading to many of the side effects common to chemotherapy. The pharmacological properties of conventional drugs can be improved by using drug delivery systems. Drug delivery systems, which include liposomes, polymeric nanoparticles, micelles, and dendrimers, are designed to protect an encapsulated therapeutic agent and preferentially accumulate at the disease site. Increased accumulation allows for a smaller drug dose, causing fewer or less severe side effects while maintaining or enhancing the therapeutic efficacy.

Liposomes are a widely studied drug delivery system. Liposomes are self-enclosed vesicles composed of amphiphilic lipids, commonly phospholipids, which self-assemble into a bilayer morphology in aqueous solutions. Liposomes are rapidly cleared from the blood by the mononuclear phagocyte system (MPS), which removes foreign particles from the blood.[169] To increase circulation time, polyethylene glycol (PEG) chains are grafted to the liposome surface. PEG functionalized liposomes, called stealth liposomes, reduce interactions through steric effects increasing circulation time. Liposomes are an excellent model drug delivery vehicle because they are well characterized and studied.

2 Development and characterization of an aptamer binding ligand of fractalkine using domain targeted SELEX*

2.1 Introduction

Fractalkine, or CX3CL1, is a member of the chemokine family that bears potential for novel therapeutics due to its unique structure and its central role in human inflammatory diseases.[95] Currently no therapeutics targeting fractalkine exist. Here, we developed an aptamer that binds with high affinity and specificity to fractalkine and can be used as a fractalkine antagonist or targeting ligand for the delivery of therapeutics.

Fractalkine is one of two chemokines, along with CXCL16, that exist in two active forms, membrane bound and soluble.[102] Membrane bound fractalkine captures circulating leukocytes through integrin independent binding with its highly specific receptor CX3CR1 expressed on leukocytes.[115, 116, 119] Fractalkine's structure facilitates leukocyte adhesion. Binding occurs exclusively through the chemokine domain of fractalkine that sits atop a heavily glycosylated mucin-like stalk (Figure 2.1) that extends the chemokine domain approximately 26 nm away from the cell membrane to increase accessibility.[104] The soluble form is produced by cleavage of membrane bound fractalkine near the cell membrane by the metalloproteinases ADAM10 and ADAM17 and is a potent

chemoattractant for natural killer cells, monocytes and subsets of T-cells.[100, 116, 119]

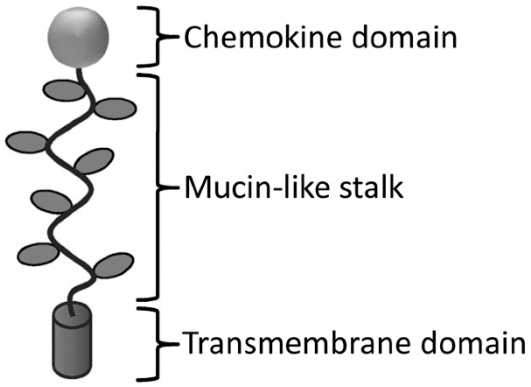

Figure 2.1: Graphic representation of fractalkine (not to scale). The chemokine domain is attached to a mucin-like stalk. A single pass transmembrane domain anchors fractalkine to the cell.

Drug delivery systems functionalized with a fractalkine ligand may have useful targeting properties because of membrane bound fractalkine's physiological role as an adhesion molecule for circulating leukocytes. Fractalkine is expressed by many cancer tissues including human glioblastoma,[126] hepatocellular carcinoma,[127] neuroblastoma,[130] epithelial ovarian cancer,[132] colorectal cancer,[136] and gastric adenocarcinoma[135] causing an increased leukocyte presence resulting in an antitumor effect. Furthermore, fractalkine has been implicated in many inflammatory diseases primarily through the recruitment and adhesion of leukocytes mediating the body inflammatory response.[95] Anti-fractalkine antibodies reduce arthritic symptoms in mouse models and elimination of fractalkine from synovial fluid reduces angiogenesis suggesting inhibition of fractalkine may be a treatment for rheumatoid arthritis.[141] Fractalkine also appears to play a role in allergic diseases, such as asthma, and local administration of a fractalkine antagonist to antigen-sensitized mice

resulted in reduced airway hyper-responsiveness and airway inflammation.[171]

Other attempts to develop a fractalkine binding molecule include a peptide ligand that bound fractalkine but lacked sufficient affinity for cellular applications.[172] Rather than a peptide, we developed an aptamer ligand. Aptamers, single stranded nucleic acid sequences that bind with high affinity and specificity, have several advantages over other ligands. Aptamers have long shelf lives, are easily refolded if denatured, are chemically synthesized allowing for precise chemical modification with little batch to batch variation, and show little to no immune response.[6] In contrast, antibodies and proteins are large, often immunogenic and require animals or cell culture methods for production increasing cost and variability.

Aptamers are identified through the systematic evolution of ligands by exponential enrichment (SELEX) process. SELEX is an iterative combinatorial method where the target molecule is exposed to 10^{14}–10^{15} random nucleotide sequences. The aptamers that bind the target are collected and amplified by polymerase chain reaction (PCR). The target is again exposed to the aptamers and the process repeated for 6 to 15 cycles at which point the aptamer pool is cloned and sequenced.

2.2 Results and discussion

SELEX was performed to identify aptamer sequences with affinity for fractalkine. Recombinant human fractalkine containing the chemokine domain and the mucin-like stalk with a polyhistidine tag attached at its end was immobilized onto magnetic agarose beads. The polyhistidine tag binds reversibly to a Ni^{2+} moiety on Ni-NTA magnetic agarose beads.

This immobilization method is advantageous because fractalkine's orientation is physiologically consistent by exposing the chemokine domain at the interface. The reversible polyhistidine-Ni^{2+} bond allows for selective elution of fractalkine–aptamer complex leaving behind non-specific binders.[88] Immobilized fractalkine was exposed to a randomized library consisting of 6×10^{14} nucleotide sequences for 1 hour. The beads were washed three times for 5 minutes to remove non-specific binders and to select aptamers with slow k_{off} kinetics.[173] The aptamers with fast k_{off} kinetics likely dissociate and are removed in the wash while the aptamers with slow off rates remain.

We reasoned that targeting the chemokine domain would produce the desirable characteristics of a fractalkine aptamer. The chemokine domain extends away from the cell increasing accessibility and improving ligand binding. Also, an aptamer that selectively binds to the chemokine domain would likely block CX_3CR1-fractalkine binding, whereas an aptamer binding other fractalkine domains, like the mucin-like stalk, may be non-specific because other proteins have similar structures. To do this, we modified the SELEX protocol to exploit the lack of secondary structure in the mucin-like stalk.[104] Heating to 95 °C eliminated the chemokine domain structure while leaving the mucin-like stalk unaffected. When the denatured fractalkine was exposed to the aptamer pool, chemokine domain aptamers remained in the supernatant while other aptamers bound and were removed. This was a simple and effective method for selecting chemokine domain aptamers.

SELEX was stopped after twelve rounds when the PCR cycles required for aptamer pool amplification levelled off indicating saturation (Figure 2.2). An electrophoretic mobility shift

assay (EMSA) confirmed that the aptamer pool bound fractalkine (Figure 2.3). The aptamer was tagged with a biotin primer and was detected using a HRP-neutravidin chemiluminescent protocol. The aptamer bound to fractalkine (FKN) appears as a strong band in lane 2. Addition of an anti-histidine antibody (His Ab) that binds fractalkine resulted in a supershift (lane 3) due to the extra mass of the antibody. The supershift confirms the aptamer binds specifically to fractalkine. The aptamer did not bind the His Ab or bovine serum albumin (BSA) controls in lanes 4 and 5 respectively. Additionally, an anti-chemokine domain antibody (FKN Ab) blocked aptamer binding demonstrating that the aptamer binds the chemokine domain (lane 6). Additional EMSA analysis is included in Figure 2.4. After confirming the aptamer pool bound fractalkine, the pool was cloned into E. coli and sequenced. Of the 85 clones sequenced, approximately 95% were the same sequence differing only by single nucleotide polymerase errors. The resulting aptamer, named FKN-S2, had the sequence 5′-GGGGTGGGTGGGGGGCACGTGTGGGGGCGGCCAGGGTGCT-3′.

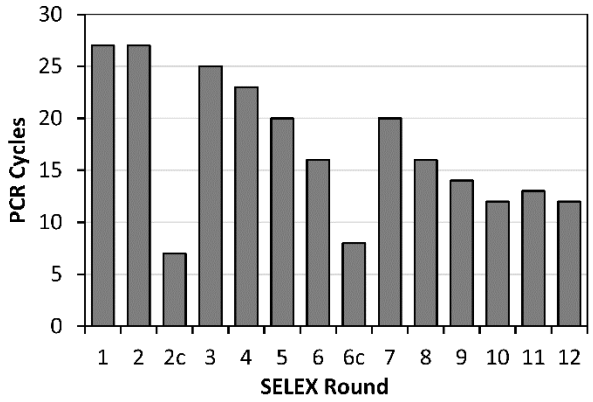

Figure 2.2: The number of PCR cycles needed for aptamer pool amplification per round. The two chemokine selection steps are denoted by 2c and 6c. The chemokine domain selection steps required fewer cycles because rather can collecting the beads, only the supernatant was amplified which contained significantly more sequences.

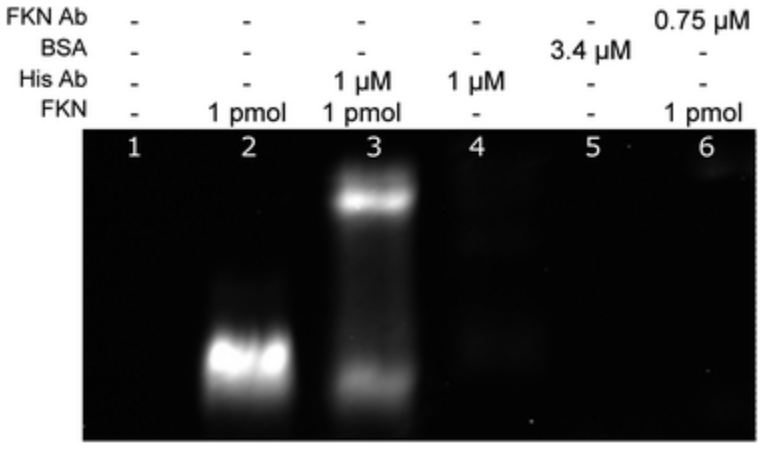

Figure 2.3: EMSA analysis of the 12th SELEX round. Lane 1: aptamer with no FKN. Unbound aptamer band removed for brevity. See below full figure (Figure 2.4). Lane 2: aptamer with FKN. Lane 3: addition of the His Ab causes a supershift. Lane 4: the aptamer does not bind the His Ab. Lane 5: the aptamer does not bind BSA. Lane 6: an anti-chemokine domain antibody blocks aptamer binding. All lanes have 5 nM aptamer concentration.

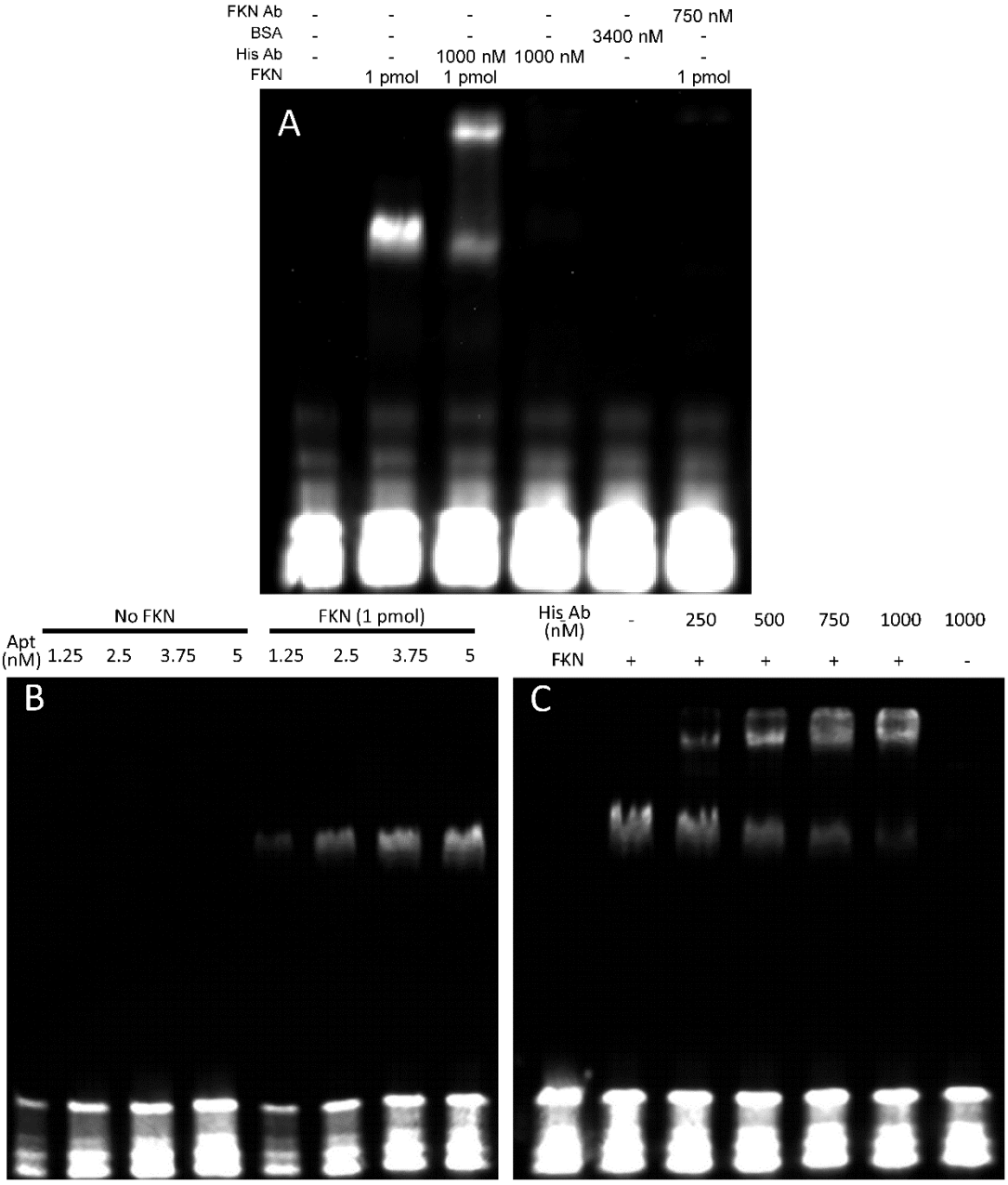

Figure 2.4: (A) Full image of Figure 2.3. EMSA analysis of the 12th SELEX round. Lane 1: Aptamer with no FKN. Lane 2: Aptamer with FKN. Lane 3: Addition of the His Ab causes a supershift. Lane 4: The aptamer does not bind the His Ab. Lane 5: The aptamer does not bind BSA. Lane 6: An anti-chemokine domain antibody blocks aptamer binding. All lanes have 5 nM aptamer concentration. (B) Increasing concentration of SELEX aptamer pool binding to fractalkine (FKN) (C) Supershift assay with increasing concentrations of an anti-polyhistidine antibody (His Ab) showing an increased supershift corresponding to the His Ab-fractalkine aptamer complex. The aptamer concentration was 5 nM with 1 pmol of FKN used in each lane.

The dissociation constant of FKN-S2 for fractalkine was determined using a radioactive homologous competition filter binding assay. Dilutions of unlabeled FKN-S2 aptamer were mixed with a constant concentration of ^{32}P ATP labeled FKN-S2. The dilutions were then incubated with 25 pM fractalkine for 1 hour at room temperature. The fractalkine concentration was iteratively decreased until it was approximately 100 times lower than the dissociation constant to prevent radioligand depletion effects. Bound aptamer was collected by filtration through a nitrocellulose membrane and the dissociation constant determined by non-linear regression analysis. The dissociation constant was determined to be 3.4 ± 0.7 nM based on the binding curve shown in Figure 2.5.

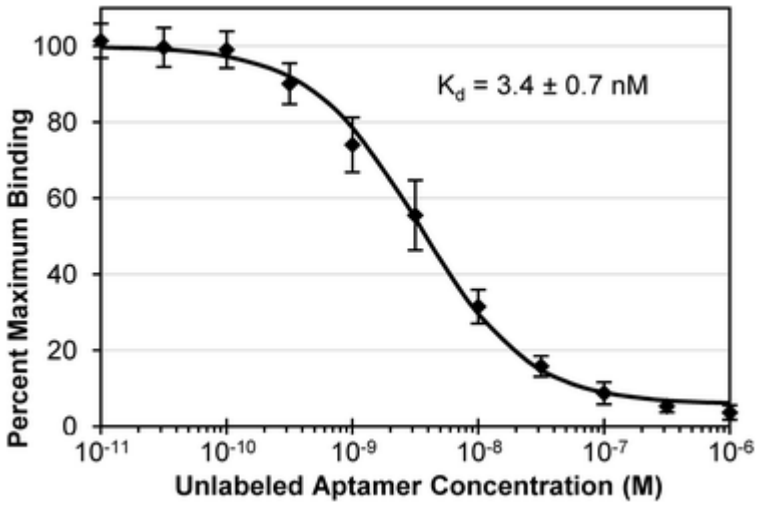

Figure 2.5: Homologous competition curve for FKN-S2. Labeled and unlabeled aptamer were incubated with 25 pM of fractalkine for 1 hour. Bound aptamer was collected by filtering through a nitrocellulose membrane. Results show the mean ± standard error from 9 independent experiments (n = 9) with each experiment performed in quadruplicate.

EMSA analysis of the aptamer pool demonstrated the aptamer bound the chemokine domain of fractalkine. However, the synthesized aptamer was significantly different from the aptamer pool due to the removal of the flanking primer sequences and because the aptamer pool contained several sequences. To ensure the aptamer was specific to fractalkine, an anti-fractalkine chemokine domain antibody (FKN Ab) was used to block aptamer binding to fractalkine. Three aptamer concentrations, with a constant labeled to unlabeled ratio, were incubated with fractalkine and fractalkine plus the antibody (Figure 2.6). Bound aptamer was collected on a nitrocellulose membrane. There was significant aptamer binding at all concentrations and the addition of the anti-chemokine domain antibody reduced binding to background levels. This demonstrates that the FKN-S2 aptamer binds directly to the chemokine domain as observed in the EMSA analysis. A similar experiment was done with a scrambled version of FKN-S2 and no binding was observed (Figure 2.7).

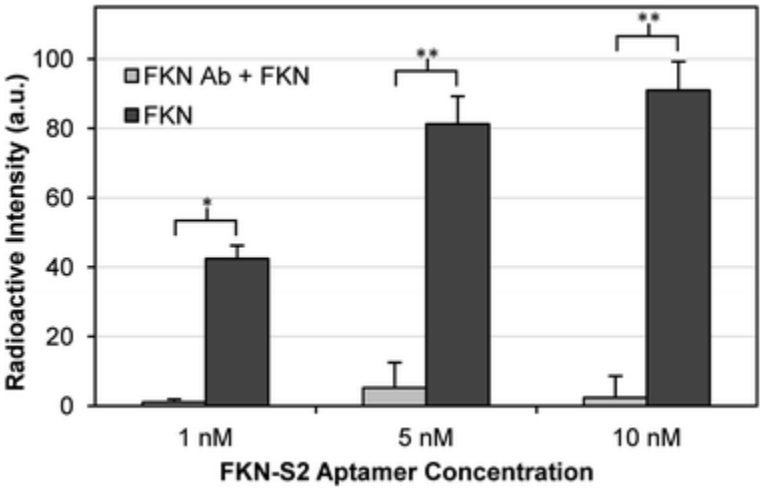

Figure 2.6: Anti-fractalkine antibody blocks binding of the FKN-S2 aptamer to fractalkine. 100 nM of antibody (FKN Ab) that is specific for the chemokine domain of fractalkine was allowed to bind for 30 minutes prior to aptamer addition. Results show the mean ± standard error from 4 independent experiments (n = 4). Two tailed t-test with unequal variances was used to determine significance, *p < 0.005, **p < 0.001.

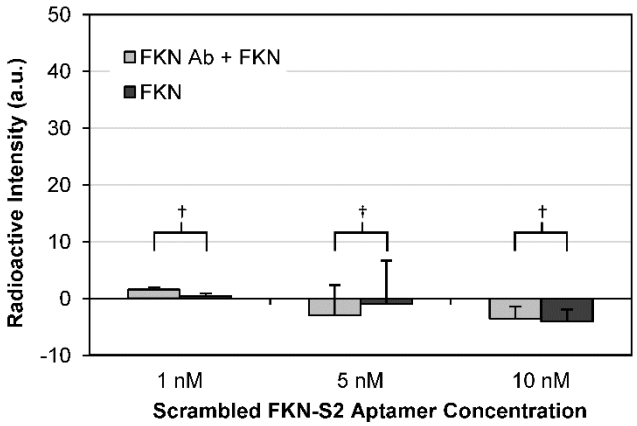

Figure 2.7: Anti-fractalkine antibody blocking of binding of the scrambled FKN-S2 aptamer to fractalkine. No binding was seen for the scrambled aptamer. 100 nM of antibody that is specific for the chemokine domain of fractalkine (FKN Ab) was allowed to bind for 30 minutes prior to aptamer addition. Results show the mean ± standard error from 4 independent experiments (n=4). Two tailed t-test with unequal variances was used to determine significance, † p > 0.01.

To further show specificity, FKN-S2 binding was tested against fractalkine, heat-denatured fractalkine and chemokines CCL8 and CXCL16. The results are shown in Figure 2.8. FKN-S2 binding to heat-denatured fractalkine was significantly reduced compared to native fractalkine while no binding was observed to either chemokines.

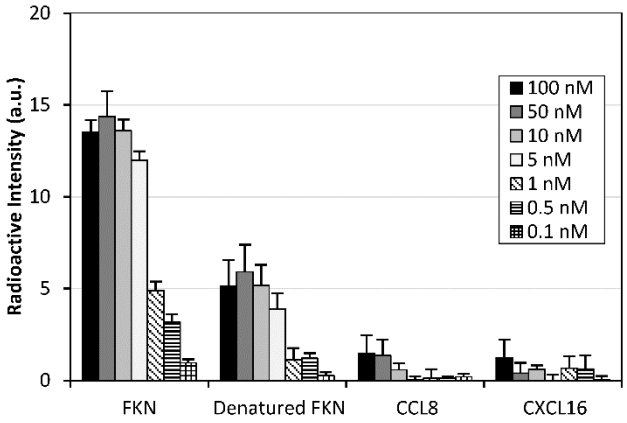

Figure 2.8: FKN-S2 binding to fractalkine, heat-denatured fractalkine, chemokine CCL8 and chemokine CXCL16. The aptamer and the protein (0.2 nM) were incubated for 1 hour at room temperature. Results show the mean ± standard error from five independent experiments (n = 5).

FKN-S2 contains 40 nucleotides and we investigated if truncation of the aptamer would result in sequences with similar affinity to fractalkine but with fewer nucleotides. Three truncated versions of the FKN-S2 aptamer were synthesized with five nucleotides removed from the 5′ end (FKN-S2a), five from the 3′ end (FKN-S2b) and five from each end (FKN-S2c). Additionally, a random 40-mer (5′-CTATCGGCGACATGAACTTTGGCAAGGGCATCTGGTCCAT-3′) was used as a control. The relative affinities of the truncated aptamers were tested using a heterogeneous competition assay with radiolabeled full length FKN-S2 (Figure 2.9). IC_{50} values (the

concentration of 50% reduction in binding) were determined by non-linear regression fitting of the data to the binding equation given in the methods section and the values are shown in Table 2.1.

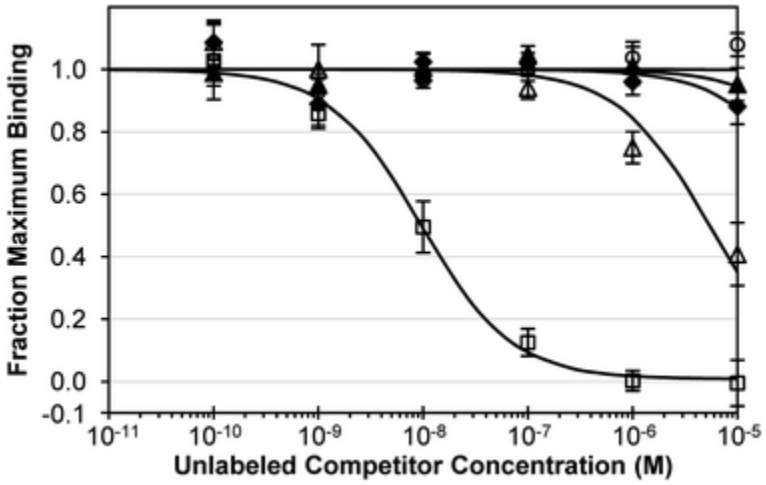

Figure 2.9: Competitive binding curves of truncated FKN-S2. Open square (□) FKN-S2; filled diamond (♦) FKN-S2a; open triangle (Δ) FKN-S2b; filled triangle (▲) FKN-S2c; open circle (○) random aptamer. Results show the mean ± standard error from 7 independent experiments (n = 7) with each experiment performed in duplicate.

Table 2.1: IC_{50} values of the truncated aptamers.

	FKN-S2	**FKN-S2a**	**FKN-S2b**	**FKN-S2c**	**Random**
IC_{50} (nM)	9.5	72 200	5410	>100 000	>100 000

Interestingly, removal of 5 nucleotides from the 5′ end (FKN-S2a) resulted in near complete loss of binding with an IC_{50} value of 72 200 nM. This suggests the 5′ end of the FKN-S2 aptamer is essential for binding. Removal from the 3′ end (FKN-S2b) similarly

gave a decrease although less drastic with an IC_{50} of 5410 nM. Sequence FKN-S2c and the random aptamer showed no binding both with IC_{50} values greater than 100 μM. The large reduction in affinity after removal of 5–10 nucleotides from the FKN-S2 sequence suggests the flanking nucleotides either participate directly in binding or are essential for stabilizing the aptamer structure. The ends may directly interact with fractalkine or may create the aptamer structure necessary for binding. Internal truncations were not investigated after observing the drastic reduction in affinity from end truncation.

We developed an aptamer via SELEX that binds with high affinity to fractalkine with a dissociation constant of 3.4 ± 0.7 nM. The aptamer was shown to be specific for the chemokine domain of fractalkine and truncation of the aptamer significantly reducing binding. This aptamer has many potential uses including as a therapeutic agent itself, as part of a targeted drug delivery system or as an investigative tool to manipulate fractalkine-CX3CR1 binding which has shown important in different diseases such as cancer, asthma and rheumatoid arthritis.

2.3 Materials and methods

2.3.1 Materials

Recombinant human fractalkine containing the chemokine domain, mucin-like stalk and a poly-histidine tag (FKN; Catalog Number 365-FR-025) and an anti-fractalkine chemokine domain antibody (FKN Ab; Catalog Number AF365) were obtained from R&D Systems (Minneapolis, MN). The anti-polyhistidine tag antibody was obtained from Millipore (His Ab; Billerica, MA, Catalog Number AB3517). The aptamer library and all primers were

obtained through Integrated DNA Technology, Inc. (Coralville, IA, USA). Ni-NTA Magnetic Agarose Beads (Catalog Number 36111) and Streptavidin MagneSphere Paramagnetic Particles (Catalog Number Z5481) were obtained from Qiagen (Valencia, CA) and Promega (Madison, WI) respectively. All PCR reagents, Hot-Start Taq DNA Polymerase (Catalog Number CB4040-1), 10x PCR buffer (Catalog Number CB3702-7) and dNTP master mix (Catalog Number CB4421- 4) were obtained from Denville Scientific (South Plainfield, NJ). The TOPO-TA cloning kit with one-shot chemically competent TOP10 E. *coli* cells (Product Number K4500-01) was obtained from Invitrogen (Carlsbad, CA). Chemokines CCL8 and CXCL16 were obtained from PeptroTech (Rocky Hill, NJ).

2.3.2 Selection of aptamers against fractalkine

The aptamer library, consisting of a 40-mer random region with flanking forward and reverse priming regions, WP-18 and WP-20 respectively, are shown below. Primer WP-20 contains a biotin tag on the 5' end to facilitate strand separation.

Aptamer Library: 5'-GTGCAGTCAAAGACGTCC-N40-GACCATGAAGTGCGATTGCC-3'

Primer WP-18: 5'-GTGCAGTCAAAGACGTCC - 3'

Primer Biotin WP-20: Biotin-5'-GGCAATCGCACTTCATGGTC -3'

The fractalkine was immobilized through a polyhistidine-Ni^{2+} interaction. Approximately 50 µL of Ni-NTA magnetic agarose beads were combined with 1 µg of fractalkine and incubating for 1 hour at room temperature on a rotisserie shaker. The beads were washed three times to remove un-immobilized fractalkine.

For the initial round of SELEX, 50 pmol of fractalkine was incubated with 500 pmol of aptamer library for 120 minutes on a rotisserie shaker at room temperature in selection buffer (phosphate buffered saline (PBS) with 10 mM imidazole and 0.005% (v/v) Tween-20, pH 7.4). The aptamer library was heat denatured and snap cooled in ice water to eliminate hybridization. Following incubation, the beads were quickly washed three times with selection buffer followed by three 5 minute washes. The aptamer-fractalkine complex was eluted by 2 additions of 50 µL of 250 mM imidazole in PBS. The aptamer pool was amplified using polymerase chain reaction (PCR) using 1 µM of primers WP-18 and WP-20, 800 µM total dNTP and 1.25 units of Taq per 50 µL reaction. Touchdown PCR was used to amplify the aptamer pool according to the following program: 5 minutes at 95°C, 10 cycles of 5 minutes at 95°C, 15 sec at 94°C, 15 sec at 72°C*, and 15 sec at 72°C with the * temperature decreased by 1°C per cycle, followed by 15 sec at 94°C, 15 sec at 62°C, and 15 sec at 72°C with an extension step of 1 minute at 72°C. The number of cycles used was adjusted depending on the SELEX round to prevent byproduct formation. The anti-sense strand was removed by denaturing the aptamer at 95°C for 5 minutes followed by snap cooling in ice water and incubation for 5 minutes on ice with Streptavidin MagneSphere Paramagnetic Particles. In subsequent rounds, the aptamer pool was reduced from 500 to 100 pmol while the fractalkine was reduced from 6 pmol to 1 pmol depending on the round to increase the stringency of selection. All binding occurred for 30 minutes at room temperature in selection buffer. SELEX was stopped after the 12th round when the PCR cycles needed for amplification of the aptamer leveled off between rounds 10 to 12 (Figure 2.2).

2.3.3 Domain targeted SELEX: Chemokine domain selection steps

Selection of chemokine domain aptamers was performed after rounds 2 and 5. Fractalkine was denatured by heating to 95°C for 10 minutes followed by snap cooling. The fractalkine was bound to Ni-NTA beads for 1 hour. The aptamer was added and incubated in selection buffer for 60 and 30 minutes at room temperature for counter selections following rounds 2 and 6 respectively. Unbound aptamer was collected and amplified by PCR.

2.3.4 EMSA analysis of aptamer pool

An electrophoretic mobility shift assay (EMSA) demonstrated binding of the aptamer pool to fractalkine. Asymmetric PCR was used to create biotinylated aptamer with the following reagent concentrations: DNA Polymerase (1.25 units per 50 µL reaction), 10x PCR buffer, dNTP (total dNTP concentration of 500 µM), Biotin-WP-18 (1 µM), WP-20 (0.01 µM), water (added to 50 µL) and SELEX round 12 aptamer template (0.1 pmol).

Varying concentrations of 5' biotinylated round 12 aptamer pool was incubated with 1 pmol of fractalkine for 30 minutes at room temperature in selection buffer. A similar procedure was used for the supershift assay. An anti-polyhistidine tag antibody, fractalkine and aptamer were incubated for 30 minutes at room temperature. For the chemokine blocking experiment, 15 pmol of anti-chemokine antibody was pre-incubated with fractalkine for 15 minutes prior to aptamer addition. After binding, the samples were run at 80V on a non-denaturing 6% polyacrylamide gel in 0.5x TBE buffer (45 mM Tris-Base, 45 mM Boric Acid, 1 mM EDTA). The samples were transferred to a nylon membrane (Pall Biodyne B) at 380 mA for 30 minutes and crosslinked by UV exposure. The membrane was developed using a LightShift Chemiluminescent EMSA Kit (Thermo Scientific; Product Number

20148) according to manufacturer's instructions.

Figure 2.3 from the main text is recreated in Figure 2.4-A to show the entire gel which shortened for space considerations. An electrophoretic mobility shift assay confirmed that the aptamer pool bound fractalkine in a dose dependent manner (Figure 2.4-B). In Figure 2.4-C an increasing concentration of an anti-polyhistidine tag antibody (His Ab) bound the polyhistidine tag of the recombinant fractalkine causing a supershift of the fractalkine-aptamer band. Increasing antibody concentrations intensified the supershift while decreasing the fractalkine aptamer band. No binding was observed in the His Ab control well indicating the aptamer does not bind the antibody.

2.3.5 Cloning and sequencing of aptamer pool

The aptamer pool was cloned into a TA vector (Invitrogen pCR2.1 Topo TA cloning kit) and heat shocked into chemically competent *E. coli* (One Shot TOP10 Chemically Competent *E. coli*; Invitrogen) according to the manufacturer's instructions. The transformed E. coli were plated onto LB agar plates with 50 µg/ml kanamycin and 40 mg/mL of X-gal and successfully transformed colonies were selected through blue/white screening. The sequencing region was amplified by colony PCR and amplicon size verified by agarose gel electrophoresis. ExoSAP-IT (Affymetrix, Inc.; Product Number 78201) was used to remove the excess primers. The clones were sequenced of the M13 Forward primer on an ABI 3730xl using ABI BigDye version 3.1 terminator chemistry by the University of Minnesota BioMedical Genomic Center sequencing facility. Aptamer candidates were aligned using MEGA 5 software.

2.3.6 FKN-S2 aptamer homologous competitive binding assay

FKN-S2 was labeled with γ-^{32}P ATP using a T4 polynucleotide kinase (PNK) (Roche Applied Science) according to the manufacturer's instructions. Briefly, 10 units of PNK were added to 25 pmol of aptamer in the supplied PNK buffer. The reaction proceeded for 45 minutes at 37°C and was stopped by the addition of 10 µL of a 0.5 M EDTA solution. Unincorporated γ-^{32}P ATP was removed using a Sephadex G-50 spin column.

The aptamer dissociation constant was measured using a homologous competitive binding assay. The aptamer concentration was quantified by UV absorbance measured using a Thermoscientific Nanodrop spectrophotometer and an extinction coefficient obtained from Integrated DNA Technology, Inc based on sequence composition.

All binding experiments occurred in binding buffer composed of PBS with 0.5 µg/mL poly dA:dT and 50 µg/mL bovine serum albumin (BSA), pH 7.4. Unlabeled full length FKN-S2 aptamer was diluted in binding buffer and a constant concentration of radiolabeled full length FKN-S2 aptamer added to each dilution. Full length fractalkine or an equivalent concentration of BSA was diluted in binding buffer to 50 pM. Aptamer and fractalkine/BSA was incubated for 1 hour at room temperature. Following incubation, samples were filtered through a nitrocellulose membrane using a bio-rad dot blot apparatus. Each well was washed 3 times with 200 µL of PBS to remove unbound aptamer. The membrane was dried and exposed to a storage phosphor screen overnight and imaged (Packard Cyclone). Binding was quantified using ImageJ and the Dot Blot Analyzer plug-in. The data was fit to the following equation $AB = AB_{MAX}\left(\frac{[A]}{[A]+[X]+K_d}\right) - b$ where AB is the

measured signal, AB_{Max} is the maximum signal, [X] is the concentration of unlabeled competitor, [A] is the hot aptamer concentration, b is the background binding, and K_d is the dissociation constant. Data was fit using non-linear regression analysis with the program Origin 8.

2.3.7 Truncated FKN-S2 aptamer competitive binding assay

Unlabeled aptamer was serially diluted from 10,000 nM to 0.1 nM in binding buffer (PBS with 0.1 µg/mL Poly (dA:dT) and 50 µg/mL BSA, pH 7.4). 1 nM of unlabeled FKN-S2 and 5,000 cpm/µL (counts per minute/µL) of radio-labeled full length FKN-S2 were heat denatured and snap cooled before addition to either fractalkine or a BSA control at a concentration of 0.1 nM and incubated for 1 hour at room temperature. The solutions were filtered through a nitrocellulose membrane and exposed to a storage phosphor film overnight and imaged. The binding was quantified using ImageJ and the Dot Blot Analyzer plug-in. Data was fit using the non-linear regression program Origin 8 to the equation $AB = AB_{MAX}\left(1 - \frac{[X]}{[X]+IC_{50}}\right)$ where AB is the measured signal, AB_{Max} is the maximum signal, [X] is the concentration of unlabeled competitor and IC_{50} is the competitor concentration at which the signal is reduced by 50%.

2.3.8 Anti-fractalkine antibody blocking assay

Unlabeled FKN-S2 and scrambled FKN-S2 aptamer (sequence 5'-GTTGGGATGAGGGTGGGCGGGCGCGGCGGCTGGGGGTCGG-3') were diluted to 10 nM in binding buffer (PBS with 50 µg/mL BSA and 2.5 µg/mL Poly (dA:dT); pH 7.4).

Approximately 75,000 cpm/well of radio-labeled aptamer was added and the samples were diluted to 5 and 1 nM. Each dilution was heat denatured and snap cooled. Full length fractalkine was diluted to 0.25 nM and approximately 100 nM of anti-chemokine domain antibody (FKN Ab) was added and allowed to bind for 30 minutes at room temperature. The aptamer was added to the protein solution and incubated at room temperature for 30 minutes. Bound aptamer was collected by filtering the samples thorough at nitrocellulose membrane and signal captured with a phosphor film and imaged. The background binding signal was removed from the FKN and FKN Ab + FKN samples by subtracting the signal from a well containing an identical concentration of BSA without FKN or FKN Ab. Binding was quantified using ImageJ. Results for the scrambled FKNS2 aptamer are shown in Figure 2.7.

2.3.9 FKN-S2 binding to heat-denatured fractalkine and chemokines CCL8 and CXCL16

A saturation binding experiment was performed examining the binding of FKN-S2 to heat-denatured fractalkine and chemokines CCL8 and CXCL16. CCL8 represents the CC family of chemokines while CXCL16 was chosen because it is structurally similar to fractalkine. CXCL16 contains a chemokine domain atop a mucin like stock which is anchored to the cell with a transmembrane domain. The membrane bound protein is cleaved to produce a soluble version of the protein. Membrane bound CXCL16 can also act as an adhesion molecule to certain T cell types. These similarities to fractalkine made it an excellent candidate to test FKN-S2 binding.

FKN-S2 was labeled with γ-32P ATP using a T4 polynucleotide kinase as described in the

FKN-S2 Aptamer Homologous Competitive Binding Assay section. Unlabeled FKN-S2 aptamer and 106 counts per minute of radiolabeled FKN-S2 aptamer were mixed in binding buffer (PBS with 50 µg/mL BSA and 2.5 µg/mL Poly (dA:dT); pH 7.4) and the aptamer was denatured at 95°C for 5 minutes followed by snap cooling in ice water for 5 minutes. The aptamer was then serial diluted in binding buffer and the dilutions added to full length fractalkine, heat-denatured fractalkine and chemokines CCL8 (PeproTech Catalog Number 300-15) and CXCL16 (PeproTech Catalog Number 300-55). All proteins were at a concentration of 0.2 nM. Fractalkine was denatured by heating to 95°C for 10 minutes followed by incubation on ice until use. The aptamer and protein were incubated for 1 hour at room temperature. Bound aptamer was collected by filtering the samples thorough at nitrocellulose membrane and signal captured with a phosphor film and imaged. The background was measured from wells containing an identical concentration of BSA without the protein. Binding was quantified using ImageJ. Results are shown in Figure 2.8. FKN-S2 did not bind to the chemokines CCL8 or CXCL16, however, some binding was seen to heat-denatured fractalkine. Heat-denaturing reduced binding by 2.5 fold at saturation. The binding that was seen may be due to incomplete denaturing or refolding of fractalkine during the experiment.

3 The effect of polyethylene glycol, alkyl, and oligonucleotide spacers on the binding, secondary structure and self-assembly of fractalkine binding FKN-S2 aptamer-amphiphiles

3.1 Introduction

The ability of antibodies to selectively bind a molecular target sparked a revolution in biotechnology leading to the creation of novel diagnostics, therapeutics, and imaging techniques.[3] Aptamers are short strands of nucleic acids that, like antibodies, bind molecular targets with high affinity and specificity. Positive characteristics of aptamers include *in vitro* selection, synthetic synthesis, reproducible and specific chemical modifications, and good chemical and thermal stability.[1, 7] Because of these advantages, aptamers are used for sensors and diagnostics,[9, 10] affinity separations,[11] and drug delivery and imaging applications.[6, 12, 15, 174]

Aptamers are often modified to reduce nuclease digestion,[12, 56] increase circulation lifetime,[175] increase association with cellular membranes,[176] induce micelle formation,[177] or functionalize liposomes.[178, 179] Commonly a polyethylene glycol (PEG) or an oligo-T (thymine) spacer is added to the aptamer, especially when attaching the aptamer to a surface.[180, 181] However, these modifications can affect the affinity of the aptamer for the target molecule through steric repulsion or alteration of the aptamer secondary structure.

Amphiphiles often form supramolecular structures.[182] Previous studies have shown that aptamer-amphiphiles can form micelles, which can be used for drug delivery or bottom up

assembly.[14, 183] Nucleic acid amphiphiles with a single nucleoside as the headgroup and a 12 carbon dialkyl tail self-assembled into cylindrical micelles and helical ribbons.[184] However, the single nucleoside headgroup lacked ligand-receptor binding capabilities. Recent work by our group has shown that aptamer-amphiphiles with a 25 nucleic acid aptamer headgroup (that binds to Muc-1 glycoprotein) and C_{16} dialkyl tails (similar to the ones used in this study) self-assembled into micelles when the amphiphile did not contain a spacer (NoSPR) or when a hydrophilic PEG_4 or PEG_8 spacers were used, but self-assembled into micelles and nanotapes, flat or twisted, when the hydrophobic C_{12} or C_{24} spacers were used.[185] The nanotapes, the presence of which could not be predicted by the standard packing parameter analysis, were bilayer structures with the hydrocarbon tails and spacers forming the hydrophobic core and the aptamer headgroups extending away from the hydrophobic interfaces.[185] We hypothesized that the hydrophobic tails and poly-carbon spacers, through attractive hydrophobic interactions, forced the aptamer headgroups together reducing the interfacial headgroup area and thereby allowing nanotape formation.

Previously, we developed the FKN-S2 aptamer that binds to the cell surface protein fractalkine (CX3CL1) with a dissociation constant (K_d) of 3.4 ± 0.7 nM.[170] Fractalkine is a chemokine involved in inflammation pathways through the recruitment and adhesion of leukocytes[95, 171, 186] and is expressed on inflamed endothelial cells and certain cancers.[126, 127, 132, 135] In this work we investigated the effects of the tail and spacer on the affinity, secondary structure and self-assembly of FKN-S2 amphiphiles. The 40-mer FKN-S2 aptamer (sequence shown in Figure 3.1A) was synthesized with a 6 carbon (C_6) amino linker added to either the 5' or 3' end of the aptamer. Tails with different spacers (a subset

of which are shown in Figure 3.1B) were then conjugated to the C_6 linker creating the aptamer-amphiphile (Figure 3.1C). The effect of the tail and different spacers on the aptamer-amphiphile binding affinity for fractalkine was measured using a competition binding assay. The aptamer and aptamer-amphiphile secondary structure were probed with circular dichroism (CD) spectroscopy and thermal melting analysis to investigate the effect of the tail on secondary structure. Cryogenic transmission electron microscopy (cryo-TEM) was used to visualize the self-assembled structures of the FKN-S2 aptamer-amphiphiles and a 40-mer oligonucleotide with a similar secondary structure. Finally, considering that the FKN-S2 aptamer can be used to functionalize nanoparticles targeted to fractalkine expressing cells, liposomes were functionalized with a FKN-S2 amphiphile and targeted to fractalkine expressing cells as a targeted drug delivery proof of concept.

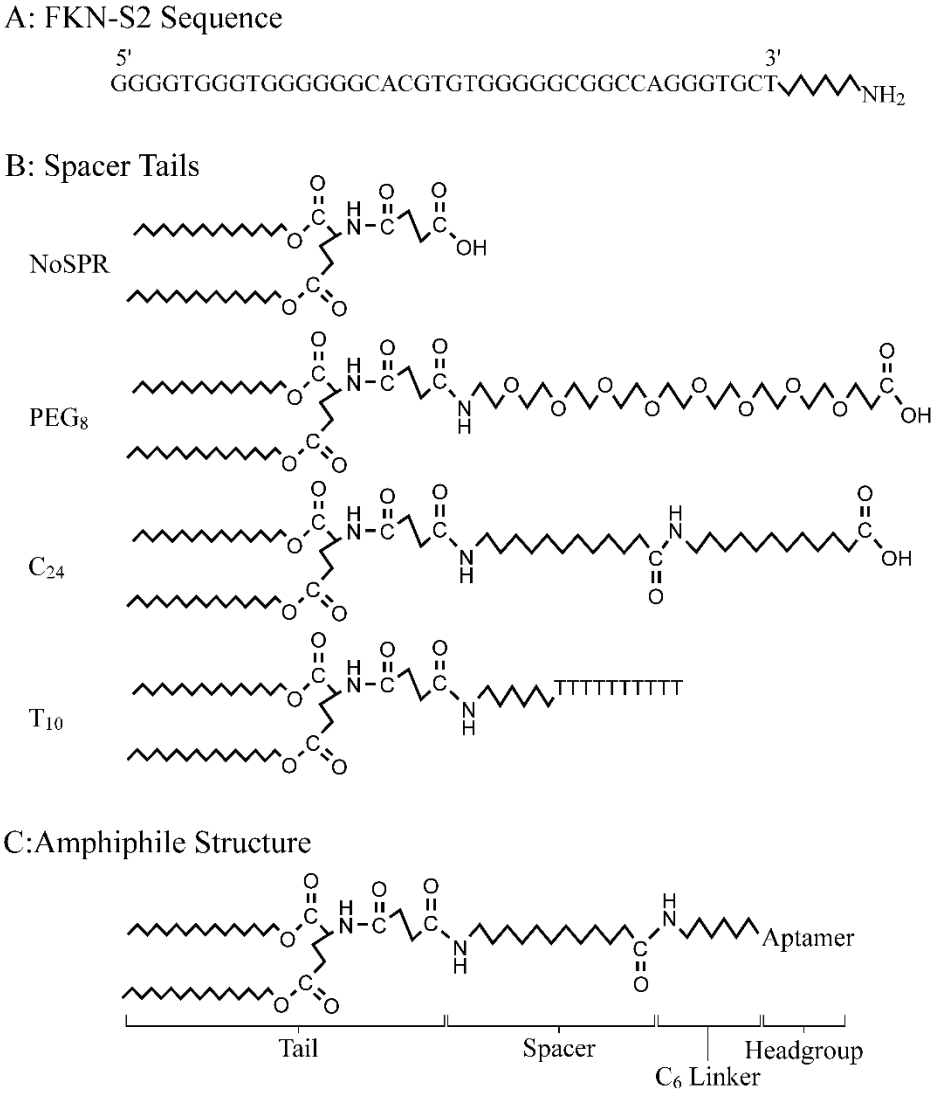

Figure 3.1: (A) The sequence of the FKN-S2 aptamer with the 3' C_6 linker, (B) structures of the tail, a saturated dialkyl C_{16} lipid like molecule, with a subset of the different spacers: NoSPR (no spacer was used), PEG_8, C_{24} and T_{10}, and (C) structure of the aptamer-amphiphile with a C_{12} spacer. The aptamer was purchased with a six carbon amino linker (C_6 Linker) on either the 5' or 3' end to which the tail was conjugated.

3.2 Materials and methods

3.2.1 Materials

All aptamers were synthesized by Integrated DNA Technologies (Coralville, IA, USA). Full length fractalkine (Product No. AF365) was purchased from R&D Systems (Minneapolis, MN). Whatman Protran nitrocellulose membrane (Product No. NBA085A) was used for the radioactive competition binding assays. The PEG spacer precursors $CA(PEG)_4$ (Product No. 26120), $CA(PEG)_8$ (Product No. 26122), and $CA(PEG)_{24}$ (Product No. 26125) were purchased from Thermo Fischer Scientific (Rockford, IL, USA). The alkyl spacers were synthesized from 12-aminododecanoic acid obtained from Sigma-Aldrich (St. Louis, MO, USA). The γ-^{32}P adenosine triphosphate (ATP) was purchased from PerkinElmer (Waltham, MA, USA) and the T4 polynucleotide kinase was purchased from Roche Applied Science (Indianapolis, IN, USA). All other solvents and reagents were purchased from Sigma Aldrich. The phosphate buffered saline (PBS) buffer was composed of 136.9 mM sodium chloride, 2.68 mM potassium chloride, 8.1 mM sodium hydrogen phosphate, and 1.76 mM potassium dihydrogen phosphate.

3.2.2 Synthesis of spacer-tails

The tails were synthesized as described previously.[187] Briefly, two cetyl alcohols were conjugated to the carboxyl groups of a L-glutamic acid through ester linkages. A succinic acid linker was reacted to the glutamic acid amino group by an amide bond.

The heterobifunctional carboxy-amine spacers PEG_4, PEG_8, PEG_{24}, and C_{12} were purchased from suppliers. The oligonucleotide spacers were added during aptamer

synthesis. The spacers were added to the carboxyl group of the succinic acid linker using the N-hydroxysuccinimide (NHS) chemistry as described previously.[185] Briefly, the tails were dissolved in ethyl acetate and N,N-dicyclocarbodiimide (DCC, 2x molar excess) and NHS (2x molar excess) were added and reacted overnight at 50 °C. The insoluble byproduct dicyclohexylurea was removed by filtration. The NHS-tails were precipitated twice in ethyl acetate and the product molecular weight verified using mass spectrometry. The NHS-tails were then reacted with excess spacer in dichloromethane for 24 hr at 50 °C. The primary amine of the heterobifunctional spacer reacted with the NHS ester of the tails forming an amide bond. The spacer tails were stored at -20 °C. The C_{24} tails were made by reacting C_{12}-tails with 12-aminododecanoic acid using the same procedure.

3.2.3 Aptamer quantification

All aptamer and aptamer-amphiphile concentrations were measured by absorbance at 260 nm. The aptamer was diluted to approximately 2.5-5.0 μM in TE buffer (10 mM Tris Base, 1 mM EDTA, pH 8.0) and the absorbance measured at 260 nm using either a Thermo Scientific Nanodrop instrument or a BioTek Synergy H1 microplate reader equipped with a take3 plate. The aptamer extinction coefficients were found using the Integrated DNA Technology OligoAnalyzer 3.1 software.

3.2.4 Synthesis of aptamer-amphiphiles

The FKN-S2 aptamer was purchased from Integrated DNA Technology with an amino-C_6 linker attached to either the 3’ or 5’ end of the aptamer. The FKN-S2 sequence is 5’-GGGGTGGGTGGGGGGCACGTGTGGGGGCGGCCAGGGTGCT-C_6 linker-3’ A 1.5x

molar excess of cetyltrimethylammonium bromide (CTAB) (excess based on the number of phosphates on the aptamer backbone) was added to the aptamer forming a CTAB-aptamer precipitate. The precipitate was collected and dried under vacuum. The CTAB-aptamer was dissolved in 1:9 volume mixture of dimethyl sulfoxide (DMSO) and N,N-dimethylformamide (DMF) and heated to 80 °C to dissolve the CTAB-aptamer. A 5x excess of NHS-tails was added and reacted at 65 °C for 24 hr. Fresh tails were added and reacted for an additional 12 hr. The DMSO and DMF was removed by evaporation. The CTAB-aptamer was dissolved in 825 µL of ethanol. 30 µL of 3 M sodium acetate and 300 µL of water were added to displace the CTAB and precipitate the aptamer. The precipitate was collected, dissolved in 300 µL of water and precipitated with sodium acetate and ethanol. The aptamer was purified by reverse phase HPLC on an Agilent Zorbax C-18 reverse phase column (4.6 x 150 mm). The mobile phase buffers were 10% methanol and 90% water (v/v) (Buffer A) and 100% methanol (Buffer B). Both buffers contained 100 mM hexafluoro-2-propanol and 14.5 mM triethylamine. The sample was separated using a linear gradient from 100% Buffer A to 100% Buffer B over 20 min at 1 mL/min. The aptamer-amphiphile peak was collected, dried, and precipitated twice with sodium acetate and ethanol. The molecular weight was verified by LC-MS. The final product was dissolved in TE buffer and stored at -20 °C.

3.2.5 Radioactive competition binding assay

FKN-S2 aptamer was radiolabeled with γ-32P ATP using a T4 polynucleotide kinase (PNK) (Roche Applied Science; Penzberg, Germany) as described previously.[170] Varying concentrations of the aptamer-amphiphile were mixed with approximately 50,000 counts per min (CPM) of radiolabeled FKN-S2, and 1 nM unlabeled FKN-S2 in binding buffer

(PBS with 50 μg/mL bovine serum albumin (BSA) and 0.1 μg/mL of poly(dA:dT), pH = 7.4). The aptamer mixture was heated to 90-95 °C in a water bath for 5 min and snap cooled in ice water to reform the aptamer into a binding conformation. The aptamer mixture was then added to fractalkine (0.1 nM final concentration) that was free in solution and incubated at room temperature for 1 hr in a 96 well plate. Following incubation, the fractalkine-aptamer solution was filtered through a nitrocellulose membrane using a dot blot vacuum apparatus. The membrane was washed three times with PBS to remove unbound aptamer, dried, and the radioactivity measured using phosphor screen (Packard Cyclone; Downers Grove, IL). Binding was quantified using ImageJ and the Dot Blot Analyzer plug-in. Non-linear regression was used to fit the data to the equation $RadAct = RadAct_{Max}\left(1 - \frac{[X]}{[X]+IC_{50}}\right)$ where RadAct is the measured radioactivity, $RadAct_{Max}$ is the radioactivity at zero competitor concentration, [X] is the competitor concentration, and IC_{50} is the competitor concentration that results in a 50% radioactivity reduction. Statistical significance was determined using a two tailed Student's t-test with unequal variances.

3.2.6 Measurement of critical micelle concentration

The critical micelle concentration (CMC) was measured using Nile red fluorescence.[188, 189] A stock solution of 1 mg/mL of Nile red (Sigma-Aldrich; microscopy grade) dissolved in acetone was diluted to 0.04 mg/mL in deionized (DI) water. 50 μL of the diluted dye was added to 50 μL of varying concentrations of aptamer-amphiphile in DI water (from 0 to 2000 nM final concentration) for 1 hr at room temperature. The fluorescent intensity was measured using a BioTek Synergy H1 microplate reader at an emission/excitation of 540/635 nm.

3.2.7 Circular dichroism spectroscopy

All CD spectroscopy spectra were measured using a Jasco J-815 CD spectrophotometer (Biophysical Spectroscopy Center at the University of Minnesota). The aptamer was precipitated using sodium acetate and ethanol and washed with 70% ethanol to remove residual salts. The aptamer was dissolved in DI water, 20 mM potassium chloride, or PBS buffer. The aptamer was heated in a 95 °C heating block for 5 min and rapidly cooled to room temperature prior to measurement. All spectra were taken within 1 hr. The CD spectrum was measured at 22 °C in a 1.0 cm quartz cuvette and the background buffer signal was subtracted.

3.2.8 Circular dichroism melting curves

The aptamer was dissolved in PBS and degassed under vacuum for 10 min. The sample was sealed in a quartz cuvette using a glass cover slip and silicone sealant to prevent evaporation. The melting curves were measured using a Jasco J-815 CD spectrophotometer (Biophysical Spectroscopy Center at the University of Minnesota) with a 6 cell Peltier heater. The samples were held at 95 °C for 10 min to fully denature the aptamer and then cooled from 95 °C to 25 °C and heated from 25 °C to 95 °C at 0.25 °C/min. No hysteresis was seen using this temperature gradient. The sample temperature was monitored using a thermocouple inserted into a buffer filled cuvette. CD absorption was measured every 1 °C at 265 and 285 nm. The melting temperature and thermodynamic parameters were determined assuming a two state model as described elsewhere.[190]

3.2.9 Cryogenic transmission electron microscopy

4.5 µL of 100-500 µM amphiphile samples were deposited onto lacey formvar/carbon copper grids that were treated for 30 sec with glow discharge to make the grids more hydrophilic. The samples were then vitrified in liquid ethane using a Vitrobot cryo-plunger (Vitrobot parameters: 5 sec blot time, -1 offset, 3 sec wait time, 3 sec relax time, 95 % humidity). Following vitrification, grids was transferred to a Tecnai G2 Spirit TWIN 20-120 kV / LaB6 Transmission Electron Microscope and imaged at using an accelerating voltage of 120 kV and an Eagle 2k CCD camera.

3.2.10 Aptamer functionalized liposome binding to MCA-38.FKN cells

The liposomes were prepared by the thin film hydration and extrusion method described elsewhere.[191] Dipalmitoylphosphatidylcholine (DPPC), cholesterol, and dipalmitoylphosphatidylethanolamine PEG2000 (DPPE-PEG2000), (purchased from Avanti Polar Lipids, Alabaster, AL) were dissolved in chloroform and mixed in a round bottom flask in a 60:35:5 molar ratio of DPPC:cholesterol:DPPE-PEG2000. The mixture was heated to 60 °C and dried into a thin film under a stream of argon. The lipids were placed under vacuum overnight to remove residual chloroform. The lipid film was hydrated with TBSE buffer with 2 mM calcein (10 mM Tris Base, 150 mM NaCl, 1 mM EDTA, 2 mM calcein pH 7.4) at a 40 mM lipid concentration and heated at 60 °C for 15 min. The liposomes were collected and freeze-thawed 5 times with liquid nitrogen and a 60 °C waterbath. Following the freeze thaw, the liposomes were extruded 21 times though a 100 nm membrane (LiposoFast extruder, Avestin, Ottawa, ON, Canada). The unincorporated calcein dye was removed through dialysis with a 50,000 MWCO dialysis membrane. A phosphorus assay was used to measure the lipid concentration of the liposomes as

described elsewhere.[192] The liposomes were functionalized with the 3' T_{10}-FKN-S2 amphiphile by the post insertion method. The liposomes (7.5 mM of lipids) and amphiphile (concentration varied from 0-50 μM) were incubated for 8 hr at 45 °C. Unincorporated aptamer-amphiphile was removed by a sepharose CL-4B gel filtration column. The aptamer-amphiphile concentration was measured after purification by first precipitating the aptamer-amphiphile with an ethanol precipitation and then measuring the absorbance at 260 nm. Mouse colon adenocarcinoma MCA-38 cells (donated by Professor Lance Augustin, University of Minnesota) were transfected with a pCAGG-Neo-fractalkine plasmid (provided by Professor Alan Fong, University of North Carolina-Chapel Hill) using X-tremeGENE 9 transfection reagent to express fractalkine. Two days after transfection the cells were cultured with media containing 500 μg/mL G418. Drug-resistance clones were picked and expanded to create a MCA-38.FKN cell line, with FKN expression confirmed after 4 weeks. The cells were grown in a T-75 tissue culture flask and maintained at 37 °C in a 5% CO_2 atmosphere. The cell media (DMEM: Life Technologies, Carlsbad, CA) was replaced every 2 days and the cells split once they reached 90% confluency. Prior to the binding experiment, the cells were seeded into a 12 well plate at $5x10^5$ cells per well and allowed to adhere for 24 hr. The liposomes added to the wells at 200 μM total lipids in PBS buffer with 0.91 mM $CaCl_2$ and 0.49 mM $MgCl_2$ and incubated at 37 °C for 1 hr. Following incubation, the cells were washed three times and lysed by the addition of 0.5 mL of 5% Triton-X100 in TBSE buffer. Cell debris was removed by centrifugation and the fluorescence was quantified using a fluorescent plate reader (Biotek Synergy H1, Winooski, VT) at excitation/emission of 490/520 nm.

3.3 Results and discussion

3.3.1 Radioactive competition binding assay

To create the aptamer-amphiphile the aptamer headgroup must be conjugated to a hydrophobic tail either directly or via a spacer. We first evaluated the effect of conjugating a hydrophobic tail directly to the aptamer (no spacer was used; NoSPR) on its binding affinity for fractalkine. The C_{16} dialkyl tail was conjugated at either the 3' or 5' end of the aptamer and the amphiphile's binding affinity for fractalkine was measured by a radioactive competition binding assay. In this assay, a varying concentration of an unlabeled competitor molecule, either aptamer or aptamer-amphiphile, was added to a constant concentration of free ^{32}P radiolabeled FKN-S2 aptamer. At high concentrations the unlabeled competitor outcompetes the radiolabeled FKN-S2 aptamer for fractalkine binding sites reducing the measured radioactivity; at low competitor concentrations, the radiolabeled FKN-S2 aptamer primarily binds to fractalkine increasing the measured radioactivity. The IC_{50} is defined as the concentration at which both FKN-S2 and the competitor bind equally and quantifies the relative affinity between the FKN-S2 aptamer and the competitor molecule.

The IC_{50} binding curves for the 3'-NoSPR-FKN-S2 (NoSPR tail conjugated to the 3' end of the aptamer) and 5'-NoSPR-FKN-S2 (NoSPR tail conjugated to the 5' end of the aptamer) amphiphiles are shown in Figure 3.2 and their IC_{50} values are given in Table 3.1. The binding curve of the free FKN-S2 aptamer is shown in black for comparison. Amphiphiles with an IC_{50} greater than that of the free FKN-S2 aptamer have lower affinity for fractalkine than the free aptamer and vice versa.

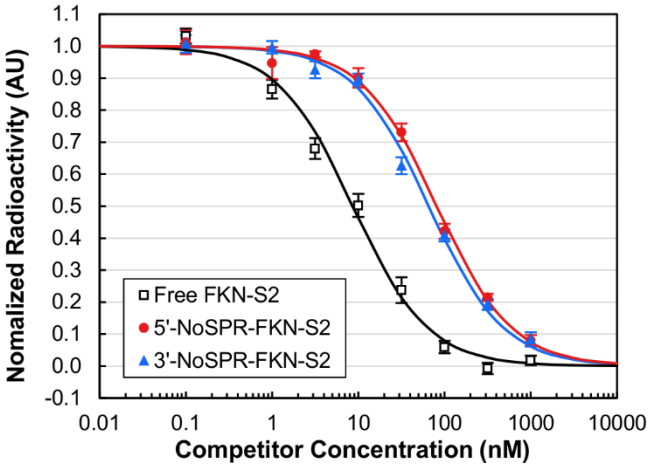

Figure 3.2: IC_{50} competition binding curves of the free FKN-S2 aptamer and FKN-S2 aptamer-amphiphiles where the tail was conjugated either at the 3' or 5' end of the aptamer in the absence of any spacer (NoSPR). The data show the mean ± standard error of the mean (SEM) of at least 6 independent experiments ($n \geq 6$) with a single repetition per experiment.

Addition of the tail significantly reduced the affinity for fractalkine and the affinity reduction was orientation specific as shown in Table 3.1. The 3'-NoSPR-FKN-S2 amphiphile (IC_{50} of 65.7 ± 3.5 nM) had a higher affinity than the 5'-NoSPR-FKN-S2 amphiphile (IC_{50} of 81.6 ± 6.6 nM) ($p < 0.05$), but both orientations had lower affinity than the free FKN-S2 aptamer (IC_{50} of 8.64 ± 0.28 nM). Future aptamer-amphiphiles were synthesized by conjugating the tails and spacers at the 3' end of the aptamer since this aptamer orientation resulted in higher binding affinity-amphiphiles.

Table 3.1: IC_{50} values of the FKN-S2 aptamer and aptamer-amphiphiles. The affinities of the amphiphiles for fractalkine were measured by competitive binding assays. The lower the IC_{50} value, the higher the binding affinity of that molecule for fractalkine. IC_{50} values are reported as the mean ± SEM (n = 3-9). p-values from the Student's t-test analysis of the IC_{50} data can be found in Table 3.2.

Sample	IC_{50} ± SEM (nM)
FKN-S2 Aptamer	8.64 ± 0.28
3' No Spr FKN-S2 Amphiphile	65.7 ± 3.5
5' No Spr FKN-S2 Amphiphile	81.6 ± 6.6
3' PEG4 FKN-S2 Amphiphile	68.6 ± 7.1
3' PEG8 FKN-S2 Amphiphile	47.5 ± 6.1
3' PEG24 FKN-S2 Amphiphile	49.6 ± 6.1
3' C12 FKN-S2 Amphiphile	75.6 ± 5.6
3' C24 FKN-S2 Amphiphile	73.5 ± 5.6
3' 10T FKN-S2 Amphiphile	21.8 ± 2.0
3' 5T FKN-S2 Amphiphile	37.6 ± 0.6
5' 10T FKN-S2 Amphiphile	55.1 ± 4.9
3' 10A FKN-S2 Amphiphile	24.8 ± 2.0

Next, the effect of different spacers on the binding affinity of the aptamer-amphiphiles for fractalkine was tested. The amphiphiles were synthesized with either PEG, alkyl (poly-carbon), or oligo thymine (oligo-T) spacers. Each spacer has different characteristics. The PEG spacer is hydrophilic and flexible, the poly-C spacer is hydrophobic, and the oligo-T spacer is negatively charged, flexible, and hydrophilic. The PEG_8 (8 PEG repeats), C_{24} (24 carbons long) and T_{10} (10 thymine nucleic acids) spacers have roughly identical lengths. Likewise, the PEG_4, C_{12} and T_5 spacers have approximately similar lengths. The binding curves of the 3'-NoSPR, 3'-PEG_8, 3'-C_{24}, and 3'-T_{10} FKN-S2 amphiphiles are shown in Figure 3.3A with the IC_{50} values shown in Table 3.1 (p-values from the Student's t-test analysis of the IC_{50} data are given in Table 3.2). The 3'-NoSPR and 3'-C_{24} spacers had similar IC_{50} values of 65.7 ± 3.5 nM and 73.5 ± 5.6 nM respectively ($p > 0.05$). The 3'-PEG_8 amphiphile (IC_{50} of 47.5 ± 6.1 nM) showed improved affinity compared to the 3'-

NoSPR amphiphile ($p < 0.05$). The best amphiphile was clearly the 3'-T_{10} (IC_{50} of 21.8 ± 2.0 nM; $p < 0.001$ with respect to 3'-NoSPR).

Table 3.2: IC_{50} p-values from the Student's t-test analysis for the FKN-S2 aptamer and aptamer amphiphile binding experiments with fractalkine. The IC_{50} values are shown in Table 3.1 (n = 3-9).

Amphiphiles											Aptamer			
3'-NoSPR	5'-NoSPR	3'-PEG_4	3'-PEG_8	3'-PEG_{24}	3'-C_{12}	3'-C_{24}	3'-T_{10}	3'-T_5	5'-T_{10}	3'-A_{10}	3'-T_5	3'-T_{10}		
< 0.001	< 0.001	< 0.001	< 0.001	< 0.01	< 0.001	< 0.001	< 0.001	< 0.001	< 0.05	< 0.001	< 0.001	< 0.001	Free FKN-S2	Aptamer
	< 0.05	> 0.3	< 0.05	> 0.05	> 0.05	> 0.1	< 0.001	< 0.001	> 0.1	< 0.001	< 0.001	< 0.001	3'-NoSPR	
		> 0.1	< 0.01	< 0.01	> 0.3	> 0.3	< 0.001	< 0.01	< 0.05	< 0.001	< 0.001	< 0.001	5'-NoSPR	
			< 0.05	> 0.05	> 0.3	> 0.3	< 0.001	< 0.01	> 0.1	< 0.001	< 0.001	< 0.001	3'-PEG4	
				> 0.3	< 0.01	< 0.01	< 0.01	> 0.1	> 0.3	< 0.01	< 0.001	< 0.001	3'-PEG8	
					< 0.05	< 0.05	< 0.01	> 0.1	> 0.3	< 0.01	< 0.001	< 0.001	3'-PEG24	
						> 0.3	< 0.001	< 0.001	< 0.05	< 0.001	< 0.001	< 0.001	3'-C12	Amphiphile
							< 0.001	< 0.01	< 0.05	< 0.001	< 0.001	< 0.001	3'-C24	
								< 0.001	< 0.05	> 0.3	< 0.001	< 0.001	3'-T10	
									> 0.05	< 0.001	< 0.001	< 0.001	3'-T5	
										< 0.05	< 0.01	< 0.01	5'-T10	
											< 0.001	< 0.001	3'-A10	
												> 0.3	3'-T5	Aptamer

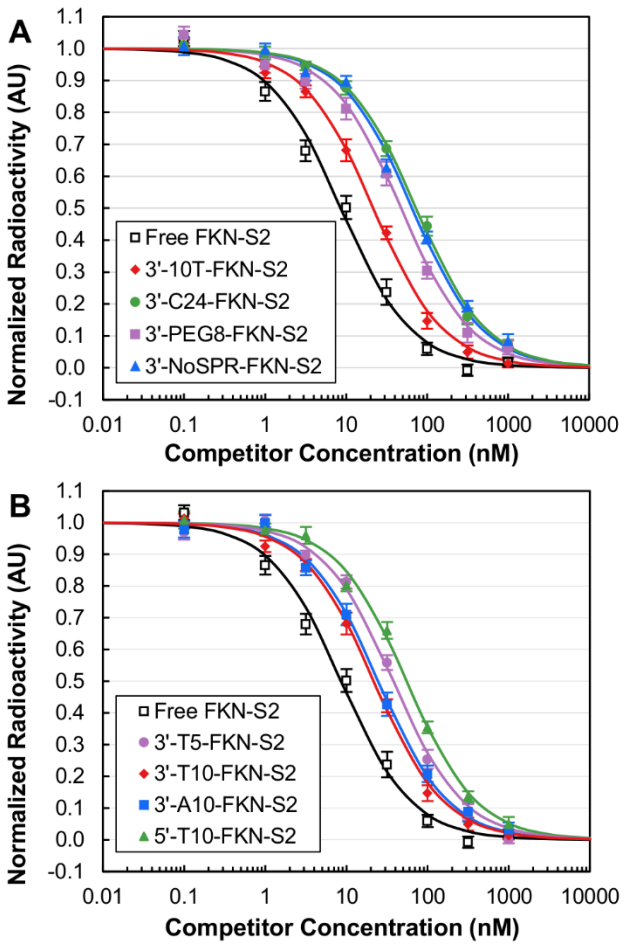

Figure 3.3: (A) IC_{50} binding curves of the free FKN-S2 aptamer and 3'-FKN-S2-amphiphiles with T_{10}, PEG_8, NoSPR and C_{24} spacers. (B) IC_{50} binding curves of the free FKN-S2 aptamer and 3'-FKN-S2-amphiphiles with T_{10}, T_5 and A_{10} spacers and 5'-T_{10}-FKN-S2 amphiphile. Data are shown as the mean ± SEM of at least 6 independent experiments ($n \geq 6$).

The spacer length had a limited effect on the affinity of some amphiphiles (binding curves are shown in Figure 3.4, the IC_{50} values are given in Table 3.1 and the p-values from the Student's t-test analysis of the IC_{50} data are given in Table 3.2). There was no difference between the C_{12} and C_{24} carbon spacers ($p > 0.05$). The affinity of the amphiphile improved from the 3'-PEG_4 amphiphile, IC_{50} of 68.6 ± 7.1 nM, to the 3'-PEG_8 amphiphile, 47.5 ± 6.1

nM, ($p < 0.05$), but there was no difference between the PEG_8 and the PEG_{24} amphiphiles, 49.6 ± 6.1 nM ($p > 0.05$). Longer oligo-T spacers seemed to improve the binding affinity of the amphiphiles for fractalkine. The 3'-T_5 amphiphile had an IC_{50} of 37.6 ± 0.6 nM and the 3'-T_{10} amphiphile had an IC_{50} of 21.8 ± 2.0 nM ($p < 0.001$).

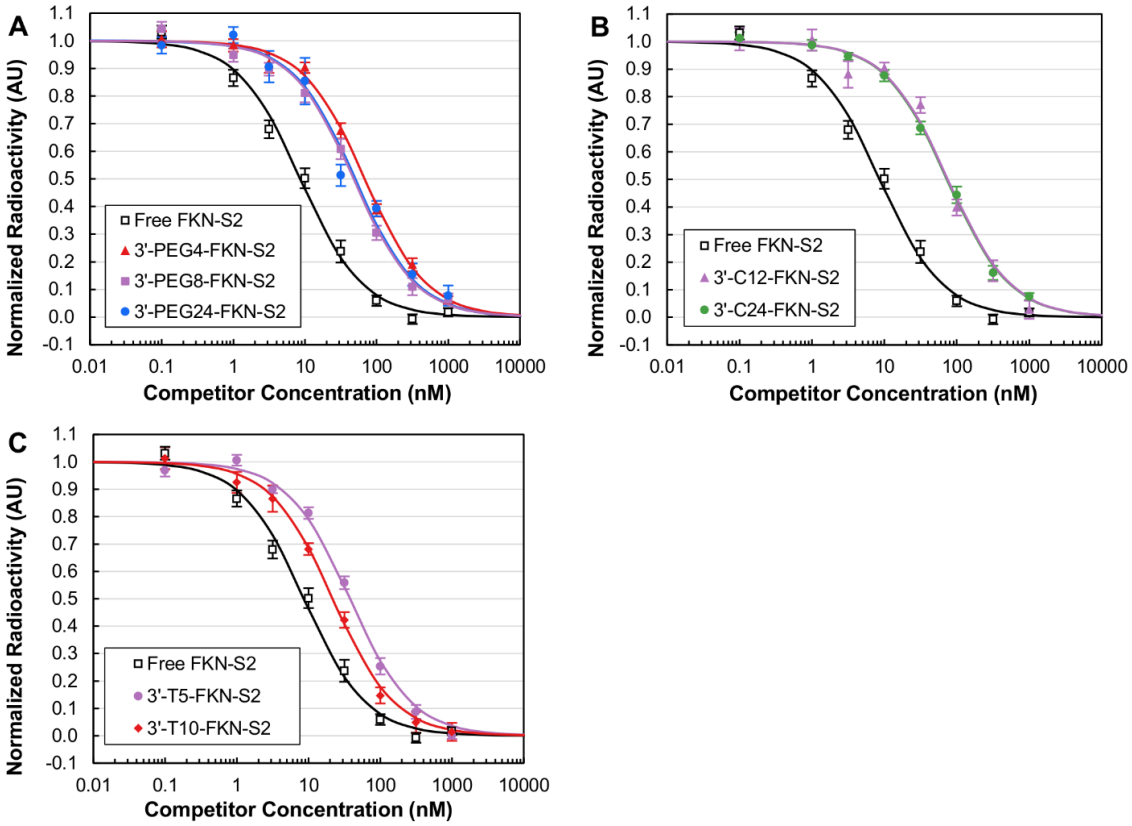

Figure 3.4: IC_{50} binding curves for the (A) PEG spacer amphiphiles, (B) Carbon spacer amphiphiles, and (C) Poly-T spacer amphiphiles. The data show the mean ± SEM (n = 3 - 9).

Because the 3'-T_{10}-FKN-S2 amphiphile was significantly better than the other amphiphiles, we tested the oligonucleotide derivatives 3'-T_5-, 5'-T_{10}-, and 3'-A_{10}-FKN-S2 amphiphiles.

The 3'-T_5-FKN-S2 amphiphile tested the effect of the oligonucleotide length, the 5'-T_{10}-FKN-S2 tested the effect of the aptamer orientation and the 3'-A_{10}-FKN-S2 amphiphile tested the effect of the oligonucleotide spacer composition. The binding curves are shown in Figure 3.3B. The 5'-T_{10}-FKN-S2 amphiphile (IC_{50} of 55.1 ± 4.9 nM) performed significantly worse ($p < 0.05$) than the 3'-T_{10}-FKN-S2 amphiphile (IC_{50} of 21.8 ± 2.0 nM). This is consistent with the preferred 3' aptamer orientation observed when the aptamer was conjugated directly to the tail in the absence of any spacer (3'-NoSPR-FKN-S2 amphiphile shown in Figure 3.3A). Reducing the oligo-T spacer from 10 to 5 nucleotides significantly reduced the amphiphile affinity. The IC_{50} value was 21.8 ± 2.0 nM for the 3'-T_{10}-FKN-S2 amphiphile versus 37.6 ± 0.6 nM for 3'-T_5-FKN-S2 ($p < 0.001$). The PEG and oligo-T IC_{50} data suggest that for short spacers, like PEG_4 and T_5, increasing spacer length increases affinity, but for spacers longer than the PEG_8 no additional gains in affinity were observed. The 3'-A_{10}-FKN-S2 amphiphile, IC_{50} of 24.8 ± 2.0 nM, performed equally well as the 3'-T_{10}-FKN-S2 amphiphile ($p > 0.05$) suggesting that the nucleotide composition does not affect the affinity.

The oligonucleotide spacer amphiphiles had higher affinities for fractalkine than the PEG or poly-carbon spacers but the reason for this improvement was uncertain. The improvement in affinity could be the result of the oligonucleotide spacer increasing the affinity of the FKN-S2 free aptamer. To test this, the IC_{50} values of 3'-T_5-FKN-S2 and 3'-T_{10}-FKN-S2 free aptamers were measured. These aptamers were synthesized as the free aptamer plus the 3' oligonucleotide spacers without the tails. The binding curves are shown in Figure 3.5. Interestingly, both the 3'-T_5- FKN-S2 (IC_{50} of 3.4 ± 0.6 nM) and the 3'-T_{10}-FKN-S2 (IC_{50} of 3.6 ± 0.9 nM) free aptamers had a higher affinity for fractalkine than

the free FKN-S2 aptamer (IC_{50} of 8.64 ± 0.28 nM; $p < 0.001$ for both 3'-T_5- FKN-S2 and 3'-T_{10}-FKN-S2 with respect to FKN-S2 aptamer). As shown in Table 3.2 there was no difference between the 3'-T_5-FKN-S2 and 3'-T_{10}-FKN-S2 free aptamers ($p > 0.05$). Because there is no difference in the affinity of the 3'-T_5-FKN-S2 and 3'-T_{10}-FKN-S2 free aptamers, the difference in the affinity of the respective amphiphiles is due to increased spacer lengths between the headgroup and the tail.

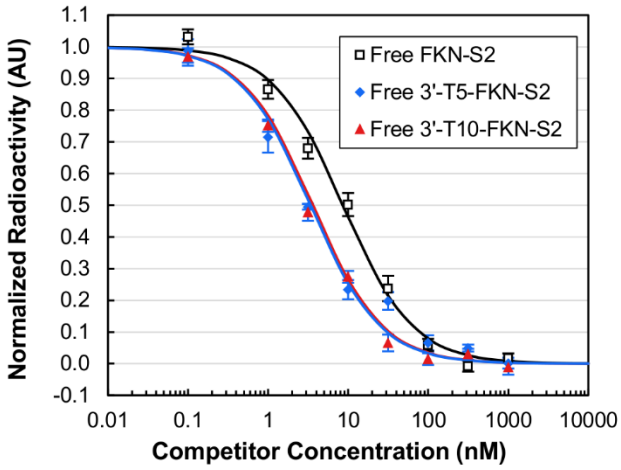

Figure 3.5: IC_{50} binding curves for the oligo-T FKN-S2 free aptamers. There was no statistical difference between the T_5 and T_{10} aptamers ($p > 0.05$). The data show the mean ± SEM ($n \geq 6$).

3.3.2 Critical micelle concentration of aptamer-amphiphiles

DNA-amphiphiles have been found to self-assemble into supramolecular structures like micelles. We used the Nile red assay to confirm self-assembly of the FKN-S2 amphiphiles and to measure their CMCs. The Nile red dye fluorescence is much greater in a lyophobic environment than in aqueous solution. At the CMC, when the amphiphiles form micelles, the dye partitions into the hydrophobic micelle core, which results in an increase in

fluorescence. Figure 3.6 shows a plot of Nile red fluorescence versus aptamer-amphiphile concentration for the 3'-NoSPR-, 3'-PEG_8, 3'-C_{24}, and 3'-T_{10}-FKN-S2 amphiphiles. The fluorescence increases above background levels around 50 nM for each of the amphiphiles, suggesting they have similar CMCs despite differences in the hydrophobicities of the spacers used to synthesize the amphiphiles. However, due to the lack of sensitivity of the Nile red assay the CMC of 50 nM should be viewed as an upper limit, which means the different spacer amphiphiles might have differing CMCs but the assay is not sensitive enough to distinguish. The aptamer-amphiphile CMC is one to two orders of magnitude lower than that of peptide-amphiphiles with similar tails. Dialkyl tail peptide-amphiphiles typically have a CMC in the μM range for peptides.[193-195] However, similar CMCs in the nM range are seen for other aptamer-amphiphiles.[177, 183]

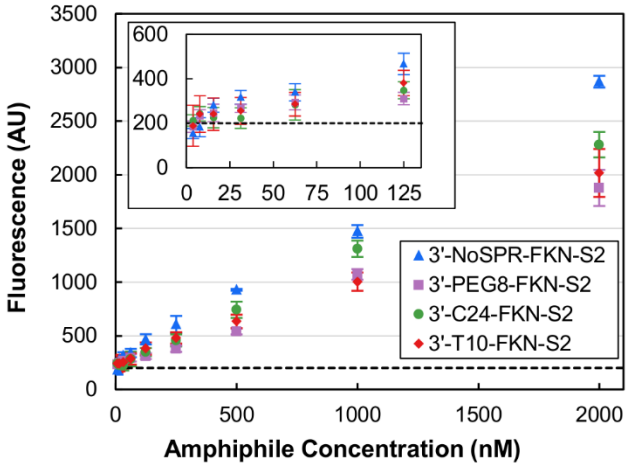

Figure 3.6: CMC curves of 3'-FKN-S2 amphiphiles with different spacers. The insert is zoomed in for a clearer view of the baseline (dotted line). The data show the mean ± SEM of 3 independent experiments (n = 3).

3.2.3 Circular dichroism spectroscopy

The secondary structure of the aptamer may be significantly different in the micelle than when free in solution. Micelles can cause unfavorable base pairing between oligonucleotides, for example, forcing parallel-strand duplex formation between oligo(dA) and oligo(dT).[196] Aptamer-aptamer interactions within a micelle may affect the structure and therefore the binding of the aptamers. Aptamers can adopt a variety of secondary structures including the standard B-form DNA and G-quadruplexes that can be probed using CD. B-form DNA forms from the standard Watson-Crick base pairing between two strands of complimentary DNA or within one strand forming stem-loop structures as shown in Figure 3.7A. G-quadruplexes are more complex. A G-quadruplex is a tertiary DNA structure composed of stacked G-quartets that form from the general sequence of $G_yX_iG_yX_jG_yX_kG_y$, where X can be any nucleotide including guanine, y is at least 2, and i, j, k are integers greater than zero.[197] A G-quartet is made up of four guanine nucleic acids arranged in a square, planar geometry stabilized by Hoogsteen hydrogen bonds. G-quartets stack due to π bond stacking forming the helical G-quadruplex structure.[69] While G-quadruplexes can form in pure water,[198] small cations, in particular, K^+ and to a lesser extent Na^+, stabilize the formation by fitting inside and between the G-quartets coordinating with the oxygen of guanine.[71] G-quadruplexes can be either parallel or anti-parallel depending on strand orientation as shown in Figure 3.7B and 3.7C.[69] In a parallel G-quadruplex all the strands share the same 5' to 3' orientation; in an anti-parallel G-quadruplex the strands are orientated in the opposing 5' to 3' and the 3' to 5' direction. The G-quadruplex can be either intramolecular (unimolecular) composed of a single aptamer, or intermolecular composed of two (bimolecular) or four (tetramolecular) strands.[70]

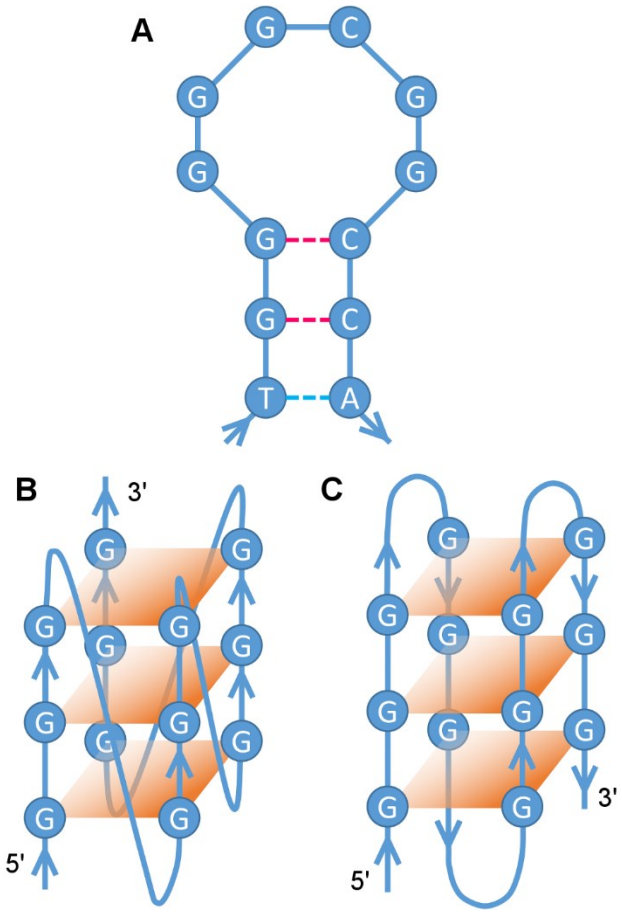

Figure 3.7: (A) Structure of a stem-loop, (B) intramolecular parallel G-quadruplex and (C) intramolecular anti-parallel G-quadruplex.

CD spectroscopy was used to probe the secondary structure of the free FKN-S2 aptamer and FKN-S2 amphiphiles. The CD spectra for the free FKN-S2 aptamer was measured in pure water, 20 mM KCl, and PBS buffer (Figure 3.8A). The water spectrum of FKN-S2 had positive peaks at 285, 258, and 211 nm and a negative peak around 235 nm. The 258 nm peak is characteristic of a parallel G-quadruplex, which typically has a positive peak between 258-265 nm, while the peak at 285 is characteristic of B-form DNA or a stem-loop structure.[73, 75, 80] The CD spectra in 20 mM KCl and PBS show a significant shift. The

addition of the salts greatly strengthened the G-quadruplex peak and shifted it to 263 nm, as the salts increase the CD signal of G-quadruplexes by stabilizing the structure.[71, 199] The stem-loop peak at 285 nm turned into a shoulder due to the strengthened G-quadruplex peak, but it is still present. The spectrum in PBS buffer is similar in shape to the KCl spectrum but with slightly less signal strength. This is probably because PBS contains mostly Na^+ which does not strengthen the G-quadruplex as strongly as K^+.[71] The G-quadruplex and stem-loop peaks in the spectrum suggest the presence of both in the aptamer structure. A hypothetical aptamer secondary structure is shown in Figure 3.8B where the first half of the aptamer, which is G rich, forms a G-quadruplex and the other half forms a stem-loop structure.

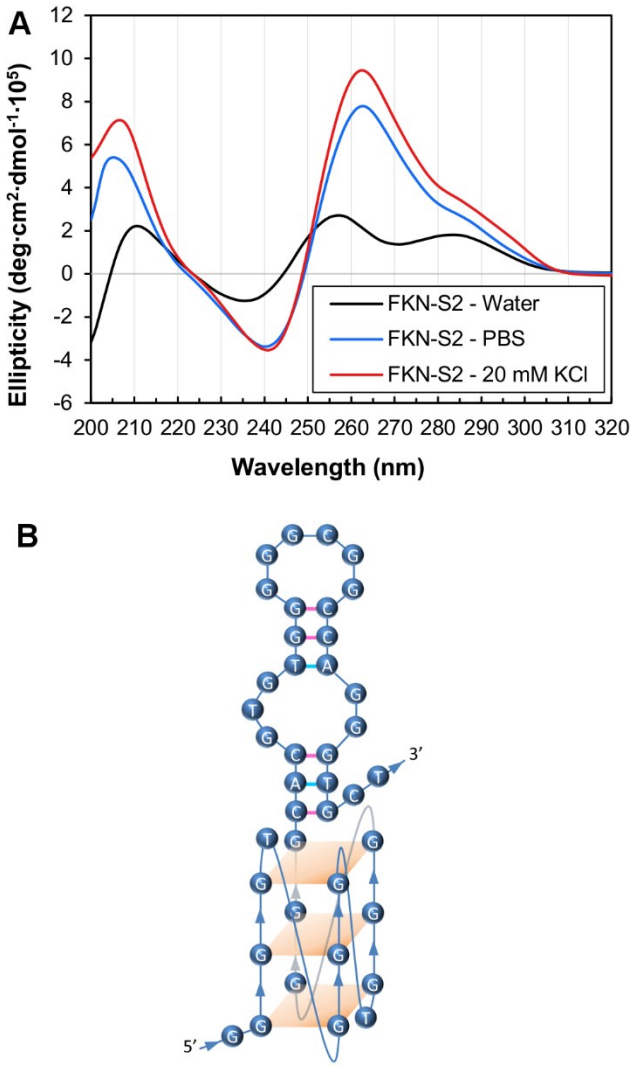

Figure 3.8: (A) CD spectra of 2.5 µM free FKN-S2 aptamer in water, 20 mM KCl and PBS. The data show the mean of four independent experiments (n = 4) with one replicate per experiment. (B) A hypothetical cartoon of the secondary structure of the FKN-S2 aptamer. The light orange represents the planes of the G-quartets. The G-quadruplex structure was predicted by the g-quadruplex prediction software QRS Mapper and the stem-loop structure was predicted by M-fold.[200]

3.3.4 Effect of the tail and spacer on the aptamer secondary structure

The CD spectra of the aptamer-amphiphiles were taken in DI water and PBS (Figure 3.9). The 3'-PEG_8-, 3'-C_{24}-, and 3'-NoSPR-FKN-S2 spectra are nearly identical in water as shown in Figure- 3.9A. Positive peaks occur at 285, 257, and 210 nm and a negative peak occurs at 236 nm. There was no statistically significant difference in the peak intensity of the 3'-NoSPR, 3'-PEG_8, and 3'-C_{24}-FKN-S2 amphiphiles ($n \geq 4$, $p > 0.05$) or the peak location indicating the secondary structure of the aptamer-amphiphile is similar between the different spacers in water. However, the 3'-T_{10}-FKN-S2 amphiphile differs significantly from the other amphiphiles; it has a much stronger stem-loop peak, the peak has shifted to 281 nm, and a weaker G-quadruplex peak at 260 nm.

The CD spectra of the 3'-NoSPR-, 3'-PEG_8-, and 3'-C_{24}-FKN-S2 amphiphiles in water (Figure 3.9A) were similar to in shape to the free FKN-S2 aptamer in water (Figure 3.8A) with the positive and negative peaks occurring at the same wavelengths. However, the G-quadruplex peak at 257-258 nm is much stronger for the free FKN-S2 aptamer (2.7 $deg \cdot cm^2 \cdot dmol^{-1} \cdot 10^{-5}$ versus $\approx$ 2.0 $deg \cdot cm^2 \cdot dmol^{-1} \cdot 10^{-5}$ for free FKN-S2 and the amphiphiles respectively; $p < 0.01$) suggesting that in water, the hydrophobic tails destabilize the G-quadruplex. There was no difference in intensity of the other spectra peaks. Comparing the 3'-T_{10}-FKN-S2 amphiphile and the free FKN-S2 aptamer, the 3'-T_{10} amphiphile had a more negative minimum at 236 nm, a depressed peak at 260 nm and a more intense peak at 281 nm ($p < 0.01$ for all peaks) than the free FKN-S2 aptamer. This suggests the 3'-T_{10} amphiphile destabilizes the G-quadruplex and stabilizes the stem-loop.

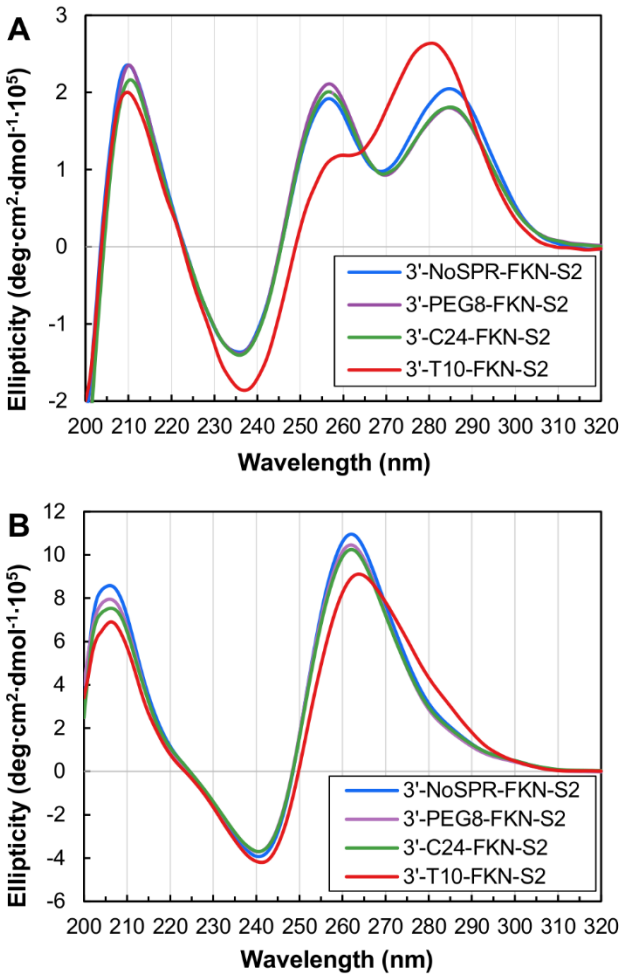

Figure 3.9: (A) CD spectra of 2.5 μM 3'-FKN-S2-amphiphiles in water at 22 °C. The data show the mean of at least 4 independent experiments (n ≥ 4). (B) CD spectra of 2.5 μM 3'-FKN-S2-amphiphiles in PBS at 22 °C. The data show the mean (n = 4).

The spectra of the aptamer-amphiphiles in PBS are shown in Figure 3.9B. There is no statistical difference between the peaks of the 3'-NoSPR, 3'-PEG_8, and 3'-C_{24}-FKN-S2 amphiphile spectra ($p > 0.05$). The spectra were strongly characteristic of a parallel G-quadruplex with positive peaks at 262 nm and 206 nm and a negative peak at 241 nm. The 3'-T_{10}-FKN-S2 amphiphile spectrum has similar characteristics but is slightly different from the other amphiphiles. The G-quadruplex peak shifts to 264 nm and is less intense.

Comparing the CD spectra of the aptamer-amphiphiles in water and PBS (Figure 3.9A and 3.9B respectively), the PBS buffer shifted the G-quadruplex peak from 257 nm to 262 nm and increases the intensity 5 fold. This was expected because the K^+ ions of the buffer can stabilize G-quadruplexes. Surprisingly, the stem-loop peak at 285 nm was not present in the aptamer-amphiphile CD spectra in PBS. The 3'-T_{10}-FKN-S2 spectrum broadens slightly at 285 nm but no peak or shoulder was seen. It is possible the stem-loop is still present in the aptamer-amphiphiles, but the signal is hidden by the large G-quadruplex peak.

The 3'-FKN-S2 amphiphiles and the free FKN-S2 aptamer CD spectra were similar in PBS except for a large change in the b-form shoulder at 285 nm. The peaks occurred at the same wavelengths and the shape was similar. However, the amphiphiles had a much stronger G-quadruplex peak at 262 nm ($p < 0.01$) than the free aptamer indicating that the addition of the tails stabilized the G-quadruplexes when dissolved in PBS. This was surprising given that the addition of tails seemed to destabilize the G-quadruplex when dissolved in pure water as described earlier. The difference may be due to the ability of PBS to screen the electrostatic repulsion from the negatively charged phosphate backbone. The charge screening of the PBS may promote the G-quadruplex structure that would otherwise be discouraged when the amphiphiles are dissolved in pure water due to electrostatic repulsion.

3.3.5 Melting curves

Thermal melting studies were performed to further characterize the aptamer and amphiphiles. All melting experiments were done in PBS buffer after we attempted melting experiments in pure water but found the aptamer rapidly degraded at high temperatures, likely through depurination, because of the lack of salts.[201] The G-quadruplex folding was monitored by CD at 265 nm and the stem-loop at 285 nm. Molar ellipticity was monitored instead of absorbance because the large signal change in CD between unfolded and folded conformations allowed for lower aptamer concentrations. The heating and melting curves of the free aptamer, shown in Figure 3.10, overlap indicating reversible melting.

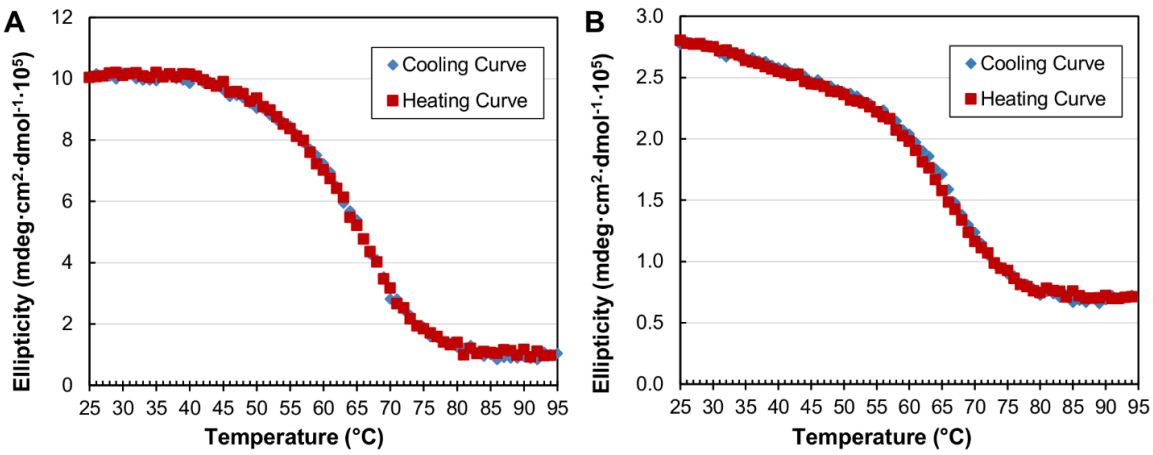

Figure 3.10: CD melting curves of 2.5 μM FKN-S2 free aptamer in PBS at (A) 265 nm and (B) 285 nm. The aptamer was heated to 95 °C and cooled to 25 °C at 0.25 °C/min followed by heating to 95 °C. Results show the mean molar ellipticity at each temperature from 4 independent experiments (n = 4).

The melting temperature (T_m) was measured as a function of the aptamer concentration to determine the molecularity of the aptamer (Figure 3.11). The melting temperature of unimolecular G-quadruplexes are concentration independent, but the melting temperature

of bimolecular and tetramolecular quadruplexes increase with increasing concentration.[190] The FKN-S2 free aptamer T_m was measured over an aptamer concentration range of 0.25 to 10 μM. The T_m was constant in the concentration range 0.25 μM to 2.5 μM (Figure 3.11; $p > 0.05$), but increased at concentrations greater than 2.5 μM. This suggests that at concentrations below 2.5 μM, the free FKN-S2 aptamer forms an intramolecular (unimolecular) G-quadruplex and at concentrations above 2.5 μM it forms an intermolecular G-quadruplex. A similar transition from intramolecular to intermolecular G-quadruplex has been observed for another aptamer as well.[202] All CD measurements were taken at 2.5 μM to ensure the aptamer is in unimolecular G-quadruplex.

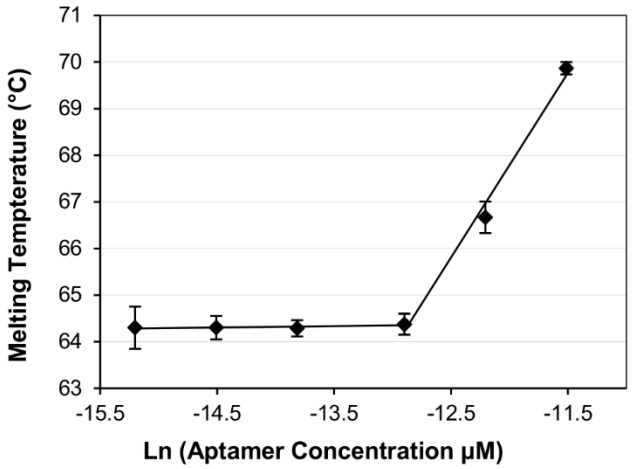

Figure 3.11: Plot of G-quadruplex melting temperature (T_m) versus the natural log of FKN-S2 free aptamer concentration. The samples were ran at 0.25 °C/min and the melting of G-quadruplexe was monitored by CD at 265 nm. The lines show the linear regression of the T_m from 0.25 μM to 2.5 μM and from 2.5 μM to 10 μM. The data points are the mean ± SEM of at least 3 independent experiments ($n \geq 3$).

The thermodynamic stability of the aptamer was assessed by thermal melting experiments. The temperature was decreased at 0.25 °C per min from 95 to 25 °C (cooling curve) and then increased from 25 to 95 °C (heating curve). No hysteresis was seen at this temperature gradient (Figure 3.10) indicating the melting process is reversible and at equilibrium. This allows for calculation of the melting temperature T_m and thermodynamic parameters such as the van't Hoff enthalpy, $\Delta H°_{vH}$, entropy, $\Delta S°$, and Gibbs free energy, $\Delta G°$. Both $\Delta H°_{vH}$ and $\Delta S°$ are model dependent. The analysis assumes two states, folded and unfolded, are present and that both states are in equilibrium at each temperature. It also assumes the entropy and enthalpy are independent of temperature.[190] The thermodynamic parameters for the FKN-S2, 3'-T_5-FKN-S2 and 3'-T_{10}-FKN-S2 free aptamers are shown in Table 3.3. There was no difference between the G- quadruplex melting temperatures of the FKN-S2, 3'-T_5-FKN-S2, and 3'-T_{10}-FKN-S2 free aptamers ($p > 0.05$). However, there was a significant difference in the Gibbs free energy. The FKN-S2 aptamer G-quadruplex was more stable ($\Delta G°_{37}$ of -13.6 ± 0.10 kJ/mol) than the 3'-T_5-FKN-S2 aptamer ($\Delta G°_{37}$ of -12.6 ± 0.14 kJ/mol; $p < 0.01$) and the 3'-T_{10}-FKN-S2 aptamer ($\Delta G°_{37}$ of -12.7 ± 0.09 kJ/mol; $p < 0.01$). There was no statistical difference between 3'-T_5 and 3'-T_{10}-FKN-S2 free aptamers; $p > 0.05$. Addition of the oligo-T spacer to the 3' end decreased the stability of the G-quadruplex. Increasing the spacer length from T_5 to T_{10} did not decrease the stability further.

Table 3.3: Thermodynamic parameters of FKN-S2, 3'-T_5-FKN-S2, and 3'-T_{10}-FKN-S2 free aptamers. Results show the mean ± SEM from 4 independent experiments (n = 4). G-quadruplex Thermodynamics: [a]Melting monitored at 265 nm. [b]Melting monitored at 285 nm.

G-Quadruplex Thermodynamic Parameters[a]

Parameter	FKN-S2	5T FKN-S2	10T FKN-S2
T_m (°C)	64.4 ± 0.2	64.1 ± 0.4	64.2 ± 0.1
$\Delta H°_{vH}$ (kJ/mol)	-174 ± 1.6	-161 ± 2.8	-164 ± 1.7
$\Delta S°$ (J/(mol·K))	-517 ± 4.9	-478 ± 8.8	-487 ± 5.3
$\Delta G°_{37}$ (kJ/mol)	-13.6 ± 0.1	-12.6 ± 0.1	-12.7 ± 0.1

Stem-Loop Thermodynamic Parameters[b]

Parameter	FKN-S2	5T FKN-S2	10T FKN-S2
T_m (°C)	67.0 ± 0.7	68.0 ± 0.4	68.5 ± 0.5
$\Delta H°_{vH}$ (kJ/mol)	-248 ± 2.2	-268 ± 3.2	-267 ± 3.8
$\Delta S°$ (J/(mol·K))	-729 ± 6.1	-786 ± 8.9	-781 ± 10.1
$\Delta G°_{37}$ (kJ/mol)	-21.8 ± 0.5	-24.2 ± 0.5	-24.6 ± 0.7

The trend was similar for the stem-loop DNA peak. The melting temperature did not change ($p > 0.05$) but the stability of the stem-loop increases from a $\Delta G°_{37}$ of -21.8 ± 0.5 kJ/mol for the free FKN-S2 to -24.2 ± 0.5 and -24.6 ± 0.7 kJ/mol for the 3'-T_5 and 3'-T_{10}-FKN-S2 free aptamers respectively ($p < 0.05$). There was no significant difference between the 3'-T_5 and 3'-T_{10}-FKN-S2 free aptamers ($p > 0.05$). The oligo-T spacer increases the stability of the stem-loop, but increasing the spacer from T_5 to T_{10} does not further increase the stability.

The thermodynamics of the aptamer were consistent with the IC_{50} data (Table 3.1). The binding curves of the 3'-T_5 and 3'-T_{10}-FKN-S2 free aptamers (Figure 3.5) were identical and so was the stability of the G-quadruplex and stem-loop secondary structures based on $\Delta G°_{37}$ (Table 3.3). Based on the $\Delta G°_{37}$ data from Table 3.3 for the FKN-S2 free aptamer, the G-quadruplex is more stable and the stem-loop less stable compared to the oligo-T

FKN-S2 free aptamers. This may suggest that destabilizing the G-quadruplex and stabilizing the stem-loop results in higher affinity of the free aptamer.

The melting curves of the aptamer-amphiphiles were also measured, but they failed to produce usable data (Figure 3.12). The melting curves did not plateau at high or low temperatures and the signal intensity did not change much from low temperature to high temperature. Other lipid-oligonucleotide melting curves have shown similar results.[203, 204] The aptamer-amphiphiles retained the G-quadruplex secondary structure even at 95 °C based on CD spectra at various temperatures (Figure 3.13). However, no G-quadruplex peak was seen in the FKN-S2 aptamer spectra at 95°C (Figure 3.14). Even at 75 °C there is only a small G-quadruplex peak present (Figure 3.14) which is consistent with the melting curves for the FKN-S2 free aptamer (Figure 3.10A). It appears that the G-quadruplex formation is stabilized when the amphiphiles are in a micellar structure. From the thermal melting experiments (Figure 3.11) we know that the FKN-S2 free aptamer forms bimolecular or tetramolecular G-quadruplexes at high concentrations. In the micelle headgroup corona layer, the concentration of the aptamer is much higher than in solution because the aptamer is confined at the surface of the micelle. Simple size arguments show the aptamer concentration within the micelle is much higher than 10 μM. The minimum possible aptamer concentration within a micelle would occur when the aptamer is fully stretched (approximately 19 nm assuming 0.34 nm/base and a 3 nm tail) and the micelle has an aggregation number of 2. The aptamer concentration in a micelle with these parameters is approximately 100 μM so it is likely that the FKN-S2 aptamer headgroup is forming intermolecular G-quadruplexes within the micelle. Thus, the high concentration of the aptamer headgroups in the micelles likely favors parallel intermolecular G-quadruplex

formation, that may be responsible for the increased melting temperature, and may be more stable than the intramolecular parallel G-quadruplexes seen for the free aptamers.

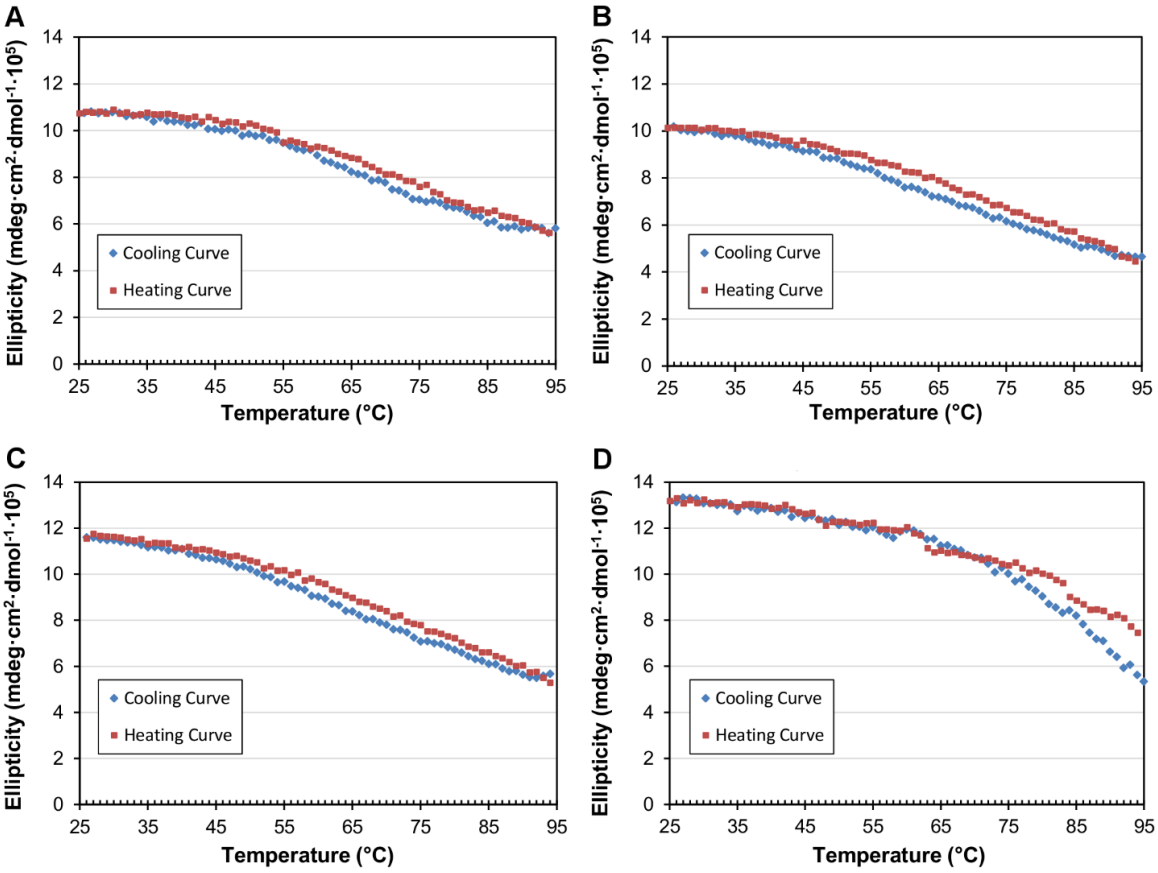

Figure 3.12: Melting curves of FKN-S2 amphiphiles measured by CD at 265 nm for the (A) 3'-NoSPR-FKN-S2 amphiphile, (B) 3'-PEG_8-FKN-S2 amphiphile, (C) 3'- C_{24}-FKN-S2 amphiphile, and (D) 3'-T_{10}-FKN-S2 amphiphiles. All melting curves are done in PBS with 2.5 μM aptamer concentration. There is a decrease in signal with temperature indicating the G-quadruplex is denaturing, but the signal does not plateau at high or low temperatures like the FKN-S2 aptamer.

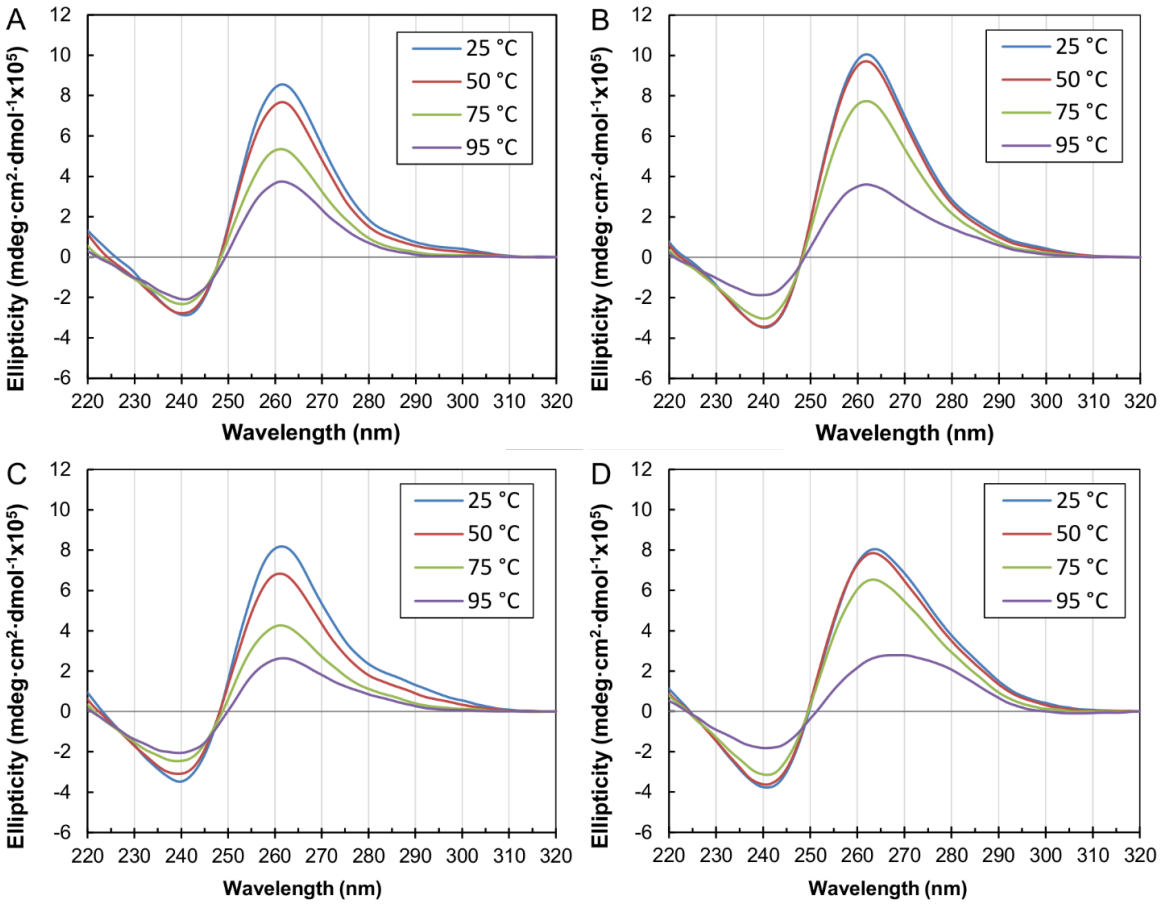

Figure 3.13: CD spectra of (A) 3'-NoSPR-FKN-S2 amphiphile, (B) 3'-PEG8-FKN-S2 amphiphile, (C) 3'-C24-FKN-S2 amphiphile, and (D) 3'-T10-FKN-S2 amphiphile in PBS at different temperatures. The aptamer-amphiphile sample, 2.5 μM aptamer-amphiphile in PBS buffer, was heated to 25 °C, 50 °C, 75 °C, and 95 °C and the spectra were taken after a 5 minute temperature equilibrium period.

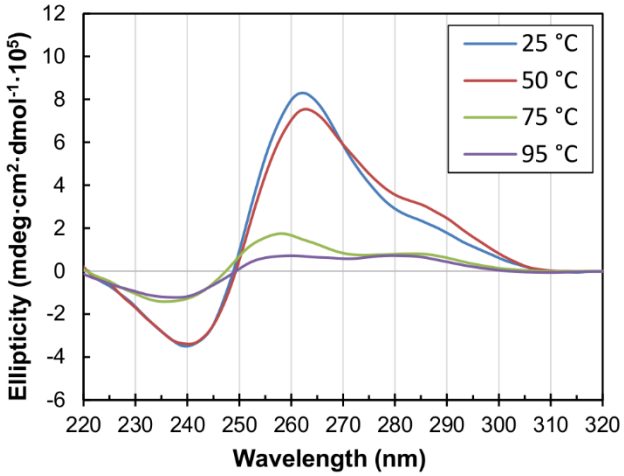

Figure 3.14: CD spectra of 2.5 μM FKN-S2 free aptamer in PBS at different temperatures. The aptamer-amphiphile sample was heated to 25 °C, 50 °C, 75 °C, and 95 °C and the spectra were taken after a 5 minute temperature equilibrium period.

3.3.6 Cryo TEM of aptamer-amphiphiles

The CMC experiments showed the presence of supramolecular structures. Cryo-TEM images of the FKN-S2 amphiphiles were taken to investigate the shape of the structures (Figure 3.15). The FKN-S2 amphiphiles formed both globular micelles and nanotapes with the majority of the structures being globular micelles. The micelles were found in all the samples and were roughly 10-20 nm in diameter. The nanotape structures were confirmed by tilting the TEM stage at different angles (representative images are shown for the 3'-C_{24}-FKN-S2 amphiphile in Figure 3.16). The nanotapes were both flat, Figure 3.15D, and twisted (Figure 3.15A-C). Flat and twisted structures were seen in all amphiphiles with similar frequency and the spacer had little effect on the shape of the nanotapes. However, the nanotapes were less prevalent in the 3'-T_{10}-FKN-S2 amphiphile compared to the other spacer amphiphiles.

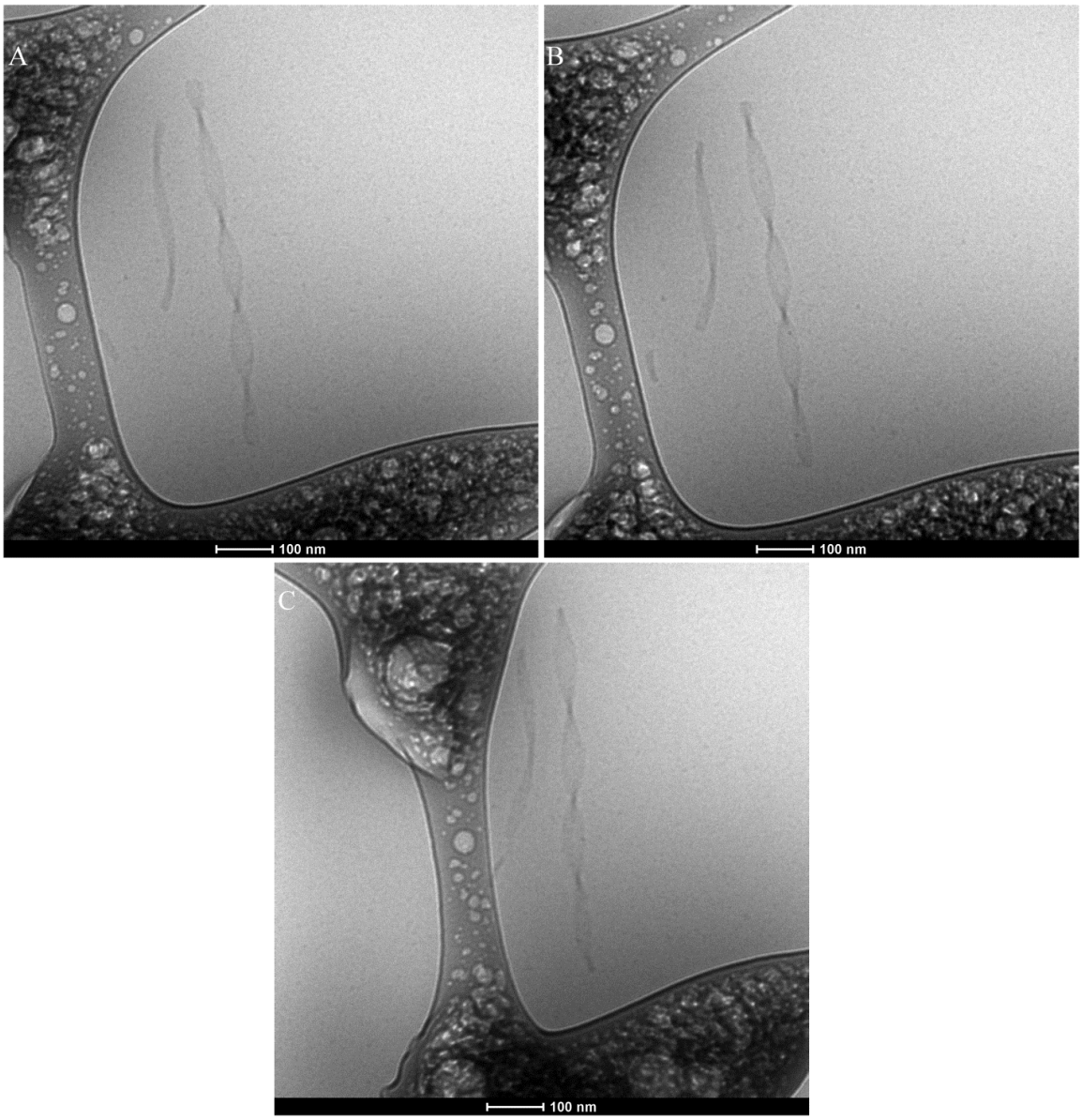

Figure 3.15: Cryo-TEM images of 3'-C24-FKN-S2 amphiphile nanotapes at (A) +30° stage tilt, (B) 0° stage tilt, and (C) -45° stage tilt. The images show twisted nanotapes.

Even though only micelles were seen in other studies with aptamer-amphiphiles,[177, 183] similar nanotapes were formed by sugar-amphiphiles,[205] or peptide-amphiphiles with strong hydrogen bonding between the peptide headgroups,[206, 207] and nucleic acid-amphiphiles.[208, 209] The nucleic acid-amphiphiles though that formed nanotape structures all had small headgroups consisting of a single nucleotide and a 12 carbon dialkyl tail.[208, 209]

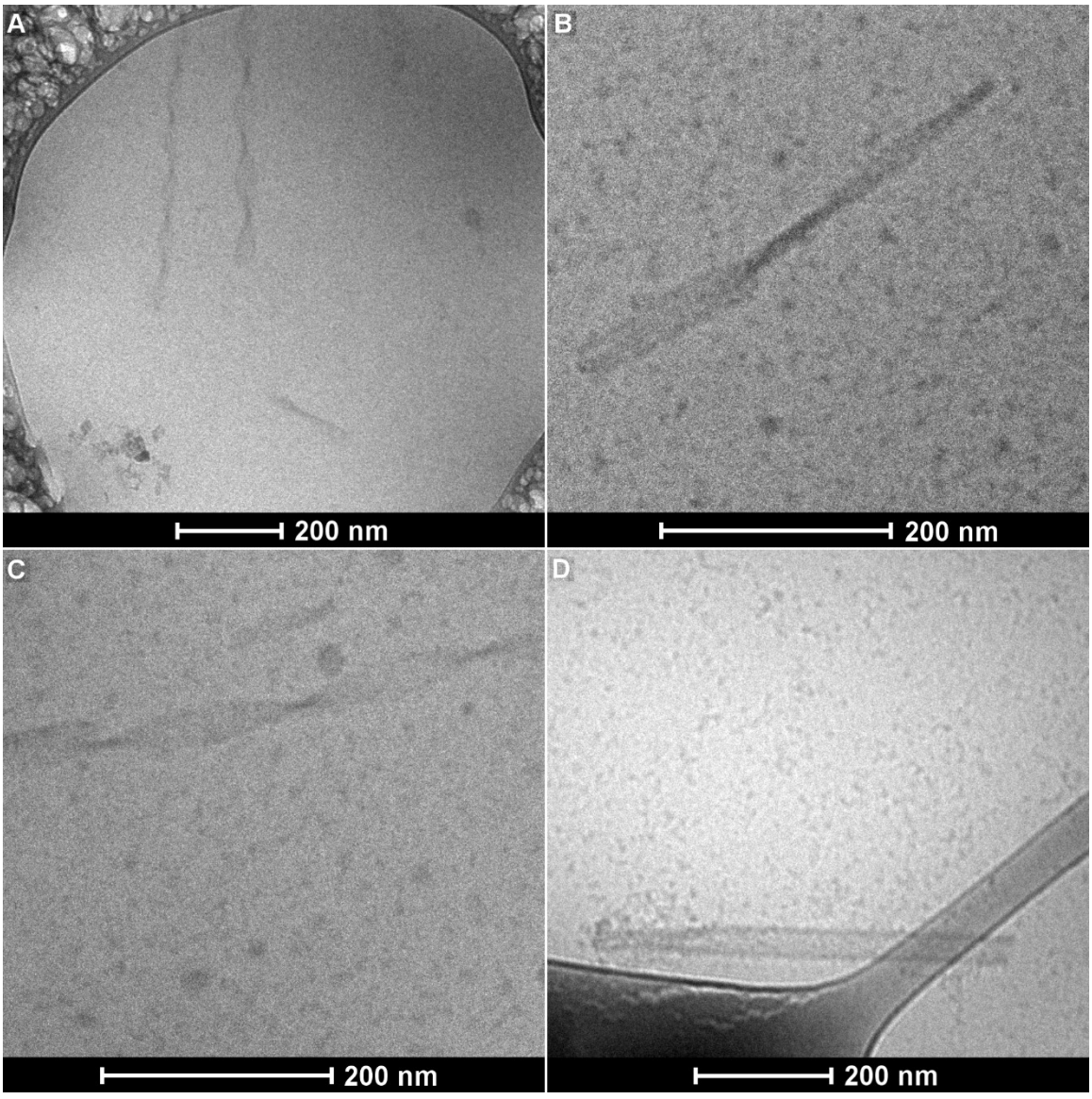

Figure 3.16: Cryo-TEM images of (A) 3'-NoSPR-FKN-S2 amphiphiles, (B) 3'-PEG_8-FKN-S2 amphiphiles, (C) 3'-C_{24}-FKN-S2 amphiphiles, and (D) 3'-T10-FKN-S2 amphiphiles. All cryo-TEM samples were prepared from stock aptamer-amphiphile at 500 μM in water.

Work by our group has showed recently that aptamer-amphiphiles can self-assemble into micelles and long nanotapes that are bilayer structures and can be flat or twisted.[185] The 25 nucleic acid aptamer used in that study (Muc-1 aptamer) had a stem-loop secondary

structure (with the potential to form G-quadruplexes as it had guanine nucleotides in its sequence) and was conjugated at its 5' end to C_{16} dialkyl tails in the absence and presence of different spacers. The aptamer-amphiphiles with NoSPR or PEG spacers self-assembled into micelles and the assembly process did not significantly alter the secondary structure of the aptamer headgroups as the amphiphiles also had a stem-loop secondary structure. However, in the presence of poly-C spacers the amphiphiles self-assembled into micelles and nanotapes, flat or twisted, with a G-quadruplex intermolecular secondary structure.[185] We hypothesized that the hydrophobic attractions between the poly-C spacers brought the aptamer headgroups together, thus reducing the aptamer headgroup area at the interface and allowing the nanotapes to assemble.

In the current study we found that in water FKN-S2 assumes a stem-loop and G-quadruplex secondary structure as a free aptamer (Figure 3.8) and as an amphiphile (Figure 3.9A), independent of the type of spacer used. Furthermore, from the thermal melting studies we postulated that it is possible for the FKN-S2 aptamer headgroup to form intermolecular G-quadruplexes within the self-assembled structures. Therefore, these interactions between adjacent aptamer headgroups could be reducing the headgroup area and favoring the assembly of bilayer nanotapes, similar to the ones observed with the Muc-1 aptamer-amphiphile in the presence of poly-C spacers.

To test this, we synthesized a 40-mer single-stranded DNA (ssDNA) sequence containing no guanine nucleotides (named NoG) thus eliminating the possibility of G-quadruplex formation. The NoG ssDNA had the following sequence, 5'-TTCTATTCTCACATTTCATCTATTAAACCACCAATTAATT-amino C_6 linker-3'. The

sequence was randomly generated from equal probabilities of A, C, and T nucleotides. The 3'-NoSPR-NoG amphiphile and 3'-C_{24}-NoG amphiphile were synthesized and imaged via cryo-TEM (Figure 3.17). The 3'-NoSPR-NoG amphiphile did not form nanotapes while the 3'-C_{24}-NoG amphiphile formed micelles and flat and twisted nanotapes. This is consistent with the findings of our previous study with the Muc-1 aptamer-amphiphile.[185] Because the NoG ssDNA headgroup does not form intermolecular G-quadruplexes, the 3'-NoSPR-NoG amphiphile does not form nanotapes in the absence of either a G-quadruplex secondary structure or a hydrophobic poly-C spacer that will reduce the aptamer headroup area by driving the aptamer headgroups in close proximity and allowing the nanotapes to form.

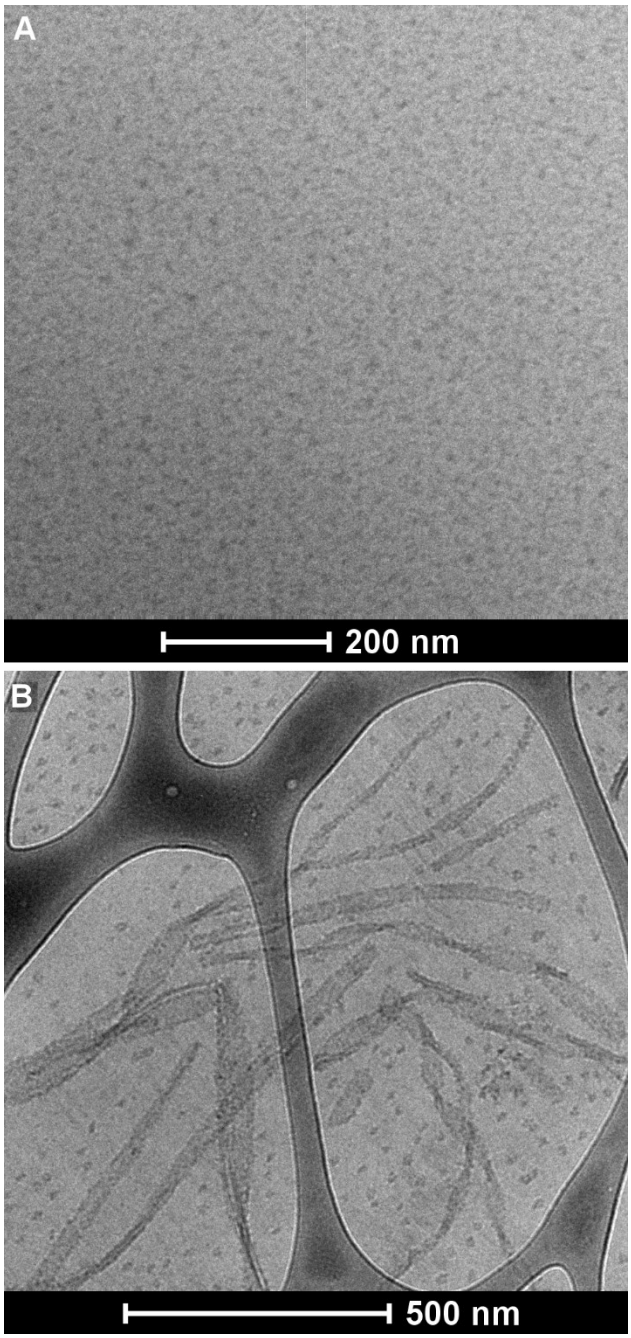

Figure 3.17: Cryo TEM images of (A) 3'-NoSPR-NoG amphiphile and (B) 3'-C_{24}-NoG amphiphile.

To assess our hypothesis even further we used a ssDNA sequence, named $(GGGT)_3$, that can form G-quadruplexes. The $(GGGT)_3$ ssDNA with the following sequence, 5'-TTCTATTCTCAC ATTTCATCTATTAAACCGGGTGGGTGGG-amino C_6 linker-3', was identical to the NoG ssDNA sequence except that 11 nucleotides at the 3' end were replaced with the GGGT repeat where a thymine nucleic acid separated 3 consecutive guanines. The 3' terminal thymine was not included because it was unlikely to participate in G-quadruplex formation. The $(GGGT)_3$ ssDNA sequence cannot form an intramolecular G-quadruplex but is capable of forming intermolecular G-quadruplexes. The CD spectra of the $(GGGT)_3$ free ssDNA, the 3'-NoSPR-$(GGGT)_3$ amphiphile, and 3'-C_{24}-$(GGGT)_3$ amphiphile are shown in Figure 3.18. The $(GGGT)_3$ free ssDNA does not form G-quadruplexes, but the 3'NoSPR-$(GGGT)_3$ and 3'-C_{24}-$(GGGT)_3$ amphiphiles do. Figure 3.19 shows cryo-TEM images of the amphiphiles. Both the 3'NoSPR-$(GGGT)_3$ and 3'-C_{24}-$(GGGT)_3$ amphiphiles form nanotape structures. In this case, we hypothesize that the intermolecular G-quadruplex formation reduces the headgroup area thus allowing for the assembly of the nanotapes.

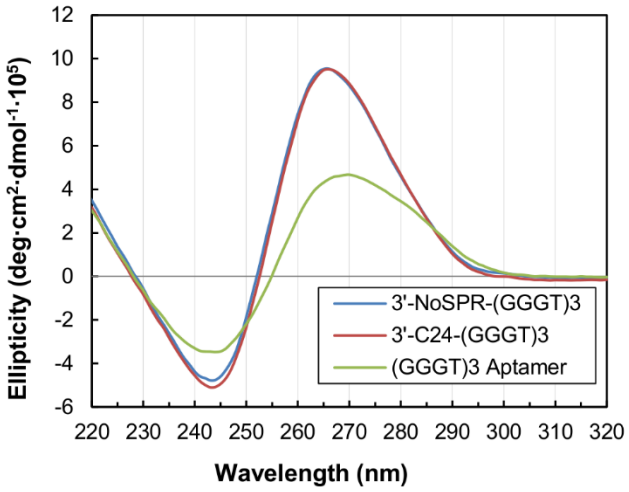

Figure 3.18: CD spectra of the $(GGGT)_3$ free ssDNA and amphiphiles in PBS at 22 °C and 2.5 μM concentration. All samples were heat denatured in a 95 °C heating block for 5 min followed by rapid cooling to room temperature.

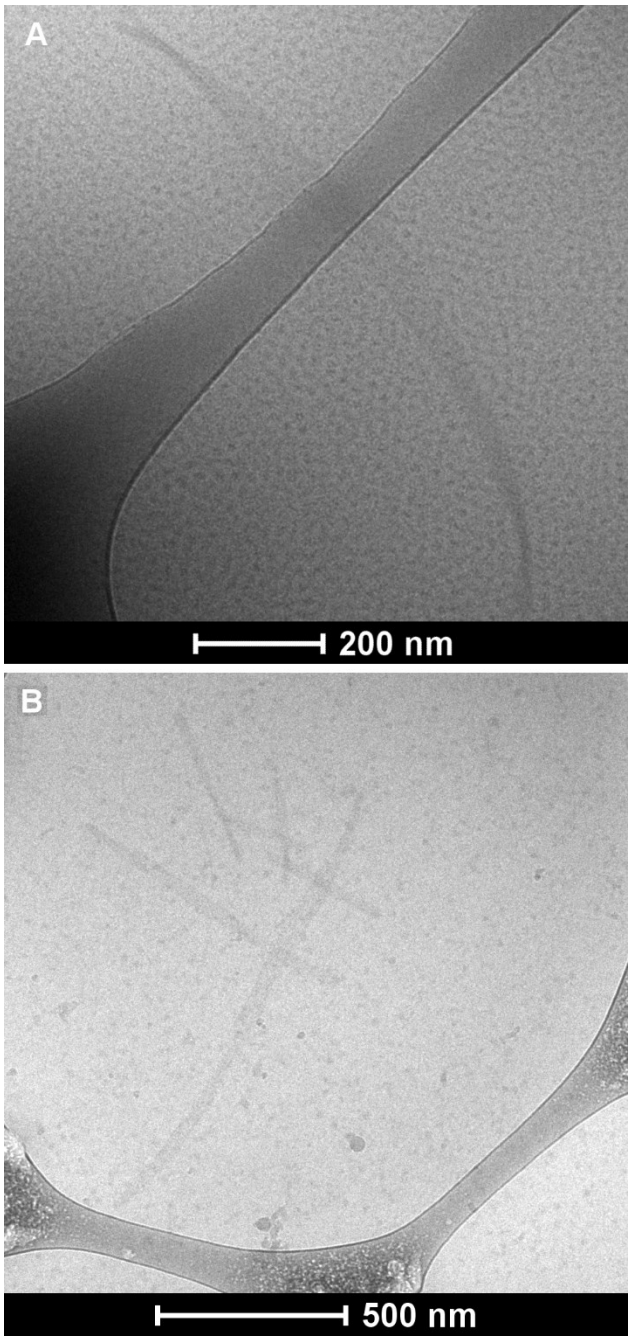

Figure 3.19: Cryo TEM images of (A) 3'-NoSPR-$(GGGT)_3$ amphiphile and (B) 3'-C_{24}-$(GGGT)_3$ amphiphile.

3.3.7 Binding of 3'-T_{10}-FKN-S2 functionalized liposomes

The aptamers are well suited for targeted drug delivery applications because they are considered to be non-immunogenic, have high affinity and specificity, and can be used to functionalize drug delivery vehicles.[174] There are a range of drug delivery vehicles from polymersomes, dendrimers, nanoparticles, liposomes, and micelles.[174] As a proof of concept, we functionalized stealth liposomes (liposomes functionalized with PEG) with the 3'-T_{10}-FKN-S2 amphiphile and targeted them to fractalkine expressing cancer cells. Liposomes were the drug delivery vehicle of choice because they are well studied and characterized, and the hydrophobic tail of the aptamer-amphiphile will spontaneously incorporate into the liposome bilayer. The liposomes were prepared with 5 mol% DPPE-PEG2000 to confer stealth properties to the liposomes. The PEG2000 coating reduces non-specific interactions with surfaces, proteins, and cells by providing a steric barrier to protein adsorption and cell adhesion.[191] The liposomes were functionalized with the 3'-T_{10}-FKN-S2 amphiphile because the IC_{50} binding experiments (Table 3.1) showed it had the highest affinity for fractalkine. The aptamer-amphiphile was incorporated into the liposomes using the post insertion method. On average, 79% of the aptamer-amphiphiles incorporated into the liposomes and all of the amphiphiles were on the outside of the liposomes because the liposomes were fully formed before addition of the amphiphile. The amount of amphiphile functionalization was controlled by changing the amount of amphiphile added to the liposomes during the post insertion step as shown in Figure 3.20.

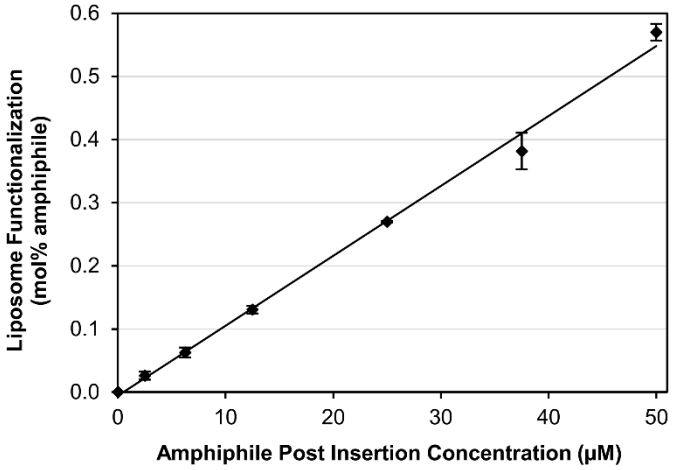

Figure 3.20: Liposome functionalization curve for the 3'-T_{10}-FKN-S2 amphiphile. The data show the mean ± SEM (n = 3).

The 3'-T_{10}-FKN-S2 functionalized stealth liposomes were loaded with the calcein dye and incubated with MCA-38.FKN mouse colon adenocarcinoma cells transfected to express fractalkine (fractalkine expression levels shown in Figure 3.21). The liposomes were incubated for 1 hr at 37 °C and the amount of binding and internalization was quantified using fluorescence as shown in Figure 3.22.

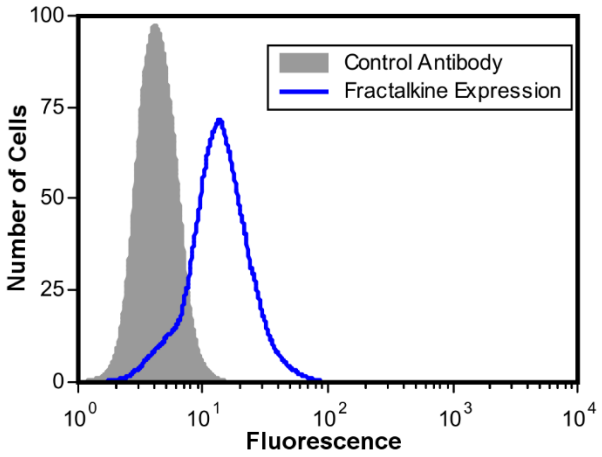

Figure 3.21: Fractalkine expression on MCA-38.FKN cells. 2 x 10^5 MCA-38.FKN cells were suspended in 200 µL of PBS buffer and 2.5 µg/mL of anti-fractalkine antibody (Cat No. AF365, R&D Systems, Minneapolis, MN) were added. After a 30 min incubation at 4 °C, the cells were centrifuged and suspended in 200 µL of PBS with a secondary antibody (Cat No. F0109, R&D Systems, Minneapolis, MN) at the concentration recommended by the manufacturer. The secondary antibody was incubated for 30 min at 4 °C and the cells were washed twice by centrifugation and imaged by flow cytometry (BD FACSCalibur, University Flow Cytometry Resource, University of Minnesota, Minneapolis, MN).

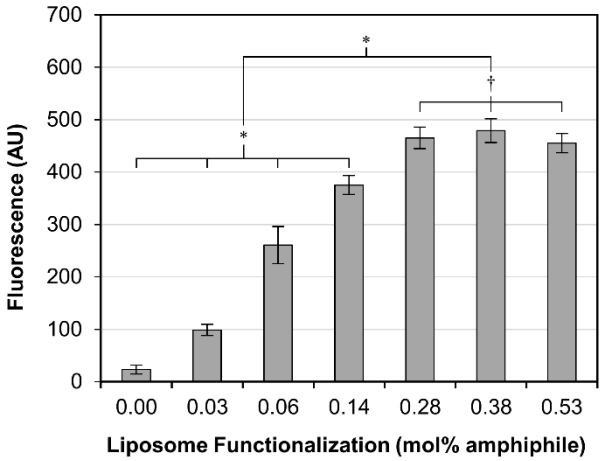

Figure 3.22: Liposome binding and internalization to fractalkine expressing MCA-38.FKN cells as a function of the concentration of the 3'-T_{10}-FKN-S2 amphiphile used to functionalize the stealth liposomes. Fluorescent liposomes were incubated with the cells for 1 hr at 37 °C and the binding and internalization was quantified by fluorescence. The data show the mean ± SEM (n = 4). Two tailed t-test with unequal variances was used to determine significance, †$p > 0.05$, *$p < 0.05$.

The 3'-T_{10}-FKN-S2 amphiphile functionalized stealth liposomes bound to the cells at all amphiphile concentrations tested ($p < 0.05$). The binding increased with increasing aptamer functionalization. This is expected because liposomes with more aptamers will likely bind with greater avidity due to multiple receptor-ligand interactions. A binding plateaued starting around 0.28 mol% aptamer-amphiphile was observed and may be a result of the liposome-fractalkine binding reaching a saturation point. This experiment showed that using the 3'-T_{10}-FKN-S2 amphiphile to functionalize stealth liposomes for targeted drug delivery applications is feasible and warrants further investigation in the future.

3.4 Conclusions

In this study we synthesized FKN-S2 aptamer-amphiphiles with different spacers and investigated their binding to fractalkine, their secondary structure and self-assembly. The addition of the tail to the aptamer reduced the affinity of FKN-S2 aptamer for fractalkine for all spacer-tail combinations tested. However, the 3'-T_{10}-FKN-S2 amphiphile had a much higher binding affinity than the other amphiphiles because of the improved affinity of the free 3'-T_{10}-FKN-S2 aptamer for fractalkine caused by the oligo-T spacer. Melting curve analysis showed that the oligo-T spacer increased the $\Delta G°_{37}$, thus decreasing stability of the G-quadruplex while increasing the stability of the stem-loop. The CMCs of the FKN-S2 aptamer-amphiphiles were less than 50 nM and all the FKN-S2 amphiphiles self-assembled into globular micelles and nanotapes, flat or twisted. For the 40-mer ssDNA sequences investigated here, nanotapes were observed in two different cases. In the first case, nanotapes formed from the FKN-S2 and $(GGGT)_3$ NoSPR amphiphiles because of the strong intermolecular G-quadruplex interactions between the ssDNA headgroups. In the second case, nanotapes did not form in the NoG-NoSPR amphiphles because the ssDNA headgroup could not form G-quadruplexes. The nanotapes only formed in the presence of a hydrophobic poly-carbon spacer. We therefore hypothesized, that in both cases, whether the driving force was the attractive interactions between the ssDNA headgroups or the attractive interactions between the hydrophobic spacers, the aptamer headroups were brought in close proximity, thus reducing the area per aptamer at the interface allowing the nanotape assemblies to form. Finally, we showed that stealth liposomes functionalized with the FKN-S2 amphiphile were able to bind to fractalkine expressing cells. Further research into the properties of ssDNA nanotapes could lead to tunable self-assembled aptamer-amphiphiles with molecular recognition properties which can be used for bottom up assembly, targeted drug delivery, and sensors.

4 Conclusion

Aptamers are an exciting and underdeveloped tool with an array of potential applications ranging from diagnostic tests and sensors to drug delivery and therapeutics. The research in this thesis was performed with the intention of developing aptamer based therapeutics against the cellular protein fractalkine. Fractalkine is expressed at sites of infection and inflammation to recruit and capture leukocytes. Because fractalkine is involved heavily with the inflammatory response, it plays a role in a variety of diseases including cancer, atherosclerosis, asthma, and arthritis. Currently there are no therapeutic agents that target fractalkine.[95] Fractalkine's structure, function, and role in disease make it an intriguing target for therapeutic applications.

In this work, an aptamer named FKN-S2 was developed that binds fractalkine with high affinity and specificity. Development of the aptamer required creative solutions to problems encountered during the SELEX process. In particular, unique methods for the immobilization of fractalkine and counter selection steps enabled the selection of the FKN-S2 aptamer where previous methods had failed. The FKN-S2 aptamer was modified by the addition of a hydrophobic tail, creating an aptamer-amphiphile. The aptamer-amphiphile had a much lower affinity for fractalkine than the free aptamer. To improve the affinity, the aptamer-amphiphiles was modified by inserting a spacer molecule between the aptamer headgroup and the tail. An optimized aptamer-amphiphile was developed by changing the length and the nature of the spacer. PEG, poly carbon, and oligonucleotide spacers were synthesized and tested. A 10 nucleotide thymidine spacer significantly improved the affinity of the amphiphile. The aptamer-amphiphiles self-assembled into micelles and nanotapes and the properties of aptamer-amphiphile self-assembly was

probed using CD spectroscopy and cryo-TEM. Finally, the FKN-S2-amphihle was incorporated into a liposome and targeted to fractalkine expressing cells as a proof of concept drug delivery system. Future work will investigate the self-assembly properties and FKN-S2 based drug delivery vehicles for therapeutic applications.

Bibliography

1. Ruigrok, V. J. B.; Levisson, M.; Eppink, M. H. M.; Smidt, H.; van der Oost, J., Alternative affinity tools: more attractive than antibodies? *Biochem. J.* **2011,** 436, (1), 1-13.
2. Jayasena, S. D., Aptamers: An Emerging Class of Molecules That Rival Antibodies in Diagnostics. *Clin. Chem.* **1999,** 45, (9), 1628-1650.
3. Laurino, J. P.; Shi, Q.; Ge, J., Monoclonal antibodies, antigens and molecular diagnostics: a practical overview. *Ann. Clin. Lab. Sci.* **1999,** 29, (3), 158-166.
4. Mascini, M.; Palchetti, I.; Tombelli, S., Nucleic Acid and Peptide Aptamers: Fundamentals and Bioanalytical Aspects. *Angew. Chem. Int. Ed.* **2012,** 51, (6), 1316-1332.
5. Bunka, D. H. J.; Stockley, P. G., Aptamers come of age - at last. *Nat. Rev. Microbiol.* **2006,** 4, (8), 588-596.
6. Cerchia, L.; de Franciscis, V., Targeting cancer cells with nucleic acid aptamers. *Trends Biotechnol.* **2010,** 28, (10), 517-525.
7. Iliuk, A. B.; Hu, L.; Tao, W. A., Aptamer in bioanalytical applications. *Anal. Chem.* **2011,** 83, (12), 4440-4452.
8. Radom, F.; Jurek, P. M.; Mazurek, M. P.; Otlewski, J.; Jeleń, F., Aptamers: Molecules of great potential. *Biotechnol. Adv.* **2013,** 31, (8), 1260-1274.
9. Song, K.-M.; Lee, S.; Ban, C., Aptamers and their biological applications. *Sensors* **2012,** 12, (1), 612-631.
10. Cho, E. J.; Lee, J.-W.; Ellington, A. D., Applications of aptamers as sensors. *Annu. Rev. Anal. Chem.* **2009,** 2, 241-264.
11. Walter, J.-G.; Stahl, F.; Scheper, T., Aptamers as affinity ligands for downstream processing. *Eng. Life Sci.* **2012,** 12, (5), 496-506.
12. Keefe, A. D.; Pai, S.; Ellington, A., Aptamers as therapeutics. *Nat. Rev. Drug Discov.* **2010,** 9, (7), 537-550.
13. Bunka, D. H. J.; Platonova, O.; Stockley, P. G., Development of aptamer therapeutics. *Curr. Opin. Pharmacol.* **2010,** 10, (5), 557-562.
14. Tan, W.; Wang, H.; Chen, Y.; Zhang, X.; Zhu, H.; Yang, C.; Yang, R.; Liu, C., Molecular aptamers for drug delivery. *Trends Biotechnol.* **2011,** 29, (12), 634-640.
15. Xiao, Z.; Farokhzad, O. C., Aptamer-functionalized nanoparticles for medical applications: challenges and opportunities. *ACS Nano* **2012,** 6, (5), 3670-3676.
16. Šmuc, T.; Ahn, I.-Y.; Ulrich, H., Nucleic acid aptamers as high affinity ligands in biotechnology and biosensorics. *J. Pharm. Biomed. Anal.* **2013,** 81–82, (0), 210-217.
17. Hermann, T.; Patel, D. J., Adaptive recognition by nucleic acid aptamers. *Science* **2000,** 287, (5454), 820-825.
18. Serganov, A.; Patel, D. J., Ribozymes, riboswitches and beyond: regulation of gene expression without proteins. *Nat. Rev. Genet.* **2007,** 8, (10), 776-790.
19. Robertson, D. L.; Joyce, G. F., Selection in vitro of an RNA enzyme that specifically cleaves single-stranded DNA. *Nature* **1990,** 344, (6265), 467-468.
20. Tuerk, C.; Gold, L., Systematic evolution of ligands by exponential enrichment: RNA ligands to bacteriophage T4 DNA polymerase. *Science* **1990,** 249, (4968), 505-510.
21. Ellington, A. D.; Szostak, J. W., In vitro selection of RNA molecules that bind specific ligands. *Nature* **1990,** 346, (6287), 818-822.

22. Dua, P.; Kim, S.; Lee, D.-k., Nucleic acid aptamers targeting cell-surface proteins. *Methods* **2011,** 54, (2), 215-225.
23. Bock, L. C.; Griffin, L. C.; Latham, J. A.; Vermaas, E. H.; Toole, J. J., Selection of single-stranded DNA molecules that bind and inhibit human thrombin. *Nature* **1992,** 355, (6360), 564-566.
24. White, R.; Rusconi, C.; Scardino, E.; Wolberg, A.; Lawson, J.; Hoffman, M.; Sullenger, B., Generation of species cross-reactive aptamers using "Toggle" SELEX. *Mol. Ther.* **2001,** 4, (6), 567-573.
25. Long, S. B.; Long, M. B.; White, R. R.; Sullenger, B. A., Crystal structure of an RNA aptamer bound to thrombin. *RNA* **2008,** 14, (12), 2504-2512.
26. Kubik, M. F.; Bell, C.; Fitzwater, T.; Watson, S. R.; Tasset, D. M., Isolation and characterization of 2'-fluoro-, 2'-amino-, and 2'-fluoro-/amino-modified RNA ligands to human IFN-gamma that inhibit receptor binding. *The Journal of Immunology* **1997,** 159, (1), 259-267.
27. Balasubramanian, V.; Nguyen, L. T.; Balasubramanian, S. V.; Ramanathan, M., Interferon-γ-inhibitory oligodeoxynucleotides alter the conformation of interferon-γ. *Mol. Pharmacol.* **1998,** 53, (5), 926-932.
28. Wiegand, T. W.; Williams, P. B.; Dreskin, S. C.; Jouvin, M. H.; Kinet, J. P.; Tasset, D., High-affinity oligonucleotide ligands to human IgE inhibit binding to Fc epsilon receptor I. *J. Immunol.* **1996,** 157, (1), 221-230.
29. Mendonsa, S. D.; Bowser, M. T., In vitro selection of high-affinity DNA ligands for human IgE using capillary electrophoresis. *Anal. Chem.* **2004,** 76, (18), 5387-5392.
30. Lauhon, C. T.; Szostak, J. W., RNA aptamers that bind flavin and nicotinamide redox cofactors. *J. Am. Chem. Soc.* **1995,** 117, (4), 1246-1257.
31. Travascio, P.; Bennet, A. J.; Wang, D. Y.; Sen, D., A ribozyme and a catalytic DNA with peroxidase activity: active sites versus cofactor-binding sites. *Chem. Biol.* **1999,** 6, (11), 779-787.
32. Walsh, R.; DeRosa, M. C., Retention of function in the DNA homolog of the RNA dopamine aptamer. *Biochem. Biophys. Res. Commun.* **2009,** 388, (4), 732-735.
33. Nimjee, S. M.; Rusconi, C. P.; Sullenger, B. A., Aptamers: An Emerging Class of Therapeutics. *Annu. Rev. Med.* **2005,** 56, (1), 555-583.
34. Carothers, J. M.; Oestreich, S. C.; Szostak, J. W., Aptamers selected for higher-affinity binding are not more specific for the target ligand. *J. Am. Chem. Soc.* **2006,** 128, (24), 7929-7937.
35. Conrad, R.; Keranen, L. M.; Ellington, A. D.; Newton, A. C., Isozyme-specific inhibition of protein kinase C by RNA aptamers. *J. Biol. Chem.* **1994,** 269, (51), 32051-32054.
36. Spoden, G. A.; Rostek, U.; Lechner, S.; Mitterberger, M.; Mazurek, S.; Zwerschke, W., Pyruvate kinase isoenzyme M2 is a glycolytic sensor differentially regulating cell proliferation, cell size and apoptotic cell death dependent on glucose supply. *Exp. Cell Res.* **2009,** 315, (16), 2765-2774.
37. Haller, A. A.; Sarnow, P., In vitro selection of a 7-methyl-guanosine binding RNA that inhibits translation of capped mRNA molecules. *Proc. Natl. Acad. Sci. USA* **1997,** 94, (16), 8521-8526.
38. Mannironi, C.; Di Nardo, A.; Fruscoloni, P.; Tocchini-Valentini, G. P., In vitro selection of dopamine RNA ligands. *Biochemistry* **1997,** 36, (32), 9726-9734.

39. Shoji, A.; Kuwahara, M.; Ozaki, H.; Sawai, H., Modified DNA aptamer that binds the (R)-isomer of a thalidomide derivative with high enantioselectivity. *J. Am. Chem. Soc.* **2007,** 129, (5), 1456-1464.
40. Michaud, M.; Jourdan, E.; Ravelet, C.; Villet, A.; Ravel, A.; Grosset, C.; Peyrin, E., Immobilized DNA aptamers as target-specific chiral stationary phases for resolution of nucleoside and amino acid derivative enantiomers. *Anal. Chem.* **2004,** 76, (4), 1015-1020.
41. Jenison, R. D.; Gill, S. C.; Pardi, A.; Polisky, B., High-resolution molecular discrimination by RNA. *Science* **1994,** 263, (5152), 1425-1429.
42. Rajendran, M.; Ellington, A., Selection of fluorescent aptamer beacons that light up in the presence of zinc. *Anal. Bioanal. Chem.* **2008,** 390, (4), 1067-1075.
43. Mann, D.; Reinemann, C.; Stoltenburg, R.; Strehlitz, B., In vitro selection of DNA aptamers binding ethanolamine. *Biochem. Biophys. Res. Commun.* **2005,** 338, (4), 1928-1934.
44. Famulok, M., Oligonucleotide aptamers that recognize small molecules. *Curr. Opin. Struct. Biol.* **1999,** 9, (3), 324-329.
45. Nonaka, Y.; Sode, K.; Ikebukuro, K., Screening and improvement of an anti-VEGF DNA aptamer. *Molecules* **2010,** 15, (1), 215-225.
46. Mehedi Masud, M.; Kuwahara, M.; Ozaki, H.; Sawai, H., Sialyllactose-binding modified DNA aptamer bearing additional functionality by SELEX. *Bioorg. Med. Chem.* **2004,** 12, (5), 1111-1120.
47. Sun, W.; Du, L.; Li, M., Aptamer-based carbohydrate recognition. *Curr. Pharm. Des.* **2010,** 16, (20), 2269-2278.
48. Lamont, E. A.; He, L.; Warriner, K.; Labuza, T. P.; Sreevatsan, S., A single DNA aptamer functions as a biosensor for ricin. *Analyst* **2011,** 136, (19), 3884-3895.
49. Eissa, S. H. H.; Ng, A.; Siaj, M.; Tavares, A. C.; Zourob, M. M., Selection and identification of DNA aptamer against okadiac acid for biosensing application. *Anal. Chem.* **2013**.
50. Kolovskaya, O. S.; Savitskaya, A. G.; Zamay, T. N.; Reshetneva, I. T.; Zamay, G. S.; Erkaev, E. N.; Wang, X.; Wehbe, M.; Salmina, A. B.; Perianova, O. V.; Zubkova, O. A.; Spivak, E. A.; Mezko, V. S.; Glazyrin, Y. E.; Titova, N. M.; Berezovski, M. V.; Zamay, A. S., Development of bacteriostatic DNA aptamers for salmonella. *J. Med. Chem.* **2013,** 56, (4), 1564-1572.
51. Wongphatcharachai, M.; Wang, P.; Enomoto, S.; Webby, R. J.; Gramer, M. R.; Amonsin, A.; Sreevatsan, S., Neutralizing DNA aptamers against swine influenza H3N2 viruses. *J. Clin. Microbiol.* **2013,** 51, (1), 46-54.
52. Stoltenburg, R.; Reinemann, C.; Strehlitz, B., SELEX—A (r)evolutionary method to generate high-affinity nucleic acid ligands. *Biomol. Eng.* **2007,** 24, (4), 381-403.
53. Mukhopadhyay, R., Aptamers are ready for the spotlight. *Anal. Chem.* **2005,** 77, (5), 114 A-118 A.
54. Cruz-Aguado, J. A.; Penner, G., Determination of ochratoxin A with a DNA aptamer. *J. Agric. Food Chem.* **2008,** 56, (22), 10456-10461.
55. André, C.; Berthelot, A.; Thomassin, M.; Guillaume, Y.-C., Enantioselective aptameric molecular recognition material: Design of a novel chiral stationary phase for enantioseparation of a series of chiral herbicides by capillary electrochromatography. *Electrophoresis* **2006,** 27, (16), 3254-3262.
56. Tolle, F.; Mayer, G., Dressed for success - applying chemistry to modulate aptamer functionality. *Chem. Sci.* **2013,** 4, (1), 60-67.

57. You, M.; Chen, Y.; Peng, L.; Han, D.; Yin, B.; Ye, B.; Tan, W., Engineering DNA aptamers for novel analytical and biomedical applications. *Chem. Sci.* **2011,** 2, (6), 1003-1010.
58. Mayer, G., The chemical biology of aptamers. *Angew. Chem. Int. Ed.* **2009,** 48, (15), 2672-2689.
59. Kuwahara, M.; Sugimoto, N., Molecular evolution of functional nucleic acids with chemical modifications. *Molecules* **2010,** 15, (8), 5423-5444.
60. Uzawa, T.; Tada, S.; Wang, W.; Ito, Y., Expansion of the aptamer library from a "natural soup" to an "unnatural soup". *Chem. Commun.* **2013,** 49, (18), 1786-1795.
61. Vaught, J. D.; Bock, C.; Carter, J.; Fitzwater, T.; Otis, M.; Schneider, D.; Rolando, J.; Waugh, S.; Wilcox, S. K.; Eaton, B. E., Expanding the chemistry of DNA for in vitro selection. *J. Am. Chem. Soc.* **2010,** 132, (12), 4141-4151.
62. Šponer, J.; Leszczynski, J.; Hobza, P., Electronic properties, hydrogen bonding, stacking, and cation binding of DNA and RNA bases. *Biopolymers* **2001,** 61, (1), 3-31.
63. Ghosal, G.; Muniyappa, K., Hoogsteen base-pairing revisited: Resolving a role in normal biological processes and human diseases. *Biochem. Biophys. Res. Commun.* **2006,** 343, (1), 1-7.
64. Watson, J. D.; Crick, F. H. C., Molecular structure of nucleic acids: A structure for deoxyribose nucleic acid. *Nature* **1953,** 171, (4356), 737-738.
65. Bansal, M., DNA structure: Revisiting the Watson–Crick double helix. *Curr. Sci.* **2003,** 85, (11), 1556-1563.
66. Richmond, T. J.; Davey, C. A., The structure of DNA in the nucleosome core. *Nature* **2003,** 423, (6936), 145-150.
67. Berg, J. M.; Tymoczko, J. L.; Stryer, L., *Biochemisty*. 5th ed.; W H Freeman: New York, 2002.
68. Senior, M. M.; Jones, R. A.; Breslauer, K. J., Influence of loop residues on the relative stabilities of DNA hairpin structures. *Proc. Natl. Acad. Sci. USA* **1988,** 85, (17), 6242-6246.
69. Huppert, J. L., Four-stranded nucleic acids: structure, function and targeting of G-quadruplexes. *Chem. Soc. Rev.* **2008,** 37, (7), 1375-1384.
70. Burge, S.; Parkinson, G. N.; Hazel, P.; Todd, A. K.; Neidle, S., Quadruplex DNA: sequence, topology and structure. *Nucleic Acids Res.* **2006,** 34, (19), 5402-5415.
71. Kankia, B. I.; Marky, L. A., Folding of the thrombin aptamer into a G-quadruplex with Sr^{2+}: stability, heat, and hydration. *J. Am. Chem. Soc.* **2001,** 123, (44), 10799-10804.
72. Hardin, C. C.; Perry, A. G.; White, K., Thermodynamic and kinetic characterization of the dissociation and assembly of quadruplex nucleic acids. *Biopolymers* **2000,** 56, (3), 147-194.
73. Kypr, J.; Kejnovská, I.; Renčiuk, D.; Vorlíčková, M., Circular dichroism and conformational polymorphism of DNA. *Nucleic Acids Res.* **2009,** 37, (6), 1713-1725.
74. Harda, K.; Frankel, A. D., Identification of two novel arginine binding DNAs. *The EMBO Journal* **1995,** 14, (23), 5798-5811.
75. Karsisiotis, A. I.; Hessari, N. M. a.; Novellino, E.; Spada, G. P.; Randazzo, A.; Webba da Silva, M., Topological characterization of nucleic acid G-quadruplexes by UV absorption and circular dichroism. *Angew. Chem.* **2011,** 123, (45), 10833-10836.

76. Rizzo, V.; Schellman, J. A., Matrix-method calculation of linear and circular dichroism spectra of nucleic acids and polynucleotides. *Biopolymers* **1984,** 23, (3), 435-470.
77. Nordén, B.; Kurucsev, T., Analysing DNA complexes by circular and linear dichroism. *J. Mol. Recognit.* **1994,** 7, (2), 141-155.
78. Ranjbar, B.; Gill, P., Circular dichroism techniques: biomolecular and nanostructural analyses- a review. *Chem. Biol. Drug Des.* **2009,** 74, (2), 101-120.
79. Masiero, S.; Trotta, R.; Pieraccini, S.; De Tito, S.; Perone, R.; Randazzo, A.; Spada, G. P., A non-empirical chromophoric interpretation of CD spectra of DNA G-quadruplex structures. *Org. Biomol. Chem.* **2010,** 8, (12), 2683-2692.
80. Gray, D. M.; Wen, J.-D.; Gray, C. W.; Repges, R.; Repges, C.; Raabe, G.; Fleischhauer, J., Measured and calculated CD spectra of G-quartets stacked with the same or opposite polarities. *Chirality* **2008,** 20, (3-4), 431-440.
81. Randazzo, A.; Spada, G. P.; da Silva, M. W., Circular dichroism of quadruplex structures. In *Quadruplex Nucleic Acids*, Chaires, J. B.; Graves, D., Eds. Springer Berlin Heidelberg: 2013; Vol. 330, pp 67-86.
82. Djordjevic, M., SELEX experiments: New prospects, applications and data analysis in inferring regulatory pathways. *Biomol. Eng.* **2007,** 24, (2), 179-189.
83. Hall, B.; Micheletti, J. M.; Satya, P.; Ogle, K.; Pollard, J.; Ellington, A. D., Design, synthesis, and amplification of DNA pools for in vitro selection. In *Current Protocols in Molecular Biology*, John Wiley & Sons, Inc.: 2009; Vol. 88, pp 24.2.1–24.2.27.
84. Gold, L., Oligonucleotides as research, diagnostic, and therapeutic agents. *J. Biol. Chem.* **1995,** 270, (23), 13581-13584.
85. Gopinath, S. C. B., Methods developed for SELEX. *Anal. Bioanal. Chem.* **2007,** 387, (1), 171-182.
86. Levine, H. A.; Nilsen-Hamilton, M., A mathematical analysis of SELEX. *Comput. Biol. Chem.* **2007,** 31, (1), 11-35.
87. Vant-Hull, B.; Payano-Baez, A.; Davis, R. H.; Gold, L., The mathematics of SELEX against complex targets. *J. Mol. Biol.* **1998,** 278, (3), 579-597.
88. Murphy, M. B.; Fuller, S. T.; Richardson, P. M.; Doyle, S. A., An improved method for the in vitro evolution of aptamers and applications in protein detection and purification. *Nucleic Acids Res.* **2003,** 31, (18), e110-e110.
89. Bibby, D. F.; Gill, A. C.; Kirby, L.; Farquhar, C. F.; Bruce, M. E.; Garson, J. A., Application of a novel in vitro selection technique to isolate and characterise high affinity DNA aptamers binding mammalian prion proteins. *J. Virol. Methods* **2008,** 151, (1), 107-115.
90. Morris, K. N.; Jensen, K. B.; Julin, C. M.; Weil, M.; Gold, L., High affinity ligands from in vitro selection: Complex targets. *Proc. Natl. Acad. Sci. USA* **1998,** 95, (6), 2902-2907.
91. Ellington, A. D.; Szostak, J. W., Selection in vitro of single-stranded DNA molecules that fold into specific ligand-binding structures. *Nature* **1992,** 355, (6363), 850-852.
92. Penner, G., Commercialization of an aptamer-based diagnostic test. *IVD Technology* **2012**, 31-37.
93. Sundaram, P.; Kurniawan, H.; Byrne, M. E.; Wower, J., Therapeutic RNA aptamers in clinical trials. *Eur. J. Pharm. Sci.* **2013,** 48, (1–2), 259-271.
94. Charo, I. F.; Ransohoff, R. M., The Many Roles of Chemokines and Chemokine Receptors in Inflammation. *N. Engl. J. Med.* **2006,** 354, (6), 610-621.

95. D'Haese, J. G.; Demir, I. E.; Friess, H.; Ceyhan, G., Fractalkine/CX3CR1: why a single chemokine-receptor duo bears a major and unique therapeutic potential. *Expert Opin. Ther. Targets* **2010,** 14, (2), 207-219.
96. Muñoz, L. M.; Holgado, B. L.; Martínez-A, C.; Rodríguez-Frade, J. M.; Mellado, M., Chemokine receptor oligomerization: A further step toward chemokine function. *Immunol. Lett.* **2012,** 145, (1–2), 23-29.
97. Zlotnik, A.; Yoshie, O., Chemokines: A New Classification System and Their Role in Immunity. *Immunity* **2000,** 12, (2), 121-127.
98. Nomiyama, H.; Osada, N.; Yoshie, O., The evolution of mammalian chemokine genes. *Cytokine Growth Factor Rev.* **2010,** 21, (4), 253-262.
99. Baggiolini, M., Chemokines and leukocyte traffic. *Nature* **1998,** 392, (6676), 565.
100. Bazan, F. J.; Bacon, K. B.; Hardiman, G.; Wang, W.; Soo, K.; Rossi, D.; Greaves, D. R.; Zlotnik, A.; Schall, T. J., A new class of membrane-bound chemokine with a CX3C motif. *Nature* **1997,** 385, (6617), 640-644.
101. Pan, Y.; Lloyd, C.; Zhou, H.; Dolich, S.; Deeds, J.; Gonzalo, J.-A.; Vath, J.; Gosselin, M.; Ma, J.; Dussault, B.; Woolf, E.; Alperin, G.; Culpepper, J.; Gutierrez-Ramos, J. C.; Gearing, D., Neurotactin, a membrane-anchored chemokine upregulated in brain inflammation. *Nature* **1997,** 387, (6633), 611-617.
102. Matloubian, M.; David, A.; Engel, S.; Ryan, J. E.; Cyster, J. G., A transmembrane CXC chemokine is a ligand for HIV-coreceptor Bonzo. *Nat. Immunol.* **2000,** 1, (4), 298-304.
103. Fong, A. M.; Robinson, L. A.; Steeber, D. A.; Tedder, T. F.; Yoshie, O.; Imai, T.; Patel, D. D., Fractalkine and CX3CR1 mediate a novel mechanism of leukocyte capture, firm adhesion, and activation under physiologic flow. *J. Exp. Med.* **1998,** 188, (8), 1413-1419.
104. Fong, A. M.; Erickson, H. P.; Zachariah, J. P.; Poon, S.; Schamberg, N. J.; Imai, T.; Patel, D. D., Ultrastructure and function of the fractalkine mucin domain in CX3C chemokine domain presentation. *J. Biol. Chem.* **2000,** 275, (6), 3781-3786.
105. Haskell, C. A.; Cleary, M. D.; Charo, I. F., Molecular Uncoupling of Fractalkine-mediated Cell Adhesion and Signal Transduction. Rapid Flow Arrest of CX3CR1-Expressing Cells is Independent of G-protein Activation. *J. Biol. Chem.* **1999,** 274, (15), 10053-10058.
106. Goda, S.; Imai, T.; Yoshie, O.; Yoneda, O.; Inoue, H.; Nagano, Y.; Okazaki, T.; Imai, H.; Bloom, E. T.; Domae, N.; Umehara, H., CX3C-chemokine, fractalkine-enhanced adhesion of THP-1 cells to endothelial cells through integrin-dependent and -independent mechanisms. *J. Immunol.* **2000,** 164, (8), 4313-4320.
107. Zanchi, C.; Zoja, C.; Morigi, M.; Valsecchi, F.; Liu, X. Y.; Rottoli, D.; Locatelli, M.; Buelli, S.; Pezzotta, A.; Mapelli, P.; Geelen, J.; Remuzzi, G.; Hawiger, J., Fractalkine and CX3CR1 Mediate Leukocyte Capture by Endothelium in Response to Shiga Toxin. *J. Immunol.* **2008,** 181, (2), 1460-1469.
108. Schulz, C.; Schafer, A.; Stolla, M.; Kerstan, S.; Lorenz, M.; von Bruhl, M.-L.; Schiemann, M.; Bauersachs, J.; Gloe, T.; Busch, D. H.; Gawaz, M.; Massberg, S., Chemokine Fractalkine Mediates Leukocyte Recruitment to Inflammatory Endothelial Cells in Flowing Whole Blood: A Critical Role for P-Selectin Expressed on Activated Platelets. *Circulation* **2007,** 116, (7), 764-773.
109. Kanazawa, N.; Nakamura, T.; Tashiro, K.; Muramatsu, M.; Morita, K.; Yoneda, K.; Inaba, K.; Imamura, S.; Honjo, T., Fractalkine and macrophage-derived chemokine:

T cell-attracting chemokines expressed in T cell area dendritic cells. *Eur. J. Immunol.* **1999,** 29, (6), 1925-1932.
110. Papadopoulos, E. J.; Sassetti, C.; Saeki, H.; Yamada, N.; Kawamura, T.; Fitzhugh, D. J.; Saraf, M. A.; Schall, T.; Blauvelt, A.; Rosen, S. D.; Hwang, S. T., Fractalkine, a CX3C chemokine, is expressed by dendritic cells and is up-regulated upon dendritic cell maturation. *Eur. J. Immunol.* **1999,** 29, (8), 2551-2559.
111. Harrison, J. K.; Jiang, Y.; Chen, S.; Xia, Y.; Maciejewski, D.; McNamara, R. K.; Streit, W. J.; Salafranca, M. N.; Adhikari, S.; Thompson, D. A.; Botti, P.; Bacon, K. B.; Feng, L., Role for neuronally derived fractalkine in mediating interactions between neurons and CX3CR1-expressing microglia. *Proc. Natl. Acad. Sci. USA* **1998,** 95, (18), 10896-10901.
112. Schwaeble, W. J.; Stover, C. M.; Schall, T. J.; Dairaghi, D. J.; Trinder, P. K. E.; Linington, C.; Iglesias, A.; Schubart, A.; Lynch, N. J.; Weihe, E.; Schäfer, M. K. H., Neuronal expression of fractalkine in the presence and absence of inflammation. *FEBS Lett.* **1998,** 439, (3), 203-207.
113. Yoshida, H.; Imaizumi, T.; Fujimoto, K.; Matsuo, N.; Kimura, K.; Cui, X.-F.; Matsumiya, T.; Tanji, K.; Shibata, T.; Tamo, W.; Kumagai, M.; Satoh, K., Synergistic stimulation, by tumor necrosis factor-α and interferon-γ, of fractalkine expression in human astrocytes. *Neurosci. Lett.* **2001,** 303, (2), 132-136.
114. Marchesi, F.; Locatelli, M.; Solinas, G.; Erreni, M.; Allavena, P.; Mantovani, A., Role of CX3CR1/CX3CL1 axis in primary and secondary involvement of the nervous system by cancer. *J. Neuroimmunol.* **2010,** 224, (1-2), 39-44.
115. Imai, T.; Hieshima, K.; Haskell, C.; Baba, M.; Nagira, M.; Nishimura, M.; Kakizaki, M.; Takagi, S.; Nomiyama, H.; Schall, T. J.; Yoshie, O., Identification and molecular characterization of fractalkine receptor CX3CR1, which mediates both leukocyte migration and adhesion. *Cell* **1997,** 91, (4), 521-530.
116. Hundhausen, C.; Misztela, D.; Berkhout, T. A.; Broadway, N.; Saftig, P.; Reiss, K.; Hartmann, D.; Fahrenholz, F.; Postina, R.; Matthews, V.; Kallen, K.-J.; Rose-John, S.; Ludwig, A., The disintegrin-like metalloproteinase ADAM10 is involved in constitutive cleavage of CX3CL1 (fractalkine) and regulates CX3CL1-mediated cell-cell adhesion. *Blood* **2003,** 102, (4), 1186-1195.
117. Ludwig, A.; Berkhout, T.; Moores, K.; Groot, P.; Chapman, G., Fractalkine Is Expressed by Smooth Muscle Cells in Response to IFN-γ and TNF-α and Is Modulated by Metalloproteinase Activity. *J. Immunol.* **2002,** 168, (2), 604-612.
118. Tsou, C.-L.; Haskell, C. A.; Charo, I. F., Tumor Necrosis Factor-alpha -converting Enzyme Mediates the Inducible Cleavage of Fractalkine. *J. Biol. Chem.* **2001,** 276, (48), 44622-44626.
119. Garton, K. J.; Gough, P. J.; Blobel, C. P.; Murphy, G.; Greaves, D. R.; Dempsey, P. J.; Raines, E. W., Tumor Necrosis Factor-alpha -converting Enzyme (ADAM17) Mediates the Cleavage and Shedding of Fractalkine (CX3CL1). *J. Biol. Chem.* **2001,** 276, (41), 37993-38001.
120. Dimberg, J.; Dienus, O.; Löfgren, S.; Hugander, A.; Wågsäter, D., Polymorphisms of Fractalkine receptor CX3CR1 and plasma levels of its ligand CX3CL1 in colorectal cancer patients. *Int. J. Colorectal Dis.* **2007,** 22, (10), 1195-1200.
121. Umehara, H.; Bloom, E. T.; Okazaki, T.; Nagano, Y.; Yoshie, O.; Imai, T., Fractalkine in vascular biology: from basic research to clinical disease. *Arterioscler. Thromb. Vasc. Biol.* **2004,** 24, (1), 34-40.

122. Yoneda, O.; Imai, T.; Goda, S.; Inoue, H.; Yamauchi, A.; Okazaki, T.; Imai, H.; Yoshie, O.; Bloom, E. T.; Domae, N.; Umehara, H., Fractalkine-mediated endothelial cell injury by NK cells. *J. Immunol.* **2000,** 164, (8), 4055-4062.
123. Lucas, A. D.; Chadwick, N.; Warren, B. F.; Jewell, D. P.; Gordon, S.; Powrie, F.; Greaves, D. R., The Transmembrane Form of the CX3CL1 Chemokine Fractalkine Is Expressed Predominantly by Epithelial Cells in Vivo. *Am. J. Pathol.* **2001,** 158, (3), 855-866.
124. Imaizumi, T.; Matsumiya, T.; Fujimoto, K.; Okamoto, K.; Cui, X.; Ohtaki, U.; Yoshida, H.; Satoh, K., Interferon-gamma; stimulates the expression of CX3CL1/fractalkine in cultured human endothelial cells. *The Tohoku Journal of Experimental Medicine* **2000,** 192, (2), 127-139.
125. Umehara, H.; Bloom, E. T.; Okazaki, T.; Domae, N.; Imai, T., Fractalkine and vascular injury. *Trends Immunol.* **2001,** 22, (11), 602-607.
126. Erreni, M.; Solinas, G.; Brescia, P.; Osti, D.; Zunino, F.; Colombo, P.; Destro, A.; Roncalli, M.; Mantovani, A.; Draghi, R.; Levi, D.; Rodriguez y Baena, R.; Gaetani, P.; Pelicci, G.; Allavena, P., Human glioblastoma tumours and neural cancer stem cells express the chemokine CX3CL1 and its receptor CX3CR1. *Eur. J. Cancer* **2010,** 46, (18), 3383-3392.
127. Matsubara, T.; Ono, T.; Yamanoi, A.; Tachibana, M.; Nagasue, N., Fractalkine-CX3CR1 axis regulates tumor cell cycle and deteriorates prognosis after radical resection for hepatocellular carcinoma. *J. Surg. Oncol.* **2007,** 95, (3), 241-249.
128. Li, F.; Wang, Z.; Liu, Y.; Li, J., Down-regulation of fractalkine inhibits the in vitro and in vivo angiogenesis of the hepatocellular carcinoma HepG2 cells. *Oncol. Rep.* **2010,** 24, (3), 669-675.
129. Ren, T.; Chen, Q.; Tian, Z.; Wei, H., Down-regulation of surface fractalkine by RNA interference in B16 melanoma reduced tumor growth in mice. *Biochem. Biophys. Res. Commun.* **2007,** 364, (4), 978-984.
130. Zeng, Y.; Huebener, N.; Fest, S.; Weixler, S.; Schroeder, U.; Gaedicke, G.; Xiang, R.; Schramm, A.; Eggert, A.; Reisfeld, R. A.; Lode, H. N., Fractalkine (CX3CL1)- and Interleukin-2-Enriched Neuroblastoma Microenvironment Induces Eradication of Metastases Mediated by T Cells and Natural Killer Cells. *Cancer Res.* **2007,** 67, (5), 2331-2338.
131. Fujimoto, K.; Imaizumi, T.; Yoshida, H.; Takanashi, S.; Okumura, K.; Satoh, K., Interferon-gamma stimulates fractalkine expression in human bronchial epithelial cells and regulates mononuclear cell adherence. *Am. J. Respir. Cell Mol. Biol.* **2001,** 25, (2), 233-238.
132. Gaudin, F.; Nasreddine, S.; Donnadieu, A.-C.; Emilie, D.; Combadière, C.; Prévot, S.; Machelon, V.; Balabanian, K., Identification of the chemokine CX3CL1 as a new regulator of malignant cell proliferation in epithelial ovarian cancer. *PLoS ONE* **2011,** 6, (7), e21546.
133. Shulby, S. A.; Dolloff, N. G.; Stearns, M. E.; Meucci, O.; Fatatis, A., CX3CR1-Fractalkine Expression Regulates Cellular Mechanisms Involved in Adhesion, Migration, and Survival of Human Prostate Cancer Cells. *Cancer Res.* **2004,** 64, (14), 4693-4698.
134. Jamieson, W. L.; Shimizu, S.; D'Ambrosio, J. A.; Meucci, O.; Fatatis, A., CX3CR1 Is Expressed by Prostate Epithelial Cells and Androgens Regulate the Levels of CX3CL1/Fractalkine in the Bone Marrow: Potential Role in Prostate Cancer Bone Tropism. *Cancer Res.* **2008,** 68, (6), 1715-1722.

135. Hyakudomi, M.; Matsubara, T.; Hyakudomi, R.; Yamamoto, T.; Kinugasa, S.; Yamanoi, A.; Maruyama, R.; Tanaka, T., Increased expression of fractalkine is correlated with a better prognosis and an increased number of both CD8+ T cells and natural killer cells in gastric adenocarcinoma. *Ann. Surg. Oncol.* **2008,** 15, (6), 1775-1782.
136. Ohta, M.; Tanaka, F.; Yamaguchi, H., The high expression of Fractalkine results in a better prognosis for colorectal cancer patients. *Int. J. Oncol.* **2005,** 26, (1), 41-47.
137. Guo, J.; Chen, T.; Wang, B.; Zhang, M.; An, H.; Guo, Z.; Yu, Y.; Qin, Z.; Cao, X., Chemoattraction, adhesion and activation of natural killer cells are involved in the antitumor immune response induced by fractalkine/CX3CL1. *Immunol. Lett.* **2003,** 89, (1), 1-7.
138. Zhang, X.; Wei, H.; Wang, H.; Tian, Z., Involvement of interaction between Fractalkine and CX3CR1 in cytotoxicity of natural killer cells against tumor cells. *Oncol. Rep.* **2006,** 15, (2), 485-488.
139. Zhang, X.; Wei, H.; Chen, Q.; Tian, Z., Activation of human natural killer cells by recombinant membrane-expressed fractalkine on the surface of tumor cells. *Oncol. Rep.* **2007,** 17, (6), 1371-1375.
140. Choy, E. H. S.; Panayi, G. S., Cytokine pathways and joint inflammation in rheumatoid arthritis. *N. Engl. J. Med.* **2001,** 344, (12), 907-916.
141. Murphy, G.; Caplice, N.; Molloy, M., Fractalkine in rheumatoid arthritis: a review to date. *Rheumatology* **2008,** 47, (10), 1446-1451.
142. Ruth, J. H.; Volin, M. V.; Haines, G. K.; Woodruff, D. C.; Katschke, K. J.; Woods, J. M.; Park, C. C.; Morel, J. C. M.; Koch, A. E., Fractalkine, a novel chemokine in rheumatoid arthritis and in rat adjuvant-induced arthritis. *Arthritis. Rheum.* **2001,** 44, (7), 1568-1581.
143. Blaschke, S.; Koziolek, M.; Schwarz, A.; Benöhr, P.; Middel, P.; Schwarz, G.; Hummel, K.-M.; Müller, G. A., Proinflammatory role of fractalkine (CX3CL1) in rheumatoid arthritis. *The Journal of Rheumatology* **2003,** 30, (9), 1918-1927.
144. Matsunawa, M.; Isozaki, T.; Odai, T.; Yajima, N.; Takeuchi, H. T.; Negishi, M.; Ide, H.; Adachi, M.; Kasama, T., Increased serum levels of soluble fractalkine (CX3CL1) correlate with disease activity in rheumatoid vasculitis. *Arthritis. Rheum.* **2006,** 54, (11), 3408-3416.
145. Yano, R.; Yamanura, M.; Sunahori, K.; Takasugi, K.; Yamana, J.; Kawashima, M.; Makino, H., Recruitment of CD16+ monocytes into synovial tissues is mediated by fractalkine and CX3CR1 in rheumatoid arthritis patients. *Acta Med. Okayama* **2007**, 98-98.
146. Sato, M.; Ohtsuka, K.; Takahashi, R.; Wakabayashi, K.; Odai, T.; Isozaki, T.; Yajima, N.; Miwa, Y.; Kasama, T., Involvement of CX3CL1/CX3CR1 axis in etanercept therapy for patients with active rheumatoid arthritis. *Open Access Rheumatology: Research and Review* **2011,** 3, (1), 1-7.
147. Nanki, T.; Urasaki, Y.; Imai, T.; Nishimura, M.; Muramoto, K.; Kubota, T.; Miyasaka, N., Inhibition of fractalkine ameliorates murine collagen-induced arthritis. *J. Immunol.* **2004,** 173, (11), 7010-7016.
148. Jeffery, P.; Haahtela, T., Allergic rhinitis and asthma: inflammation in a one-airway condition. *BMC Pulm. Med.* **2006,** 6, (Suppl 1), S5.
149. Barnes, P. J., Immunology of asthma and chronic obstructive pulmonary disease. *Nat. Rev. Immunol.* **2008,** 8, (3), 183-192.

150. Larché, M.; Robinson, D. S.; Kay, A. B., The role of T lymphocytes in the pathogenesis of asthma. *J. Allergy Clin. Immunol.* **2003,** 111, (3), 450-463.
151. Meyer, E. H.; DeKruyff, R. H.; Umetsu, D. T., T Cells and NKT Cells in the Pathogenesis of Asthma. *Annu. Rev. Med.* **2008,** 59, (1), 281-292.
152. Holgate, S. T.; Polosa, R., Treatment strategies for allergy and asthma. *Nat. Rev. Immunol.* **2008,** 8, (3), 218-230.
153. El-Shazly, A.; Berger, P.; Girodet, P.-O.; Ousova, O.; Fayon, M.; Vernejoux, J.-M.; Marthan, R.; Tunon-de-Lara, J. M., Fraktalkine Produced by Airway Smooth Muscle Cells Contributes to Mast Cell Recruitment in Asthma. *J. Immunol.* **2006,** 176, (3), 1860-1868.
154. Rimaniol, A.-C.; Till, S. J.; Garcia, G.; Capel, F.; Godot, V.; Balabanian, K.; Durand-Gasselin, I.; Varga, E. M.; Simonneau, G.; Emilie, D.; Durham, S. R.; Humbert, M., The CX3C chemokine fractalkine in allergic asthma and rhinitis. *J. Allergy Clin. Immunol.* **2003,** 112, (6), 1139-1146.
155. Bosson, J.; Stenfors, N.; Bucht, A.; Helleday, R.; Pourazar, J.; Holgate, S. T.; Kelly, F. J.; Sandström, T.; Wilson, S.; Frew, A. J.; Blomberg, A., Ozone-induced bronchial epithelial cytokine expression differs between healthy and asthmatic subjects. *Clinical & Experimental Allergy* **2003,** 33, (6), 777-782.
156. Braunersreuther, V.; Mach, F.; Steffens, S., The specific role of chemokines in atherosclerosis. *Thromb. Haemostasis* **2007,** 97, (5), 714-721.
157. McDermott, D. H.; Halcox, J. P. J.; Schenke, W. H.; Waclawiw, M. A.; Merrell, M. N.; Epstein, N.; Quyyumi, A. A.; Murphy, P. M., Association Between Polymorphism in the Chemokine Receptor CX3CR1 and Coronary Vascular Endothelial Dysfunction and Atherosclerosis. *Circ. Res.* **2001,** 89, (5), 401-407.
158. Moatti, D.; Faure, S.; Fumeron, F.; Amara, M. E. W.; Seknadji, P.; McDermott, D. H.; Debré, P.; Aumont, M. C.; Murphy, P. M.; de Prost, D.; Combadière, C., Polymorphism in the fractalkine receptor CX3CR1 as a genetic risk factor for coronary artery disease. *Blood* **2001,** 97, (7), 1925-1928.
159. Combadière, C.; Potteaux, S.; Gao, J.-L.; Esposito, B.; Casanova, S.; Lee, E. J.; Debré, P.; Tedgui, A.; Murphy, P. M.; Mallat, Z., Decreased Atherosclerotic Lesion Formation in CX3CR1/Apolipoprotein E Double Knockout Mice. *Circulation* **2003,** 107, (7), 1009-1016.
160. Lesnik, P.; Haskell, C. A.; Charo, I. F., Decreased atherosclerosis in CX3CR1-/- mice reveals a role for fractalkine in atherogenesis. *J. Clin. Investig.* **2003,** 111, (3), 333-340.
161. Teupser, D.; Pavlides, S.; Tan, M.; Gutierrez-Ramos, J.-C.; Kolbeck, R.; Breslow, J. L., Major reduction of atherosclerosis in fractalkine (CX3CL1)-deficient mice is at the brachiocephalic artery, not the aortic root. *Proc. Natl. Acad. Sci. USA* **2004,** 101, (51), 17795-17800.
162. Saederup, N.; Chan, L.; Lira, S. A.; Charo, I. F., Fractalkine Deficiency Markedly Reduces Macrophage Accumulation and Atherosclerotic Lesion Formation in CCR2−/− Mice. *Circulation* **2008,** 117, (13), 1642-1648.
163. Nishiyori, A.; Minami, M.; Ohtani, Y.; Takami, S.; Yamamoto, J.; Kawaguchi, N.; Kume, T.; Akaike, A.; Satoh, M., Localization of fractalkine and CX3CR1 mRNAs in rat brain: does fractalkine play a role in signaling from neuron to microglia? *FEBS Lett.* **1998,** 429, (2), 167-172.
164. Milligan, E. D.; Zapata, V.; Chacur, M.; Schoeniger, D.; Biedenkapp, J.; O'Connor, K. A.; Verge, G. M.; Chapman, G.; Green, P.; Foster, A. C.; Naeve, G. S.; Maier, S.

F.; Watkins, L. R., Evidence that exogenous and endogenous fractalkine can induce spinal nociceptive facilitation in rats. *Eur. J. Neurosci.* **2004,** 20, (9), 2294-2302.
165. Milligan, E.; Zapata, V.; Schoeniger, D.; Chacur, M.; Green, P.; Poole, S.; Martin, D.; Maier, S. F.; Watkins, L. R., An initial investigation of spinal mechanisms underlying pain enhancement induced by fractalkine, a neuronally released chemokine. *Eur. J. Neurosci.* **2005,** 22, (11), 2775-2782.
166. Verge, G. M.; Milligan, E. D.; Maier, S. F.; Watkins, L. R.; Naeve, G. S.; Foster, A. C., Fractalkine (CX3CL1) and fractalkine receptor (CX3CR1) distribution in spinal cord and dorsal root ganglia under basal and neuropathic pain conditions. *Eur. J. Neurosci.* **2004,** 20, (5), 1150-1160.
167. Staniland, A. A.; Clark, A. K.; Wodarski, R.; Sasso, O.; Maione, F.; D'Acquisto, F.; Malcangio, M., Reduced inflammatory and neuropathic pain and decreased spinal microglial response in fractalkine receptor (CX3CR1) knockout mice. *J. Neurochem.* **2010,** 114, (4), 1143-1157.
168. Clark, A. K.; Yip, P. K.; Grist, J.; Gentry, C.; Staniland, A. A.; Marchand, F.; Dehvari, M.; Wotherspoon, G.; Winter, J.; Ullah, J.; Bevan, S.; Malcangio, M., Inhibition of spinal microglial cathepsin S for the reversal of neuropathic pain. *Proc. Natl. Acad. Sci. USA* **2007,** 104, (25), 10655-10660.
169. Furth, R. v.; Cohn, Z. A.; Hirsch, J. G.; Humphrey, J. H.; Spector, W. G.; Langevoort, H. L., The mononuclear phagocyte system: a new classification of macrophages, monocytes, and their precursor cells. *Bull. W.H.O* **1972,** 46, (6), 845-852.
170. Waybrant, B.; Pearce, T. R.; Wang, P.; Sreevatsan, S.; Kokkoli, E., Development and characterization of an aptamer binding ligand of fractalkine using domain targeted SELEX. *Chem. Commun.* **2012,** 48, (80), 10043-10045.
171. Julia, V., CX3CL1 in allergic diseases: not just a chemotactic molecule. *Allergy* **2012**.
172. Kokkoli, E.; Kasinskas, R. W.; Mardilovich, A.; Garg, A., Fractalkine Targeting with a Receptor-Mimicking Peptide-Amphiphile. *Biomacromolecules* **2005,** 6, (3), 1272-1279.
173. Drolet, D. W.; Jenison, R. D.; Smith, D. E.; Pratt, D.; Hicke, B. J., A high throughput platform for systematic evolution of ligands by exponential enrichment (SELEX). *Comb. Chem. High Throughput Screen.* **1999,** 2, (5), 271-278.
174. Pangburn, T. O.; Petersen, M. A.; Waybrant, B.; Adil, M. M.; Kokkoli, E., Peptide- and aptamer-functionalized nanovectors for targeted delivery of therapeutics. *J. Biomech. Eng.* **2009,** 131, (7), 074005.
175. Bouchard, P. R.; Hutabarat, R. M.; Thompson, K. M., Discovery and development of therapeutic aptamers. *Annu. Rev. Pharmacol. Toxicol.* **2010,** 50, (1), 237-257.
176. Borisenko, G. G.; Zaitseva, M. A.; Chuvilin, A. N.; Pozmogova, G. E., DNA modification of live cell surface. *Nucleic Acids Res.* **2009,** 37, (4), e28.
177. Liu, H.; Zhu, Z.; Kang, H.; Wu, Y.; Sefan, K.; Tan, W., DNA-based micelles: synthesis, micellar properties and size-dependent cell permeability. *Chem. Eur. J.* **2010,** 16, (12), 3791-3797.
178. Willis, M. C.; Collins, B.; Zhang, T.; Green, L. S.; Sebesta, D. P.; Bell, C.; Kellogg, E.; Gill, S. C.; Magallanez, A.; Knauer, S.; Bendele, R. A.; Gill, P. S.; Janjic, N., Liposome-anchored vascular endothelial growth factor aptamers. *Bioconjug. Chem.* **1998,** 9, (5), 573-582.

179. Cao, Z.; Tong, R.; Mishra, A.; Xu, W.; Wong, G. C. L.; Cheng, J.; Lu, Y., Reversible cell-specific drug delivery with aptamer-functionalized liposomes. *Angew. Chem. Int. Ed.* **2009,** 48, (35), 6494-6498.
180. Shchepinov, M. S.; Case-Green, S. C.; Southern, E. M., Steric factors influencing hybridisation of nucleic acids to oligonucleotide arrays. *Nucleic Acids Res.* **1997,** 25, (6), 1155-1161.
181. Lao, Y.-H.; Peck, K.; Chen, L.-C., Enhancement of aptamer microarray sensitivity through spacer optimization and avidity effect. *Anal. Chem.* **2009,** 81, (5), 1747-1754.
182. Kokkoli, E.; Mardilovich, A.; Wedekind, A.; Rexeisen, E. L.; Garg, A.; Craig, J. A., Self-assembly and applications of biomimetic and bioactive peptide-amphiphiles. *Soft Matter* **2006,** 2, (12), 1015-1024.
183. Wu, Y.; Sefah, K.; Liu, H.; Wang, R.; Tan, W., DNA aptamer–micelle as an efficient detection/delivery vehicle toward cancer cells. *Proc. Natl. Acad. Sci. USA* **2010,** 107, (1), 5-10.
184. Baglioni, P.; Berti, D., Self assembly in micelles combining stacking and H-bonding. *Curr. Opin. Colloid Interface Sci.* **2003,** 8, (1), 55-61.
185. Pearce, T. R.; Waybrant, B.; Kokkoli, E., The role of spacers on the self-assembly of DNA aptamer-amphiphiles into micelles and nanotapes. *Chem. Commun.* **2013,** 50, (2), 210-212.
186. Jones, B. A.; Beamer, M.; Ahmed, S., Fractalkine/CX3CL1: a potential new target for inflammatory diseases. *Mol. Interv.* **2010,** 10, (5), 263-270.
187. Mardilovich, A.; Kokkoli, E., Biomimetic peptide−amphiphiles for functional biomaterials: the role of GRGDSP and PHSRN. *Biomacromolecules* **2004,** 5, (3), 950-957.
188. Rexeisen, E. L.; Fan, W.; Pangburn, T. O.; Taribagil, R. R.; Bates, F. S.; Lodge, T. P.; Tsapatsis, M.; Kokkoli, E., Self-assembly of fibronectin mimetic peptide-amphiphile nanofibers. *Langmuir* **2009,** 26, (3), 1953-1959.
189. Lau, C.; Bitton, R.; Bianco-Peled, H.; Schultz, D. G.; Cookson, D. J.; Grosser, S. T.; Schneider, J. W., Morphological characterization of self-assembled peptide nucleic acid amphiphiles. *J. Phys. Chem. B* **2006,** 110, (18), 9027-9033.
190. Mergny, J.-L.; Lacroix, L., Analysis of thermal melting curves. *Oligonucleotides* **2003,** 13, (6), 515-537.
191. Garg, A.; Tisdale, A. W.; Haidari, E.; Kokkoli, E., Targeting colon cancer cells using PEGylated liposomes modified with a fibronectin-mimetic peptide. *Int. J. Pharm.* **2009,** 366, (1-2), 201-210.
192. Chen, P. S.; Toribara, T. Y.; Warner, H., Microdetermination of Phosphorus. *Anal. Chem.* **1956,** 28, (11), 1756-1758.
193. Tu, R. S.; Marullo, R.; Pynn, R.; Bitton, R.; Bianco-Peled, H.; Tirrell, M. V., Cooperative DNA binding and assembly by a bZip peptide-amphiphile. *Soft Matter* **2010,** 6, (5), 1035-1044.
194. Black, M.; Trent, A.; Kostenko, Y.; Lee, J. S.; Olive, C.; Tirrell, M., Self-assembled peptide amphiphile micelles containing a cytotoxic T-cell epitope promote a protective immune response *in vivo*. *Adv. Mater.* **2012,** 24, (28), 3845-3849.
195. Lim, Y.-b.; Lee, E.; Lee, M., Controlled bioactive nanostructures from self-assembly of peptide building blocks. *Angew. Chem. Int. Ed.* **2007,** 46, (47), 9011-9014.

196. Letsinger, R. L.; Chaturvedi, S. K.; Farooqui, F.; Salunkhe, M., Use of hydrophobic substituents in controlling self-assembly of oligonucleotides. *J. Am. Chem. Soc.* **1993,** 115, (16), 7535-7536.
197. Williamson, J. R., G-quartet structures in telomeric DNA. *Annu. Rev. Biophys. Biomol. Struct.* **1994,** 23, 703-730.
198. Choi, E. W.; Nayak, L. V.; Bates, P. J., Cancer-selective antiproliferative activity is a general property of some G-rich oligodeoxynucleotides. *Nucleic Acids Res.* **2010,** 38, (5), 1623-1635.
199. Penázová, H.; Vorlicková, M., Guanine tetraplex formation by short DNA fragments containing runs of guanine and cytosine. *Biophys. J.* **1997,** 73, (4), 2054-2063.
200. Zuker, M., Mfold web server for nucleic acid folding and hybridization prediction. *Nucleic Acids Res.* **2003,** 31, (13), 3406-3415.
201. Marguet, E.; Forterre, P., Protection of DNA by salts against thermodegradation at temperatures typical for hyperthermophiles. *Extremophiles* **1998,** 2, (2), 115-122.
202. Trajkovski, M.; Webba da Silva, M.; Plavec, J., Unique structural features of interconverting monomeric and dimeric G-quadruplexes adopted by a sequence from the intron of the N-myc gene. *J. Am. Chem. Soc.* **2012,** 134, (9), 4132-4141.
203. Shea, R. G.; Marsters, J. C.; Bischofberger, N., Synthesis, hybridization properties and antiviral activity of lipid-oligodeoxynucleotide conjugates. *Nucleic Acids Res.* **1990,** 18, (13), 3777-3783.
204. Gosse, C.; Boutorine, A.; Aujard, I.; Chami, M.; Kononov, A.; Cogné-Laage, E.; Allemand, J. F.; Li, J.; Jullien, L., Micelles of lipid−oligonucleotide conjugates: implications for membrane anchoring and base pairing. *J. Phys. Chem. B* **2004,** 108, (20), 6485-6497.
205. Jung, J. H.; Do, Y.; Lee, Y.-A.; Shimizu, T., Self-assembling structures of long-chain sugar-based amphiphiles influenced by the introduction of double bonds. *Chem. Eur. J.* **2005,** 11, (19), 5538-5544.
206. Missirlis, D.; Chworos, A.; Fu, C. J.; Khant, H. A.; Krogstad, D. V.; Tirrell, M., Effect of the peptide secondary structure on the peptide amphiphile supramolecular structure and interactions. *Langmuir* **2011,** 27, (10), 6163-6170.
207. Ziserman, L.; Lee, H.-Y.; Raghavan, S. R.; Mor, A.; Danino, D., Unraveling the mechanism of nanotube formation by chiral self-assembly of amphiphiles. *J. Am. Chem. Soc.* **2011,** 133, (8), 2511-2517.
208. Shimizu, T.; Iwaura, R.; Masuda, M.; Hanada, T.; Yase, K., Internucleobase-interaction-directed self-assembly of nanofibers from homo- and heteroditopic 1,ω-nucleobase bolaamphiphiles. *J. Am. Chem. Soc.* **2001,** 123, (25), 5947-5955.
209. Baldelli Bombelli, F.; Berti, D.; Keiderling, U.; Baglioni, P., Giant polymerlike micelles formed by nucleoside-functionalized lipids. *J. Phys. Chem. B* **2002,** 106, (44), 11613-11621.